INSTITUTO
UNIVERSITÁRIO
DE LISBOA

Impact of physical layer impairments on large ROADM architectures

Diogo Miguel Cigarro Morão

Master in Telecommunications and Computer Engineering,

Supervisor:
Doctor Luís Gonçalo Lecoq Vences e Costa Cancela, Assistant Professor,
ISCTE-IUL

Co-Supervisor:
Doctor João Lopes Rebola, Assistant Professor,
ISCTE-IUL

October 2020

TECNOLOGIAS
E ARQUITETURA

Impact of physical layer impairments on large ROADM architectures

Diogo Miguel Cigarro Morão

Master in Telecommunications and Computer Engineering,

Supervisor:
Doctor Luís Gonçalo Lecoq Vences e Costa Cancela, Assistant Professor,
ISCTE-IUL

Co-Supervisor:
Doctor João Lopes Rebola, Assistant Professor,
ISCTE-IUL

October 2020

Agradecimentos

Quero agradecer ao ISCTE-IUL por estes cinco anos e a todos os docentes que fizeram parte do meu percurso, e em especial, aos meus orientadores, Prof. Luís Cancela e Prof. João Rebola por todo o apoio e trabalho a analisar as diferentes versões que lhes apresentei. Um agradecimento também ao Instituto de Telecomunicações, pelo acesso dado às suas instalações e material.

Quero também agradecer à minha família, que sempre me apoiou em todas as ocasiões, e à minha namorada que esteve presente em todos os altos e baixos dos últimos anos.

Um obrigado também a todos os meus colegas de curso, em especial ao Rafael Dias, pelo seu companheirismo e apoio.

Por último, mas nunca o menos importante, agradecer ao meu avô, que estaria certamente muito orgulhoso por esta meta alcançada.

Resumo

A maioria das redes óticas são atualmente compostas por multiplexadores óticos de inserção/extração reconfiguráveis (ROADMs, em inglês) nos nós, cuja arquitetura tem evoluído para se tornarem mais dinâmicos e flexíveis. As funcionalidades *colorless*, *directionless* e *contentionless* estão hoje normalizadas, no entanto, as arquiteturas atuais tornam-se pouco escaláveis para ROADMs de elevada dimensão, devido a limitações nos comutadores seletivos no comprimento-de-onda.

Neste trabalho, a comparação entre os custos associados e a geração de *crosstalk* homódino em diferentes arquiteturas propostas para ROADMs de elevada dimensão e as arquitecturas tradicionais é efetuada. É também analisado o impacto da filtragem ótica, ruído de emissão espontânea amplificada (ASE, em inglês) e *crosstalk* homódino no desempenho de uma rede com nós baseados na arquitetura denominada "*Interconnected A*". A avaliação é feita através de simulação Monte-Carlo com sinais multiplexados por divisão na polarização e modulação de amplitude em quadratura, PDM-16QAM e PDM-32QAM a 200 Gb/s e 250 Gb/s, respetivamente. Foram consideradas duas configurações para os ROADMs estudados, *Broadcast and Select* e *Route and Select* (B&S e R&S, em inglês) e uma estrutura de inserção/extração denominada "*bank-based*".

Quando considerados todos os efeitos, o alcance máximo da rede é de 4 e 7 nós para um sinal 16QAM, respetivamente, para configurações B&S e R&S. Para um sinal 32QAM, é de 3 e 4 nós, respetivamente, para configurações B&S e R&S. A principal penalidade na transmissão deve-se ao ruído ASE gerado nos amplificadores óticos ao longo da rede, tendo a penalidade devido ao *crosstalk* homódino e a filtragem ótica uma menor contribuição.

Palavras-chave: crosstalk homódino, estrutura de inserção/extracção bank based, filtragem ótica, ROADMs de grandes dimensões, ruído ASE.

Abstract

Most of today's optical networks, use reconfigurable optical add/drop multiplexers (ROADMs) as nodes. To become more dynamic and flexible, these nodes architectures evolved over the years. The colorless, directionless and contentionless functionalities are now standard, however, current architectures have poor scalability due to limitations on wavelength selective switches dimensions. Hence, due to constant increase in data traffic, current architectures might become a bottleneck to manufacture future large-scale ROADMs.

In this work, the hardware cost and in-band crosstalk generation inside different large-scale ROADM architectures, is compared with conventional architectures. Moreover, an analysis of optical filtering, amplified spontaneous emission (ASE) noise and in-band crosstalk impact in the performance of an optical network, with nodes based on the most promising large-scale architecture, the interconnected A architecture, is performed. This performance is assessed through Monte-Carlo simulation with 16 point quadrature amplitude modulation with polarization-division multiplexing (PDM-16QAM) and PDM-32QAM signals with 200 Gb/s and 250 Gb/s, respectively. Two architectures are considered for the interconnected A express structure, Broadcast and Select (B&S) and Route and Select (R&S). For the add/drop structure, a bank-based structure is considered.

The maximum number of cascaded ROADMs, considering all the studied impairments, is 5 and 7 nodes for a 32 GBaud 16QAM signal, respectively, for B&S and R&S architectures. A 32QAM signal reaches 3 and 4 nodes, respectively, for B&S and R&S architectures. The main penalty in transmission is the ASE noise generated by optical amplifiers throughout the network, having the in-band crosstalk and optical filtering penalties a lower contribution.

Keywords: amplified spontaneous emission noise, bank based add/drop, in-band crosstalk, large-scale ROADMs, optical filtering.

Contents

List of Figures

List of Tables

List of Acronyms

A/D	**A**dd/**D**rop
ADM	**A**dd/**D**rop **M**ultiplexers
AWG	**A**rrayed **W**aveguide **G**rating
B&S	**B**roadcast and **S**elect
CDC	**C**olorless, **D**irectionless and **C**ontentionless
DC	**D**elivery and **C**oupling
DSP	**D**igital **S**ignal **P**rocessing
DWDM	**D**ense **W**avelength **D**ivision **M**ultiplexing
EDFA	**E**rbium-**D**oped **F**iber **A**mplifier
FEC	**F**orward **E**rror **C**orrection
IP	**I**nternet **P**rotocol
ISI	**I**nter-**S**ymbolic **I**nterference
ITU	**I**nternational **T**elecommunication **U**nion
LCoS	**L**iquid **C**rystal **o**n **S**ilicon
MCS	**M**ulti**c**ast **S**witch
MEMS	**M**icro-**E**lectro-**M**echanical **S**ystems
NLI	**N**on **L**inear **I**nterference
NRZ	**N**on-**R**eturn-to-**Z**ero
OADM	**O**ptical **A**dd/**D**rop **M**ultiplexers
OSNR	**O**ptical **S**ignal-to-**N**oise **R**atio
OXC	**O**ptical **C**ross-**C**onnects
PDM	**P**olarization **D**ivision **M**ultiplexing
PLI	**P**hysical **L**ayer **I**mpairments
PSD	**P**ower **S**pectral **D**ensity
QAM	**Q**uadrature **A**mplitude **M**odulation
ROADM	**R**econfigurable **O**ptical **A**dd/**D**rop **M**ultiplexer
RWA	**R**outing and **W**avelength **A**ssignment
R&S	**R**oute and **S**elect
SDH	**S**ynchronous **D**igital **H**ierarchy
SNR	**S**ignal-to-**N**oise **R**atio

SONET	**S**ynchronous **O**ptical **N**etwork
WDM	**W**avelength-**D**ivision **M**ultiplexing
WSS	**W**avelength **S**elective **S**witch

List of Symbols

A	Blocking amplitude
b	Number of input fibers per bank
B_o	–3 dB bandwidth of the optical filters
B_{OSA}	Bandwidth of the optical spectrum analyzer
B_{ref}	Reference optical bandwidth
B_{RRC}	Bandwidth of the RRC filter
B_{sim}	Simulation bandwidth
BW_{mdB}	$-m$ dB bandwidth of the superGaussian filter
D	ROADM degree
D_L	Size of large port count WSS
D_S	Size of small port count WSS
$E_{in}(t)$	Photodetector incident electrical field
$E_{LO}(t)$	Local oscillator electric field
$E_r(t)$	Received signal electric field
f_d	Number of fibers per degree
f_{intra}	Number of intra-node fibers
G	Optical amplifier gain
G_{add}	Add structure optical amplifier gain
G_{drop_1}	First drop structure optical amplifier gain
G_{drop_2}	Second drop structure optical amplifier gain
G_{inter}	Inter subsystems optical amplifier gain
G_{pre}	Optical pre-amplifier gain
G_{post}	Optical post-amplifier gain
$H_{RRC}(f)$	Transfer function of the RRC filter
$H_p(f)$	Transfer function of optical passband filter
$H_b(f)$	Transfer function of optical stopband filter
$I_i(t)$	Detected signal in-phase component
$I_p(t)$	Current produced by the received optical signal
$I_q(t)$	Detected signal quadrature component
IL	Insertion loss

IL_{excess}	Excess insertion loss
$IL_{splitter}$	Optical splitter insertion loss
IL_{WSS}	WSS insertion loss
K	ROADM scale
M	Modulation order format
N_a	Number of samples per symbol
N_{ASE}	PSD of ASE noise
N_b	Number of transmitted bits
N_e	Number of counted bit errors
N_{MC}	Number of generated sample functions
N_R	Number of traversed ROADMs
N_s	Number of simulated symbols
N_{SUB}	Number of subsystems in a interconnected architecture
N_{inter}	Number of WSSs needed to interconnect the subsystems
NX_{FLEX}	Number of in-band crosstalk terms generated inside the FLEX architecture
NX_{inter_A}	Number of in-band crosstalk terms generated inside the interconnected A architecture
NX_{inter_B}	Number of in-band crosstalk terms generated inside the interconnected B architecture
NX_{prim}	Number of primary subsystem interferers
NX_{adj}	Number of adjacent subsystems interferers
P_{ASE}	Power of the ASE noise
$P_{ASE,\,add}$	Power of the ASE noise generated in the add structure optical amplifier
$P_{ASE,\,drop1}$	Power of the ASE noise generated in the drop structure first optical amplifier
$P_{ASE,\,drop2}$	Power of the ASE noise generated in the drop structure second optical amplifier
$P_{ASE,\,inter}$	Power of the ASE noise generated in the inter subsystems optical amplifier
$P_{ASE,\,pre}$	Power of the ASE noise generated in optical pre-amplifier
$P_{ASE,\,post}$	Power of the ASE noise generated in optical post-amplifier
P_{filt}	Filtering penalty
P_{in}	Optical signal power at the photodetector input
P_{LO}	Local oscillator power
P_{out}	Signal power at the optical amplifier output

P_{Tx}	Transmitted signal power
P_{xtalk}	Inter carrier crosstalk penalty
ρ	RRC filter roll-off factor
$R_{b,\,i}$	Information bit rate
R_s	Symbol rate
SM	Safety margin of the optical network
T	Total number of transponders
T_{bank}	Number of transponders per bank
W_{conv}	Number of WSS required to build a conventional architecture
W_{inter}	Total number of WSSs required to build an interconnected architecture
W_B	Number of waveband groups in the FLEX architecture
Δf	WDM channel spacing

Chapter 1

Introduction

The Internet traffic is still nowadays in an exponential growth trend, mainly due to the increase in the number of devices connected worldwide, cloud services (many network functionalities are being implemented in the cloud) and video-on-demand [1]. Over the previous 20 years, the Internet Protocol (IP) traffic has grown by a factor of 10^4 worldwide and the capacity of wavelength-division multiplexed (WDM) fiber-optic communication systems transporting the IP traffic across the globe has grown by a factor of 1000 [2]. These numbers reflect the enormous growth in the demand for data traffic and its support through information and communications technologies [2]. Fiber optic network technologies are in continuous development in order to be able to accommodate this data traffic growth and technologies such as dense wavelength multiplexing (DWDM) [3], flexible grid [4], high order modulation formats [5], coherent detection and advanced digital signal processing (DSP) [6] are still necessary today in order to accomplish the enormous transport capacity needed by the overall telecommunications infrastructure.

The optical transport networks (OTN) are now evolving using the concept of elastic optical network (EON) that take advantage of the variable bandwidth wavelength selective switches (WSS) inside the reconfigurable optical add/drop multiplexers (ROADMs) and also the improved routing and spectrum assignment algorithms.

As the ROADMs are upgraded, the optical network physical layer limitations also require a deep study because the optical signal, along its light-path, passes through optical fiber links as well as many network components inside the ROADMs, such as WSSs, optical switches, (de)multiplexers or splitters/couplers. Consequently, all losses, noises and interferences arising along the light-path will degrade the signal transmission along the optical network.

1.1 Road to future large-scale ROADMs

Optical networks have and continue to evolve in order to accommodate all the traffic that flows through it. Nowadays, the traffic requires a flexible and dynamic network, since it is primarily based on IP packets [7].

Increased demand for traffic also leads to the need for higher bit rates per optical channel in the fiber. The widely used fixed grid, standardized in the 1990s, with an optical channel width of 50 GHz and even

with complex modulation schemes, no longer complies with above 200 Gb/s per channel. Therefore, a new grid has been standardized, the flexible grid [4].

In this case, the optical channel width can be modified accordingly with the network requirements, leading to optical channels with a larger bandwidth and higher granularity, so that they can support higher bit rates than the ones supported by the fixed grid. The International Telecommunication Union (ITU) proposed a grid granularity of 6.25 GHz with a minimum frequency slot of 12.5 GHz [8], [9]. For example, in the flexible grid, we can have optical channels with 37.5 GHz or 75 GHz bandwidth instead of the most common ones with 50 GHz and 100 GHz spacings. Recent studies have shown that a grid granularity of 6.25 GHz gives a greater freedom to adjust the gap between optical channels and avoid portions of unused spectrum, hence, increasing network efficiency [10], [11].

Hence, given the increased traffic demand and the introduction of a more versatile optical network, all the optical network components and ROADM nodes must be developed to address these new characteristics. The key improvements in the ROADM nodes are seen in the add/drop architectures, with the introduction of colorless, directionless, contentionless and gridless features [7].

With the major increase in traffic, we are now heading to large-scale ROADMs that become somewhat expensive with the currently available components. Nowadays, since the maximum WSS dimension is 1×35, a larger WSS dimension, probably needed in large-sale ROADMs, could only be implemented by cascading several WSS, which has high insertion losses and a high cost [12]. New ROADM architectures have been proposed in order to reduce the need for much more expensive components and therefore make the large-scale ROADMs more economic to manufacture [12], [13].

In this work, different proposed express architectures, named FLEX [13], interconnected A and B [14] and the bank-based add/drop (A/D) structure [14], are studied and compared in terms of hardware cost reduction and in-band crosstalk generation. Then, the performance of an optical network based on interconnected A and bank-based A/D architecture ROADM nodes is assessed using simulation, considering the transmission of 200 Gb/s 16 quadrature amplitude modulation (QAM) and 250 Gb/s 32QAM signals, regarding the impact of the physical layer impairments, optical filters cascading, noise from amplification and in-band crosstalk.

1.2 Dissertation organization

This dissertation is organized as follows. Chapter 2 is focused on the study of ROADMs nodes and its components. We present a summary of the evolution of its characteristics and main architectures until

today and study new proposals for the architectures of express and add/drop structures of large-scale ROADMs. A hardware cost comparison between each architecture is also performed.

Chapter 3 is dedicated to study the in-band crosstalk generated inside large-scale ROADM architectures in the express structure and A/D structure. We also quantify the number of interferers in each large-scale ROADM architecture studied and perform a comparison with the conventional node architectures.

In Chapter 4, the optical network simulator developed in MATLAB is described, from the modeling of the optical components and corresponding assumptions, to the optical signals generation and also to the metrics used to evaluate the network performance.

In Chapter 5, the performance and the maximum reach of an optical network impaired by optical filtering cascading, amplified spontaneous emission (ASE) noise and in-band crosstalk based on interconnected A ROADMs and bank-based A/D architectures is evaluated. The network models used in each study are also presented.

Chapter 6 summarizes the main conclusions of this dissertation and provides some study ideas for future work.

1.3 Dissertation main contributions

This work has the following main contributions:

- We show that large-scale ROADM architectures studied based on interconnected sub-systems, based on joining wavelengths and also based on A/D banks can bring a considerable cost reduction in terms of hardware components in comparison with the conventional ROADM architectures.
- We show that the large-scale ROADM architectures studied reduce the number of in-band crosstalk interferers in comparison to conventional architectures, being the interconnected A architecture the best in terms of in-band crosstalk reduction
- We assess the network performance and concluded that the main physical impairment along the ROADM cascade based on the interconnected A architecture that limits the network reach, is the accumulation of ASE noise along the primary signal optical path.

Chapter 2

ROADM fundamentals - components, properties and architectures

2.1 Introduction

In this chapter, we discuss and analyze the optical network nodes, nowadays known as ROADMs. We describe the evolution of ROADMs, from the first generation to the latest and current generation, in Section 2.2, and then, their main characteristics are presented in Section 2.3. Section 2.4 shows a little overview of the ROADM and its structure, the express and A/D structures. In Section 2.5, the components used (e.g. splitters/couplers, switches) in these nodes and their characteristics are presented. After that, in Section 2.6, the properties of ROADM nodes and their implementations are explained, from colorless (C) to colorless, directionless and contentionless (CDC) ROADMs. In Section 2.7, the conventional and recently proposed large-scale ROADM architectures with the main goal of reducing the hardware cost are presented: the interconnected ROADM subsystems, FLEX and bank-based A/D architectures. Their advantages, besides reducing hardware cost, and disadvantages are also discussed. Lastly, in Section 2.8, the conclusions of the chapter are presented.

2.2 ROADMs evolution

ROADMs arose from the need to make transport networks more flexible and reduce their implementation cost. Before its existence, in synchronous digital hierarchy (SDH) and synchronous optical (SONET) transport networks, WDM technology was used with the goal of increasing the network capacity. WDM technology was implemented mainly in networks with ring-topology, so that a fiber could carry more SONET or SDH channels [7]. In SDH/SONET networks, the signal was transmitted in the optical domain, but the signal processing, e.g. switching, in the node occurred in the electrical domain. These nodes were named optical cross connect (OXC) nodes with electrical switching. For the signal processing at these network nodes, a conversion of the signal from the optical to the electrical domain, and then again to the optical domain was required as shown in Fig. 2.1. This conversion is dependent on the bit-rate and signal format. These networks were named opaque networks [15].

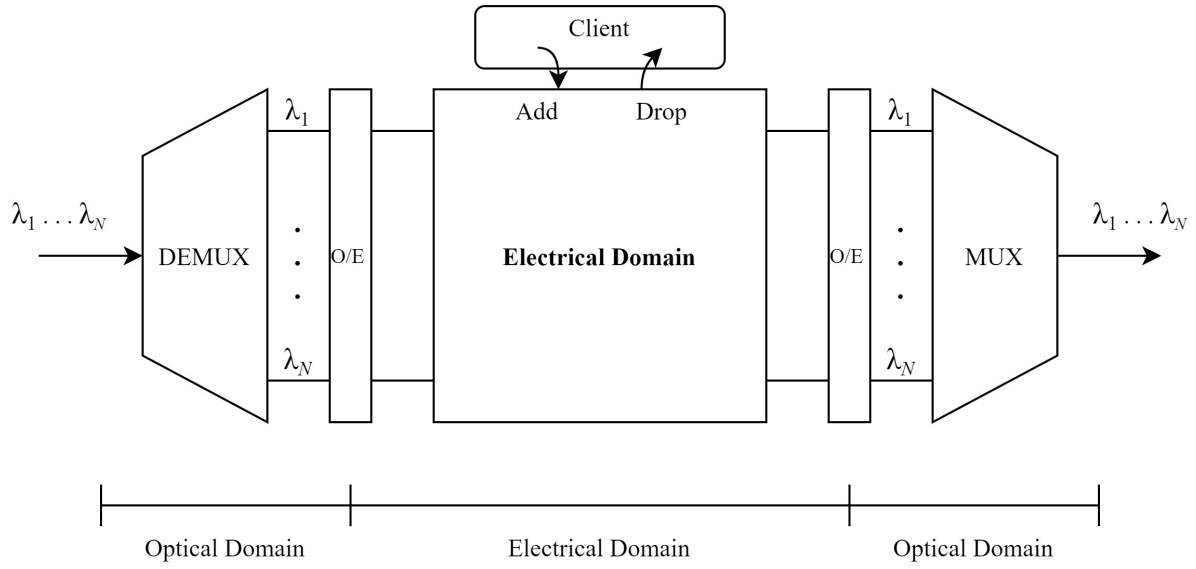

FIGURE 2.1: Node of an opaque optical network with O/E/O conversions.

As the volume of traffic increased and the type of traffic changed from voice signals to IP data signals, limitations due to processing times and bit rate began to appear in opaque networks, due to the need of optical-electrical-optical conversion. To support this traffic with more flexibility and capacity, it was necessary that all network nodes route the signal regardless of bit rates or signal format, taking only into account the signal wavelength. With the evolution of the optical technology, the term transparent arose, linked to the fact that optical networks do not need to convert the signal to the electrical domain to route the signal in the nodes, unlike in opaque networks (Fig. 2.2) [16]. Based on this concept, the second-generation of optical networks emerged. With this evolution, it became possible to pre-plan the network, using for example Routing and Wavelength Assignment (RWA) algorithms, that define which wavelengths are added/dropped on each node and which wavelengths pass through the node - express signals [7]. These network nodes became known as optical add/drop multiplexers (OADMs). They are similar to SDH or SONET add/drop multiplexers (ADM), except that they work in the optical domain.

The next improvement to network nodes was to increase network dynamism, i.e., being able to establish/release connections by software. It became possible to change the pre-planned network, allowing to reconfigure which wavelengths are dropped or added on each node dynamically accordingly to traffic demands. Derived from this reconfiguration property, these OADMs are called ROADMs [7].

ROADMs can have different degrees, associated with the number of fiber pairs (or directions) that are attached to the node. At the beginning of the implementation of these nodes, the typical network topology was the ring, Fig. 2.3 a), and therefore each node was served only by two fiber pairs (one for each

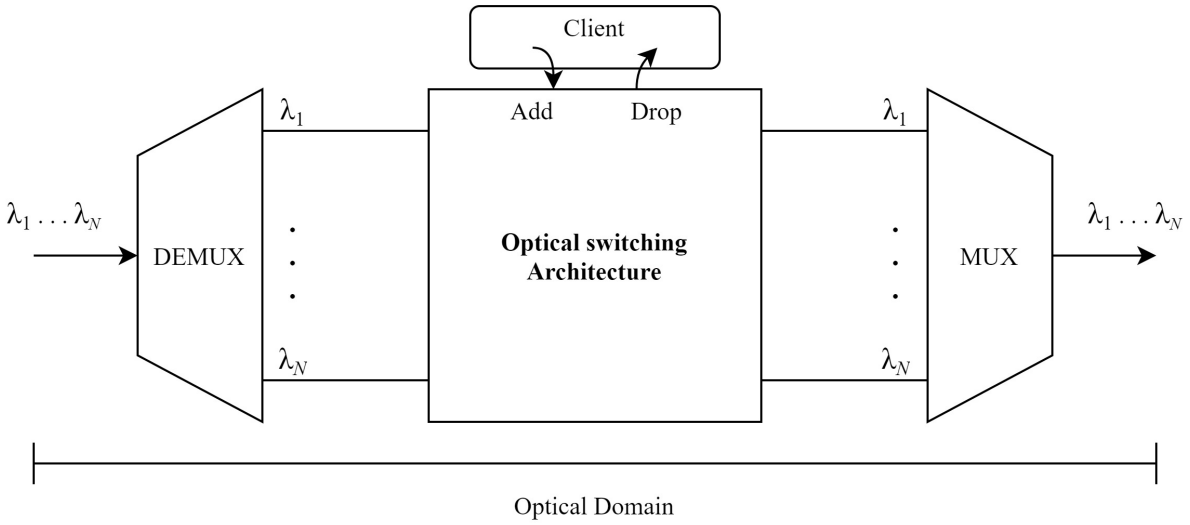

FIGURE 2.2: Node of the transparent optical network without O/E/O conversion.

direction). The nodes in this topology are known as 2-degree ROADMs [16]. As it became necessary to link various ring networks together to increase network connectivity, *D*-degree ROADMs emerged served by *D* fiber pairs, as many as the number of nodes attached directly to the ROADM, and the network topology evolved to more complex scenarios, such as the one shown in Fig. 2.3 b).

2.3 ROADM characteristics

The ROADMs main features are connectivity, scalability, A/D capability, cascadeability and possibility of channel monitoring, which are detailed below [17]:

- Connectivity : The basic function of ROADMs is to provide connectivity between network nodes. They can be full-ROADMs, if they have no wavelength restrictions or partial-ROADMs, if they can only process certain wavelengths.

- Scalability: ROADMs can be scalable, if the degree/direction of the node can be increased, while the ROADM is working on the network, hence, avoiding traffic congestion. Networks that have WSS based ROADMs have the advantage of being easily scalable over OXCs with electrical switching based networks.

- Add/drop capability: a ROADM can have a 100% A/D ratio, if it can A/D all the wavelengths from all directions.

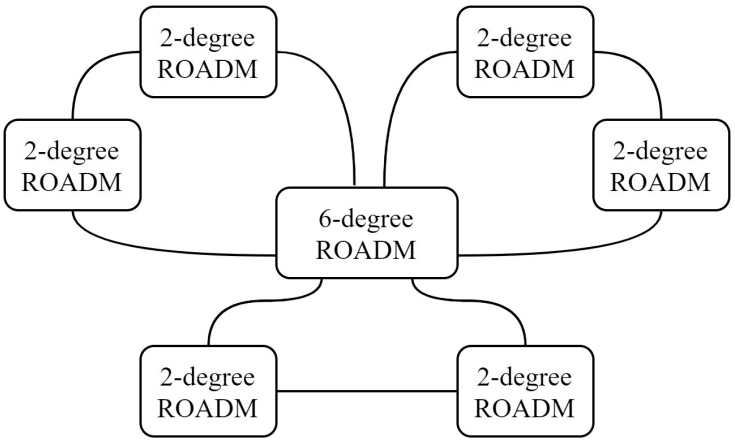

a) Multi-ring topology

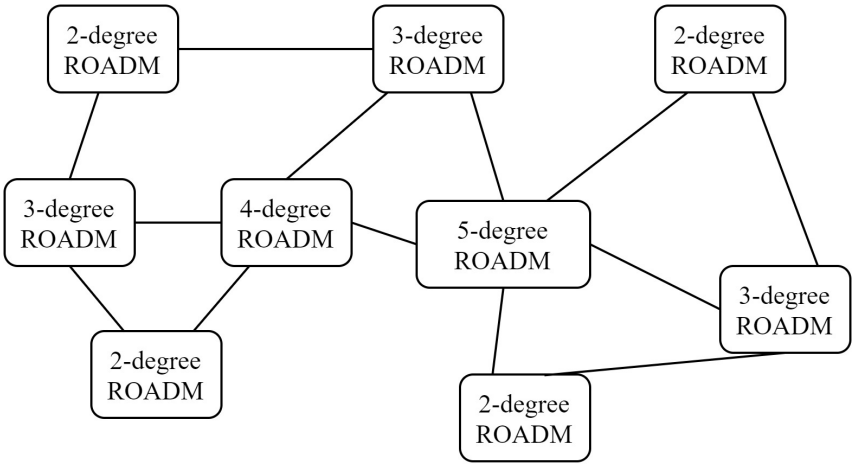

b) Mesh topology

FIGURE 2.3: Different ROADM network topologies.

- Cascadeability: When the optical signal passes through several cascaded ROADMs, it may suffer from enhanced inter-symbolic interference (ISI) and signal degradation by the optical filtering bandwidth narrowing, crosstalk from poor component isolation, and noise addition by the optical amplifiers. These penalties become larger as the number of ROADMs the signal passes through increases, thus limiting the maximum number of cascaded ROADM nodes in a network [17].

- Channel monitoring: The signal inside the ROADM can be monitored so that the power of each channel can be adjusted in order to have a uniform power per channel at the output of the ROADM.

In order to build a flexible network and increase its reconfigurability as well as its flexibility, technology developments have been made and the following features are now available on ROADMs [4]:

- Gridless property: usually, a standard frequency fixed grid with 50 GHz spacing between channels is typically used for WDM transmission [4]. This fixed grid does not allow efficient use of the available spectrum, which led to the appearance of the flexible grid. With this grid, it is possible to adjust the frequency spacing between channels accordingly with network requirements. Instead of the traditional 50 GHz spacing, channel spacings of 25 GHz or 37.5 GHz can be used, for example. This concept allows to save spectrum, as can be seen in Fig. 2.4, where the transmission of 4 quadrature phase-shift keying (QPSK) channels with 40 Gb/s using the fixed grid and also the flexible grid, is schematically represented. As can be observed, a spectral saving of 50 GHz is attained with the flexible grid.

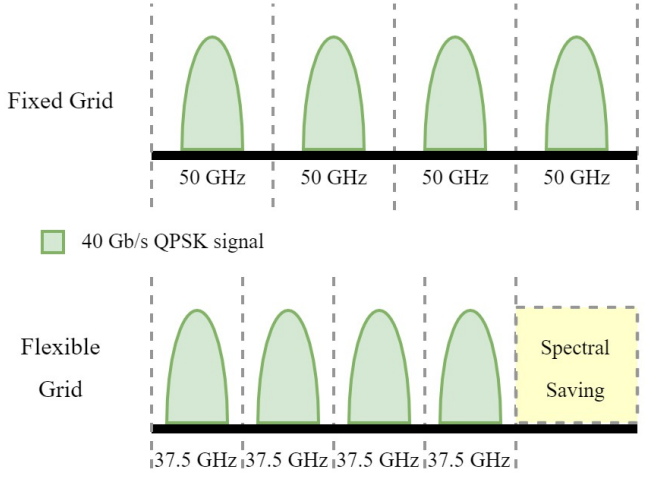

FIGURE 2.4: Comparison between fixed grid channels and flexible grid channels.

- Flexible transponders that increase spectral efficiency: Transponders that must support any type of traffic (e.g. Ethernet, SDH), bit rate (e.g. 10 Gb/s, 40 Gb/s, 100 Gb/s) and modulation format (e.g. M-QAM and QPSK).

- Switching speed: as nodes become more flexible and reconfigurable, a high switching speed is required. The speed is measured by the time the 2×2 switching element takes to change from a cross state to a bar state. These states of a 2×2 switching element are illustrated in Fig. 2.5. The micro-electro-mechanical switching systems (MEMS) are widely used in the fixed grid [18], with switching speeds less than a millisecond. The technology Liquid Crystal on Silicon (LCoS) that has a switching speed in the order of microseconds, is more suitable to work with the flexible grid [19].

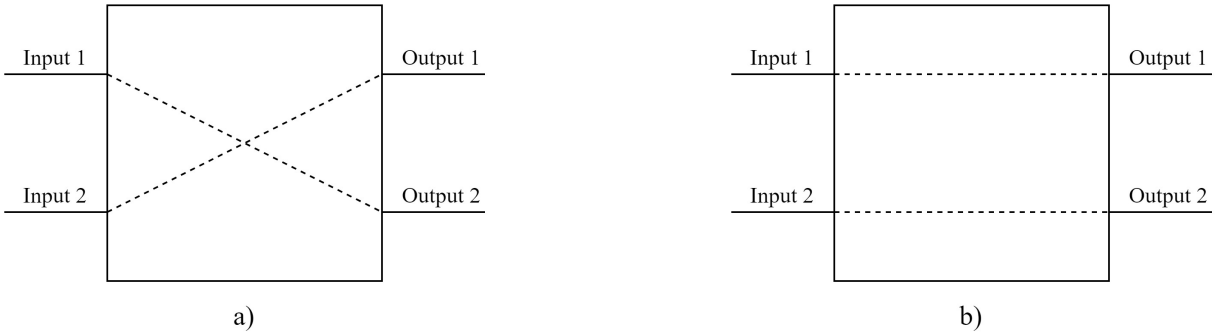

FIGURE 2.5: Cross (a) and bar (b) states of a 2×2 switching element.

2.4 Overview of the ROADM structure

A ROADM is composed by two structures: the A/D structure and the express structure, as shown in Fig. 2.6.

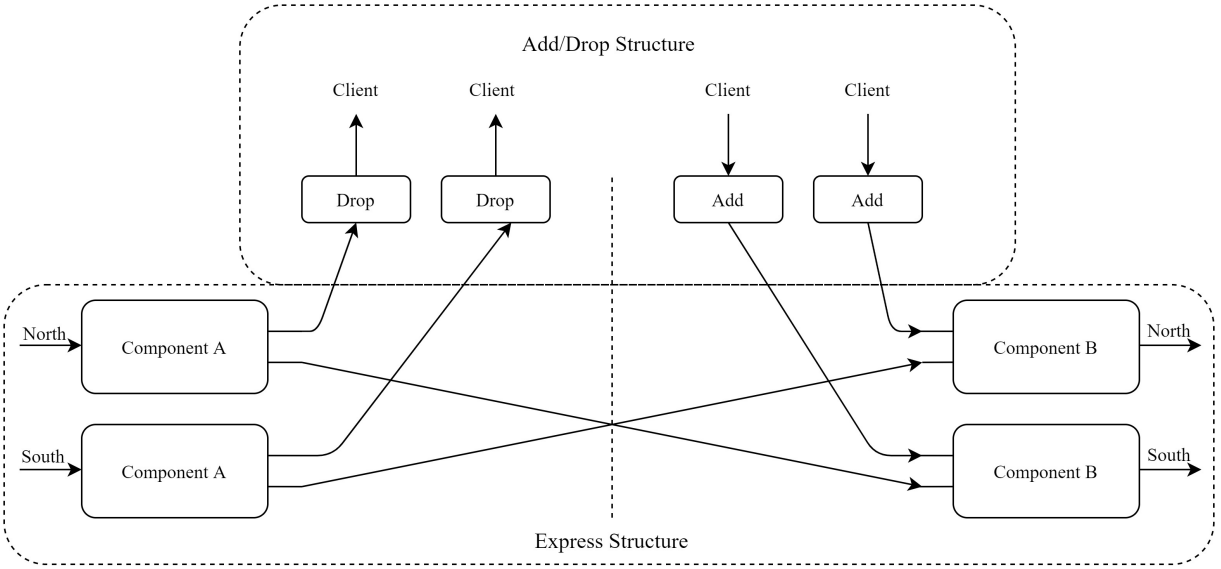

FIGURE 2.6: 2-degree ROADM structures schematic.

The express structure is responsible for routing the wavelengths to another ROADM direction. These structures can have different architectures, like the Broadcast and Select (B&S) or Route and Select (R&S) which are described in Section 2.7.

The A/D structure, as the name implies, is where a wavelength can be dropped or added to the optical network. These structures can be based on multicast switches (MCSs) or WSSs. These components will be explained with more detail in the next section.

2.5 ROADM components

The evolution of ROADMs components has been a key factor for the nodes being able to support the increase of data traffic and also being able to increase network flexibility. The main used components in a ROADM are [17], [18]:

- Optical coupler/splitter: an $N\times1$ coupler receives N optical signals and couples them into one output, as depicted in Fig. 2.7 a). An $1\times N$ optical splitter receives an optical signal and splits its signal power equally into N outputs, as we can see in Fig. 2.7 b). By assembling the two previous components together, it is possible to form an $N\times N$ splitter/coupler, as depicted in Fig. 2.7 c). In this way, it is possible to have many input signals coupled/splitted to many outputs in a static way.

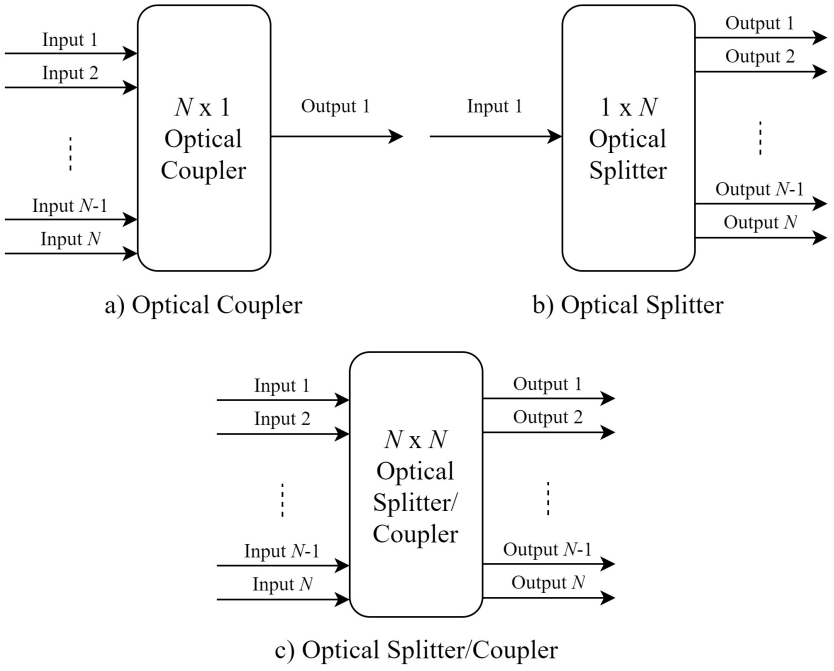

FIGURE 2.7: Optical coupler and splitter: (a) $N\times1$ optical coupler, (b) $1\times N$ optical splitter and (c) $N\times N$ optical splitter/coupler.

- Wavelength splitter/coupler: unlike the previous component, this component receives a WDM signal and demultiplexes it, sending each wavelength to a specific output port as shown schematically in Fig. 2.8. The wavelength splitter used in the opposite direction works as a $N\times1$ wavelength coupler.

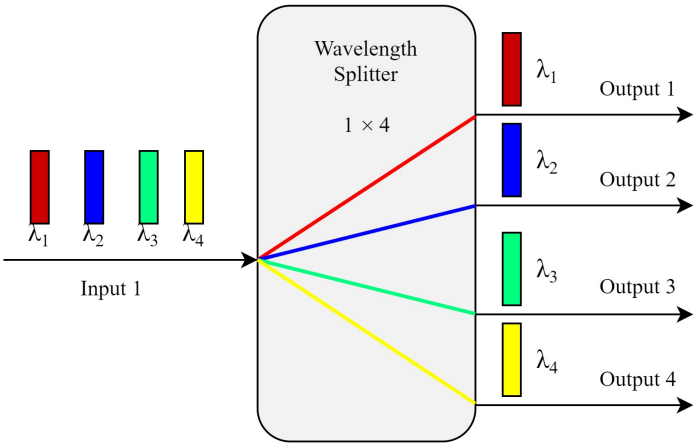

FIGURE 2.8: 1×4 wavelength splitter example.

- Optical switch: it is responsible for routing the optical signal transparently (i.e. based only on the signal wavelength). The most widely used technology is MEMS, which consists of micro-mirrors that route the signal through the optical switch [20]. This component can introduce several physical impairments on the routed signals, such as insertion losses and crosstalk [18].

- Wavelength selective switches (WSSs): they are a combination of optical switches with wavelength (de)multiplexers, being the most important component in today's ROADMs. Nowadays, LCoS is the chosen technology for its implementation [21], [22]. The typical size of an WSS is not higher than 1x35 [23]. There are three types of WSS-based structures:

  - 1×N WSS: one input with multiple wavelengths (WDM signal) and each one can be assigned to a selected output. In Fig. 2.9, an example of a 1×4 WSS is shown.

  - N×1 WSS: N input signals with multiple wavelengths (WDM signals) and the desired wavelengths are assigned to the output. An example of this component is the one in Fig. 2.9, but used in reverse.

  - N×M WSS: N input signals with multiple wavelengths and the desired wavelengths are assigned to the M desired outputs. Normally, N represents the number of ROADM directions (degree) and M is the number of connections with the A/D ports [24]. This WSS type has high manufacturing costs, but avoids wavelength contention and minimizes crosstalk [25].

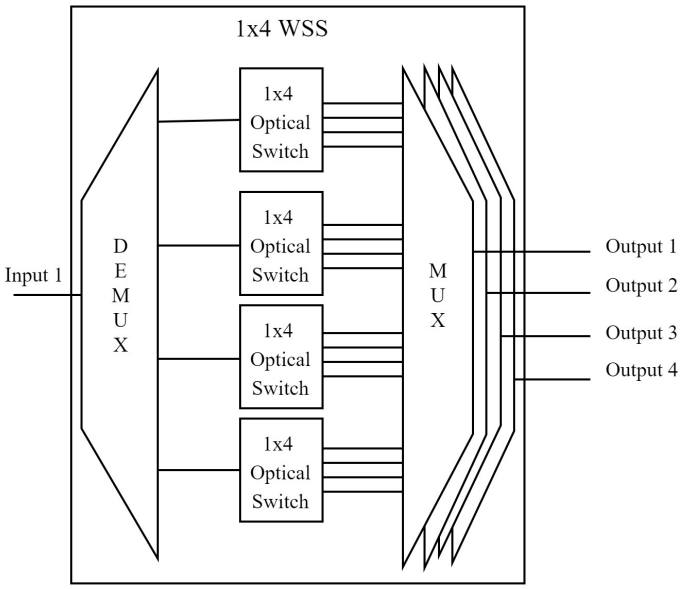

FIGURE 2.9: 1×4 WSS diagram.

- Multicast switches (MCSs): they are a cheaper alternative to $N \times N$ WSSs, implemented with optical splitters/couplers and switches, that are not wavelength selective [21]. In Fig. 2.10, a 2×8 MCS is represented. They are the most common structure in the current A/D structures [26]. Recently, A/D structures based on $N \times M$ WSSs are being investigated [27].

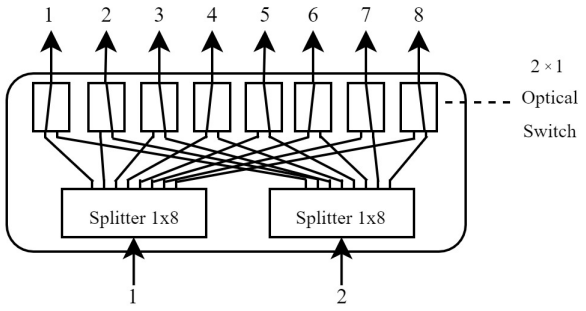

FIGURE 2.10: 2×8 MCS diagram.

2.6 ROADM properties

One important function of the ROADM nodes, in addition to routing optical signals, is adding or dropping wavelengths to the client networks [28]. The A/D structure properties of ROADMs have evolved as networks required greater flexibility.

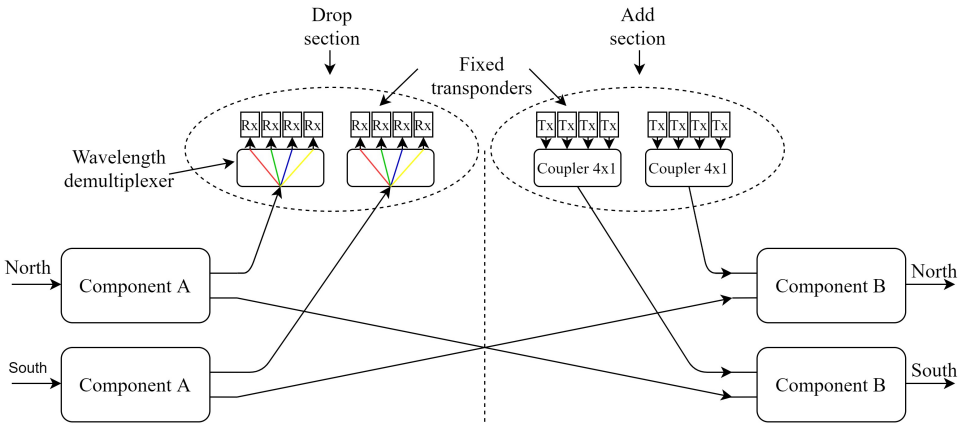

FIGURE 2.11: 2-degree colored ROADM.

In the first generation of A/D structures, the add section was implemented with optical couplers and the drop section with wavelength (de)multiplexers, as depicted in Fig. 2.11. Each port was set to operate in a certain fixed wavelength and therefore this structures were called colored [7]. Because of that, node transponders were, therefore, fixed to a wavelength in these structures, which quickly became a limitation.

2.6.1 Colorless ROADM

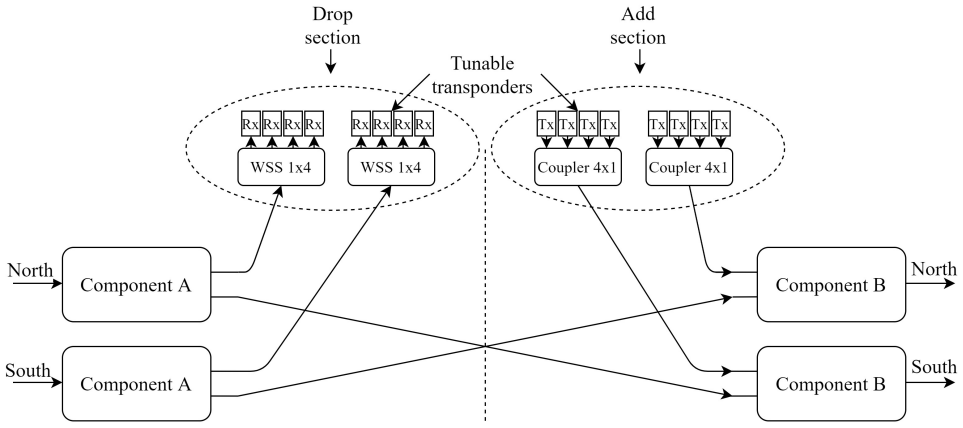

FIGURE 2.12: 2-degree colorless ROADM.

Technology evolved and transponders become tunable and the first WSSs emerged. By using these two components in A/D structure, the limitation imposed on the previous structure by wavelength demultiplexers and fixed transponders was overcome. It was then possible to A/D any wavelength in any port of the ROADM A/D structure. The ROADMs nodes with this property are now known as Colorless - C ROADMs and a 2-degree C ROADM is shown in Fig. 2.12. In this figure, each WDM signal has four

different wavelengths, tunable transponders and optical couplers are used in the add section, and 1×4 WSSs are used in the drop section.

2.6.2 Colorless and directionless ROADM

Another property of ROADM A/D structures arose with the need to redirect any input signal from one direction to any output direction, the so-called Directionless - D ROADMs. To be able to implement this property, more robust components were needed both in the ROADM inputs/outputs and in the A/D section.

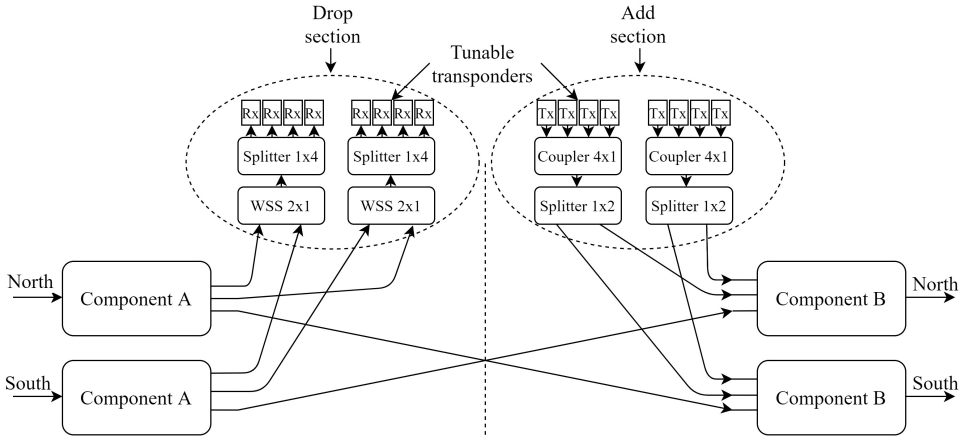

FIGURE 2.13: 2-degree colorless and directionless ROADM.

For example, considering a 2-degree D-ROADM, with A/D structures in all degrees/directions, the component A at each ROADM input will have a 1×3 dimension ($1 \times [2D - 1]$), being D the degree of the ROADM), as depicted in Fig. 2.13. The component A can be an optical splitter or WSS, depending on the ROADM architecture [28]. A ROADM with A/D structures in all directions was considered in Fig. 2.13, but this is only required if there is the need to add or drop two or more optical signals with the same wavelength in the same A/D section. Hence, the ROADM degree gives us the maximum number of A/D structures. Therefore, if there is the need to drop three optical signals with the same wavelength on 3-degree ROADMs with only two A/D structures, wavelength contention could occur inside the ROADM [29]. The wavelength contention can also appear when two signals, with equal wavelength, are dropped in the same drop structure.

2.6.3 Colorless, directionless and contentionless ROADM

In order to avoid wavelength contention inside the ROADMs, the A/D structures must be contentionless. A full-ROADM, as defined in section 2.3, must be colorless, directionless and contentionless - CDC ROADM.

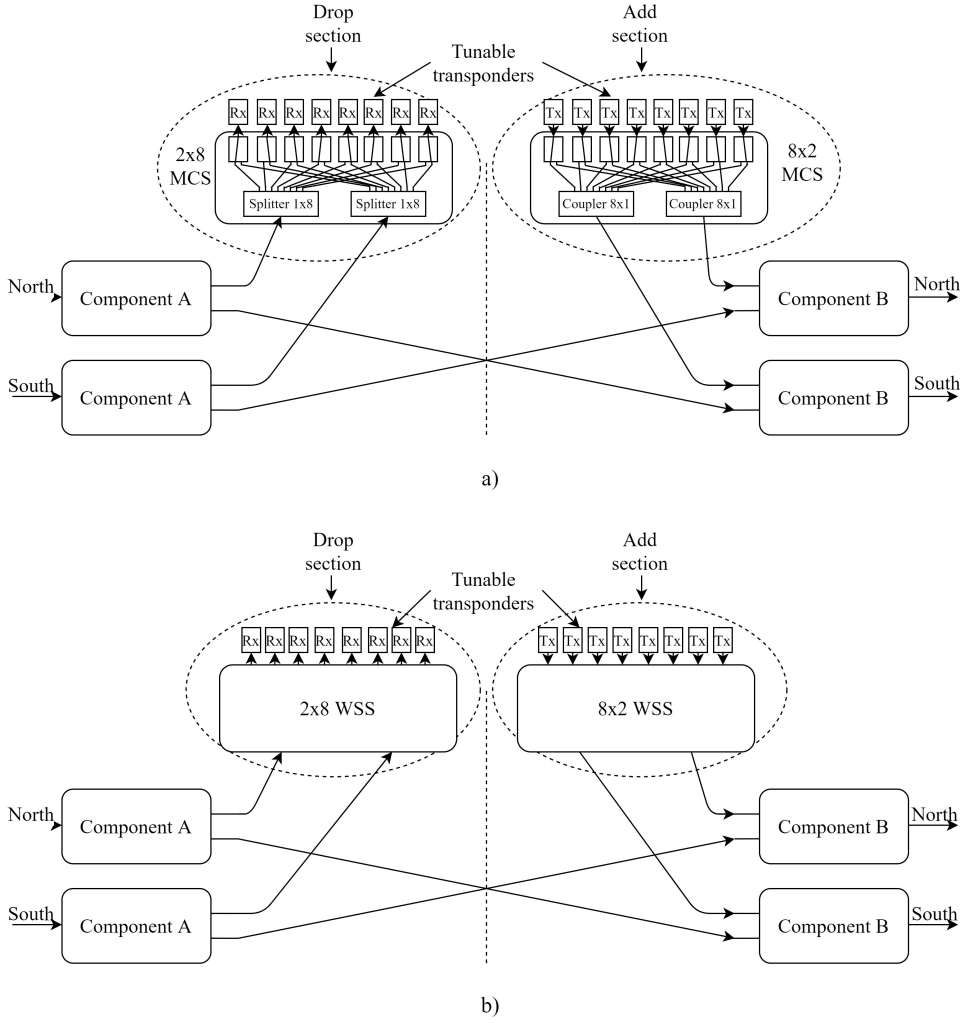

FIGURE 2.14: 2-degree colorless, directionless and contentionless (CDC) ROADM implemented with (a) 2×8 MCSs and (b) 2×8 WSS.

Today, the CDC ROADMs A/D structures are usually build with MCS [26], like in Fig. 2.14 a), or with $N \times M$ WSS [30], [31], as shown in Fig. 2.14 b) with 2×8 WSSs, for a 2-degree ROADM. The MCSs are not selective in wavelength as WSSs, leading to ROADMs more vulnerable to in-band crosstalk [21].

Finally, the gridless property is also applied to flexible grid-based ROADMs structures [32], [33]. These ROADMs can adapt to network demands and routing, switching and adding/dropping any traffic that reaches the node.

2.7 ROADM architectures

2.7.1 Broadcast & Select and Route & Select architectures

The conventional ROADM architectures are the B&S and R&S [16]. These architectures have influence on the components used in ROADMs inputs and outputs.

In a conventional B&S architecture (Fig. 2.15), the optical input signal is sent to all ROADM degrees (outputs) via an optical splitter. Each output WSS then selects which wavelength to transmit.

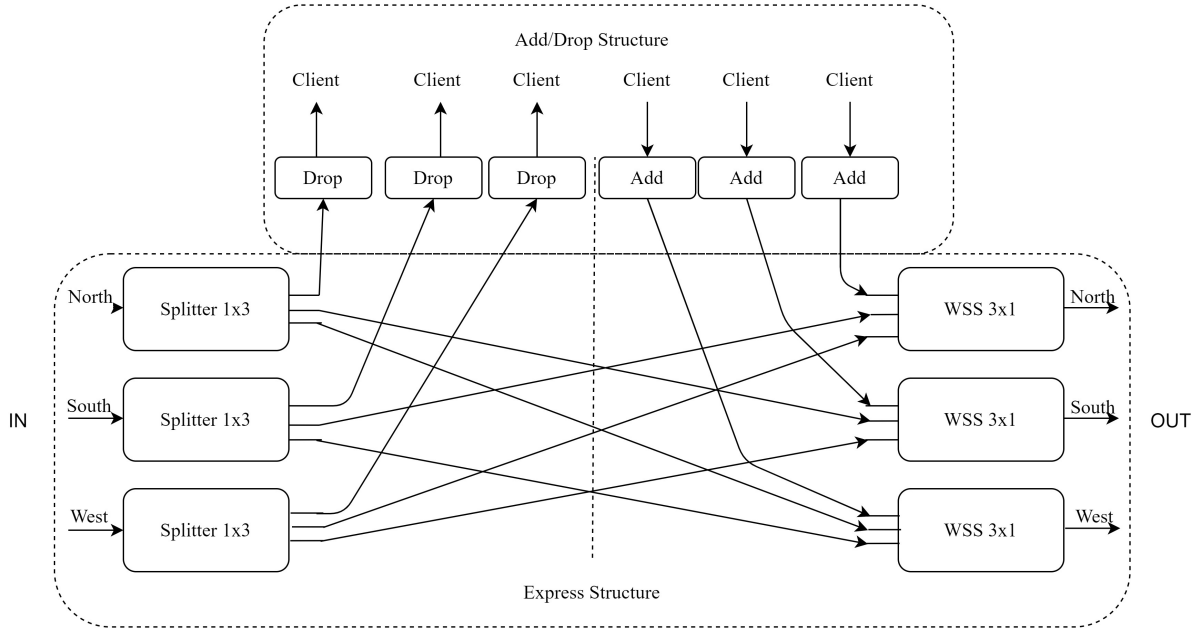

FIGURE 2.15: 3-degree ROADM B&S architecture.

In a conventional R&S architecture (Fig. 2.16), instead of broadcasting the optical input signal, there is a selection of the signal using a "route" WSS. Thus, there are two phases of wavelength selection, at the ROADM input and output. For this reason, the signal goes through one more filtering stage than in the conventional B&S architecture.

The conventional B&S architecture is better suited to ring networks when the optical signal goes through multiple nodes [34], because it has less filtering penalty than the conventional R&S architecture. However, the conventional R&S has one more WSS stage than the conventional B&S, so the cost of implementation becomes higher, although there is the advantage of a reduced crosstalk penalty.

For a ROADM node size (K) with multiple fibers per degree (f_D), where $K = f_D \times D$, or with a higher degree (e.g. $D \geq 16$), these architectures become somewhat expensive because of the WSS components available, as large port-count WSSs are difficult to manufacture and the highest port count commercially

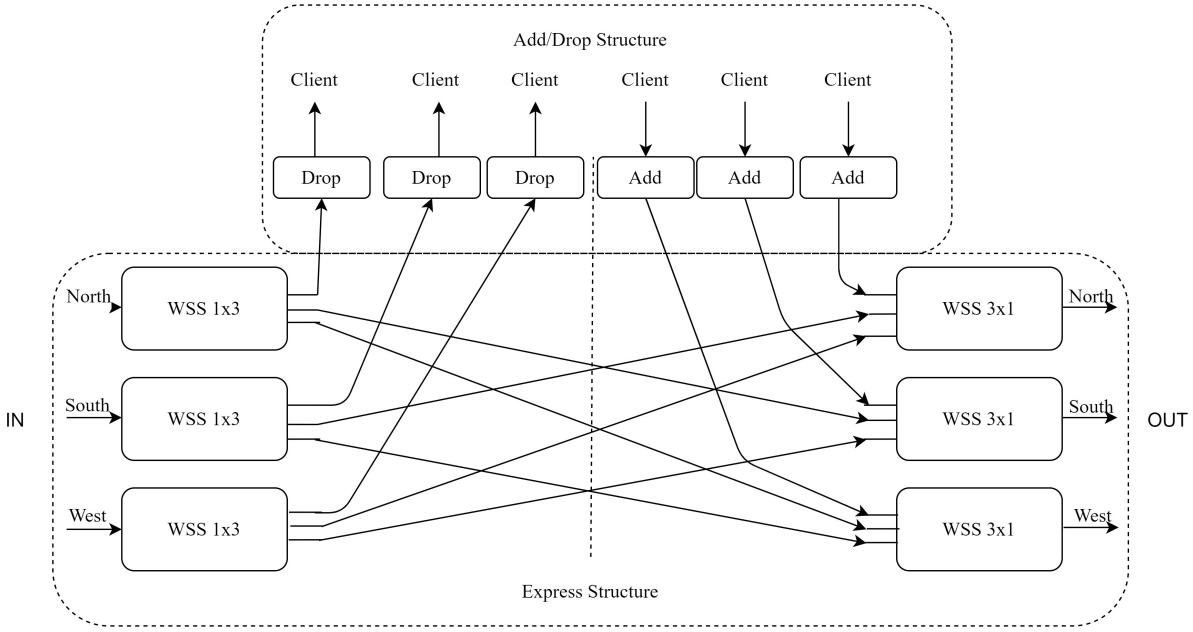

FIGURE 2.16: 3-degree ROADM R&S architecture.

available currently is 35 [23]. However, a large degree WSS, for the ROADM inputs or outputs, can be created by cascading multiple WSSs using an optical splitter, or a smaller WSS, that splits the signal to the n cascaded WSSs, as shown in Fig. 2.17 [13] .

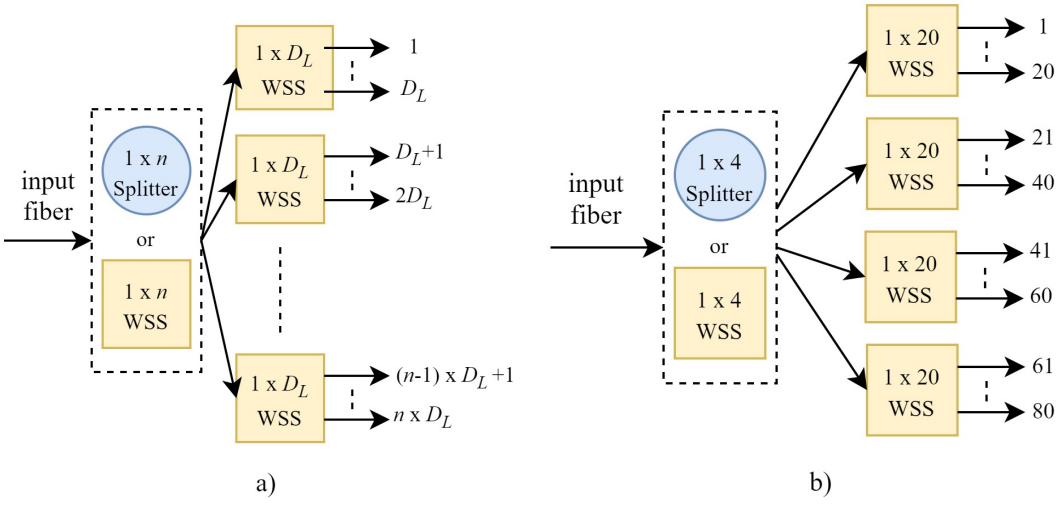

FIGURE 2.17: WSS cascading using a splitter or WSS (a) and an example 1×80 cascaded WSS (b), with $n = 4$ and $D_L = 20$.

The number of WSS, n, required to build a cascaded WSS, can be calculated using the following expression, where K is the ROADM size and D_L is the size of each WSS [12]:

$$n = \left\lceil \frac{K}{D_L} \right\rceil \tag{2.1}$$

The total number of WSS required to build all the cascaded WSSs for the two conventional architectures, since each input/output requires a WSS, is therefore:

$$W_{conv} = K \times n \text{ , for a B\&S} \tag{2.2}$$

$$W_{conv} = 2K \times n \text{ , for a R\&S} \tag{2.3}$$

In addition, K input or $2K$ input/output $1\times n$ optical splitters or WSS are required, respectively, for a B&S and a R&S node. For example, if we have a ROADM node whose physical degree (D) is 8 and each incoming/outgoing link has 10 fibers (f_D), the size of the ROADM (K) needed is 80×80. Since the typical port count WSS is 20 [12], using four 1×20 WSS and one 1×4 splitter, it is possible to build a 1×80 WSS with this solution, as shown in Fig 2.17b, with a total of 320 or 640 WSS and 80 or 160 1×4 splitters , for a B&S and R&S architecture, respectively. However, this approach results in a high number of WSS with large port count and a very high optical loss [12]. Another major limitation of this larger ROADMs is the nodes cost due to the large number of WSSs required. In Sections 2.7.2 and 2.7.3, alternative solutions for large ROADM architectures with the goal of reducing the WSSs size and number are presented.

2.7.2 Interconnected ROADM-subsystems architecture

A ROADM architecture named interconnected ROADM-subsystems has been proposed to reduce the WSSs number and size required to implement ROADMs with larger dimension [12], [14], [35]. This proposed architecture is shown in Fig. 2.18. It consists of multiple interconnected small ROADM-subsystems, whose port count is much lower than the cascaded large port count WSS (D_L) used in conventional larger ROADMs. Each subsystem is a conventional ROADM architecture, be it a B&S or a R&S, but with smaller size ($D_S \times D_S$). In a later evolution, there is also the possibility to use $M \times M$ WSSs as subsystems [35]. The node has K pairs of inter-node fibers that connect the node to the other nodes in the optical network, and each subsystems has $2f_{intra}$ pairs of intra-node fibers that inter-connect adjacent subsystems, where f_{intra} denotes the number of fibers connected to an adjacent subsystem.

There are two possible implementations of this architecture. The first one, where the A/D fibers are placed outside the express part (architecture A), shown in Fig 2.19 a), and the second one where the signal A/D shares the routing capability of the express structure (architecture B), shown in Fig. 2.19 b) [14]. In

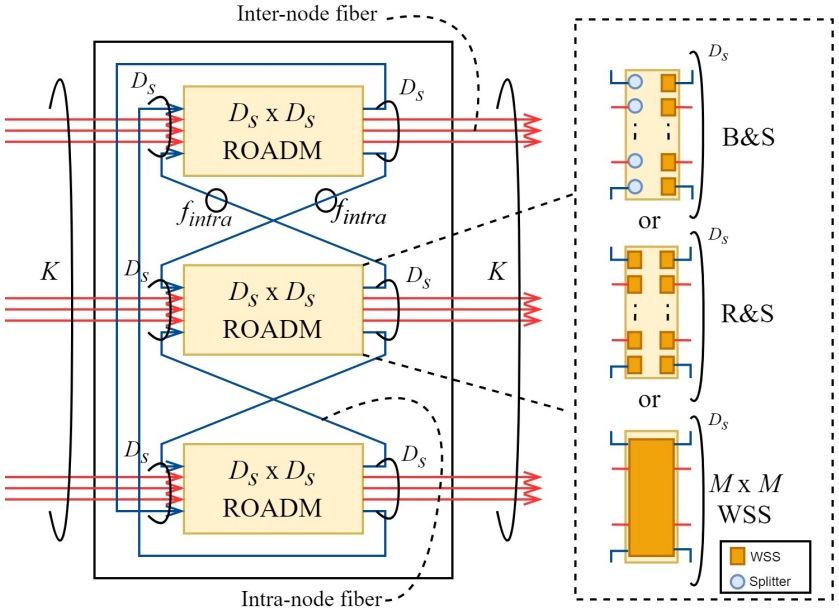

FIGURE 2.18: Interconnected ROADM-subsystems node architecture [12], [35].

the first one, the signal is sent to/from the A/D structure using a 1×2 splitter/coupler or WSS, before entering the ROADM through one port of one of the subsystems. The latter, has $(D_S - 2f_{intra})$ / 2 pairs of inter-node fibers, $2f_{intra}$ pairs of intra-node fibers, and $(D_S - 2f_{intra})$ / 2 pairs of A/D fibers in each sub-ROADM. The signal is sent to/from the A/D structure through the A/D fibers that are connected directly into the subsystems, thus being capable of using the routing capability. This port assignment can support any A/D ratio, since the number of A/D fibers is the same as the number of inter-node fibers. The total number of subsystems in an interconnected architecture node, N_{SUB}, is given by

$$N_{SUB_A} = \left\lceil \frac{K}{D_S - 2f_{intra}} \right\rceil \text{, for architecture A} \tag{2.4}$$

$$N_{SUB_B} = \left\lceil \frac{K + A/D_{fibers}}{D_S - 2f_{intra}} \right\rceil \text{, for architecture B} \tag{2.5}$$

To build a $K \times K$ ROADM, the number of WSSs needed to interconnect the subsystems together, N_{inter}, is given by:

$$N_{inter} = 2f_{intra} \cdot N_{SUB} \tag{2.6}$$

therefore, the total number of WSSs required to build an interconnected architecture, W_{inter}, is given by

$$W_{inter_A} = K + N_{inter} \text{ , for an architecture A B\&S} \tag{2.7}$$

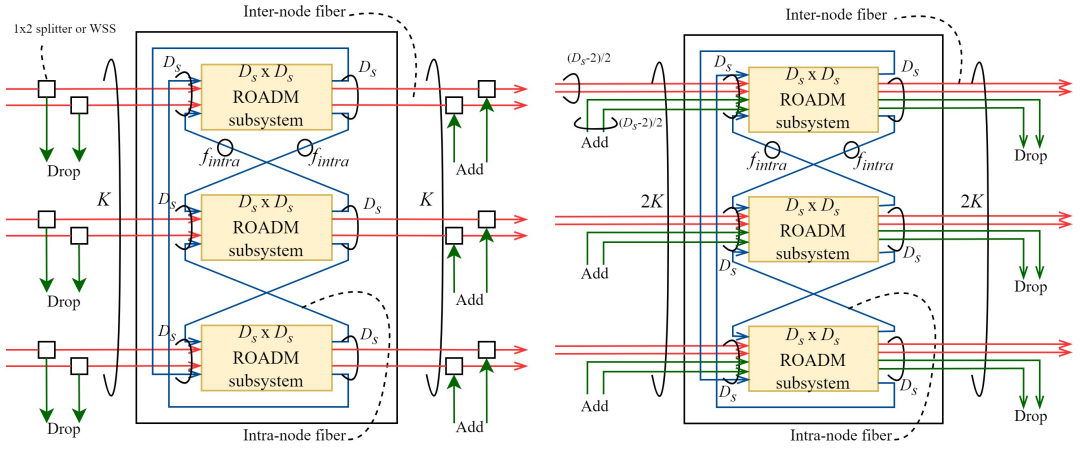

FIGURE 2.19: Two different interconnected architecture implementations: with A/D fibers outside the express structure (a) and with A/D fibers sharing the express structure routing capability (b).

$$W_{inter_A} = K + A/D_{fibers} + N_{inter} \text{ , for an architecture B B\&S} \tag{2.8}$$

$$W_{inter_B} = 2(K + N_{inter}) \text{ , for an architecture A R\&S} \tag{2.9}$$

$$W_{inter_B} = 2(K + A/D_{fibers} + N_{inter}) \text{ , for an architecture B R\&S} \tag{2.10}$$

As a numerical example, suppose that we have a node with 10 fibers per degree (f_D) and an 8-degree node (D), same as in Section 2.7.1, hence, the required size of the ROADM is 80×80. Let $D_L = 20$, $D_S = 9$ and $f_{intra} = 1$. Using Eqs. (2.4), (2.6) and (2.7), for a B&S architecture, the conventional node requires 320 1×20 WSSs, while the proposed node, with architecture A, needs only 104 1×9 WSSs. Also, using Eqs. (2.4), (2.6) and (2.9), in a R&S architecture, with the conventional architectures, 640 1×20 WSSs are required, while the proposed node, with architecture A, requires only 208 1×9 WSSs. The total number of WSSs used is approximately one third of the total used in a conventional node.

The major advantage of this structure, based on the above calculations, is that it is possible to build the same scale ROADM system using small port-count WSSs (D_s), which are more accessible and cheaper than larger ones [12]. Furthermore, by lowering the number of total WSSs used in the overall structure, the hardware cost is also reduced [12]. However, if a wavelength has to travel through multiple subsystems inside the interconnected architecture, the number of WSSs traversed increases, which can lead to enhanced physical layer impairments (PLIs), such as in-band crosstalk and distortion due to optical filtering in comparison with conventional ROADM architectures.

Lastly, by using $D_S \times D_S$ WSSs as subsystems, the number of required WSSs is even more reduced.

For example, instead of using 18 1×9 WSSs for a 9×9 subsystem, a single 9×9 WSS can be employed. Although being a more complex component, the ROADM sub-system with $D_S \times D_S$ WSSs becomes more affordable than using multiple $1 \times D_S$ WSSs, as concluded in [14].

2.7.3 FLEX - Flexible waveband architecture

Recently, another architecture, known as FLEX, has been proposed as a solution to deploy large-scale ROADMs with high port count WSSs [13]. In the FLEX architecture, the WDM signals from the several input directions are grouped together in W_B groups and then switched to one of the output fibers, as a whole signal. The bandwidth allocation is specific for each fiber, which enables a fully flexible reconfiguration in terms of paths carried, as shown in Fig. 2.20 [13].

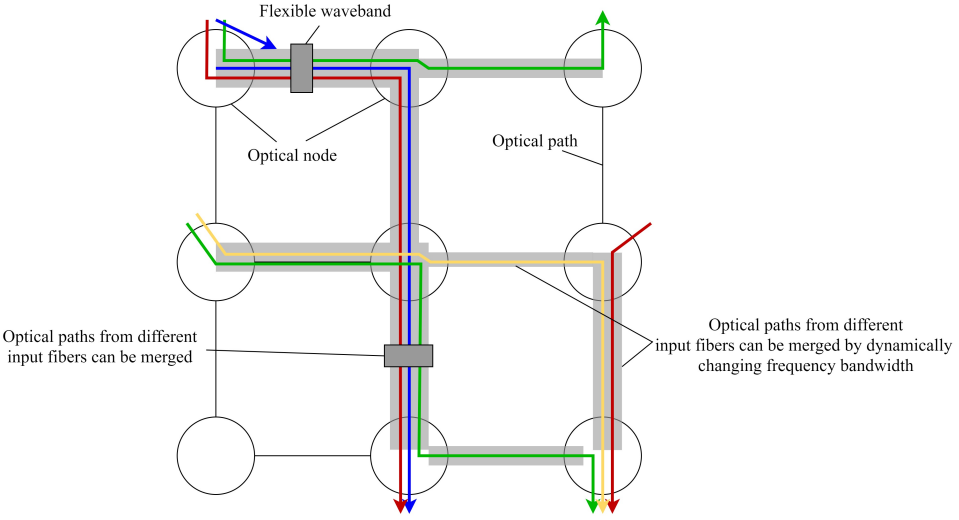

FIGURE 2.20: Example of wavebands routing in an optical network with FLEX ROADMs.

This architecture, as depicted in Fig. 2.21, is composed of $2K$ small-port-count flex-grid WSSs with dimension $1 \times W_B$ and W_B and $K \times K$ matrix switches, which are named as cost-effective delivery and coupling (DC) matrix switches [13]. In this figure, we considered that each ROADM degree (D) contains several optical fibers, represented by f_D. The A/D is performed through 1×2 WSSs that send the signal to the drop structure and receive the signal from the add structure to the output. The DC matrix switches, as depicted in Fig. 2.22, are composed by 1×K optical switches and K×1 optical couplers.

In order to group the signals together, the FLEX architecture is in a R&S configuration [13]. This allows the WSSs size to be smaller, compared to switching each channel independently, and because W_B can be much smaller than K, the hardware cost can be reduced [36]. However, the switching capability

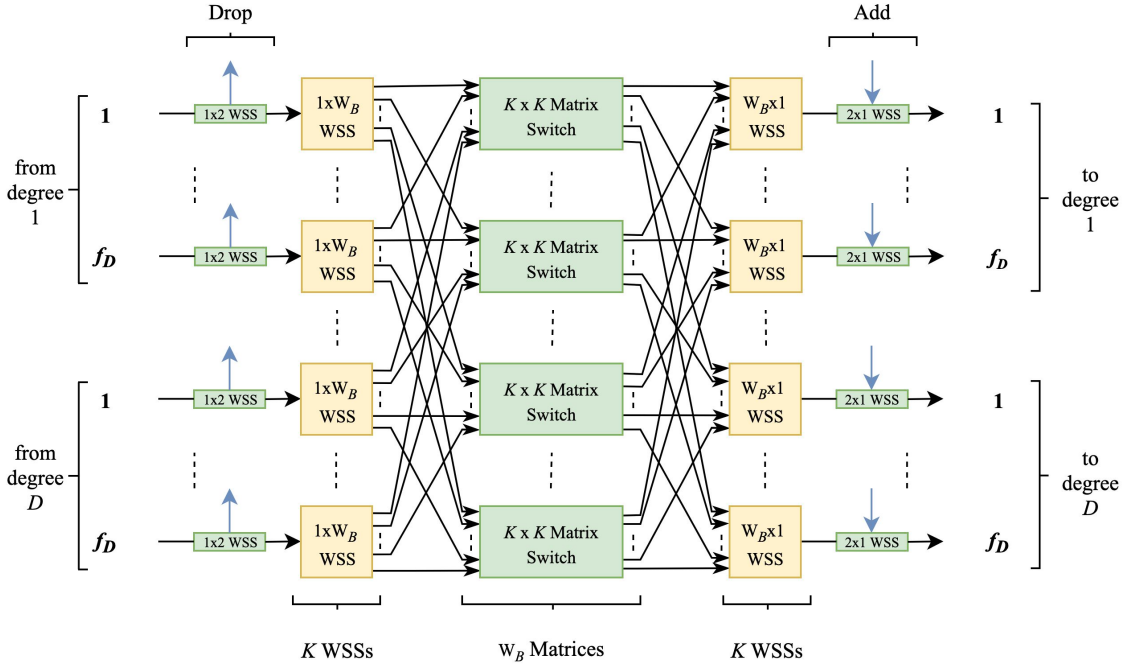

FIGURE 2.21: $K \times K$ ROADM with flexible waveband architecture.

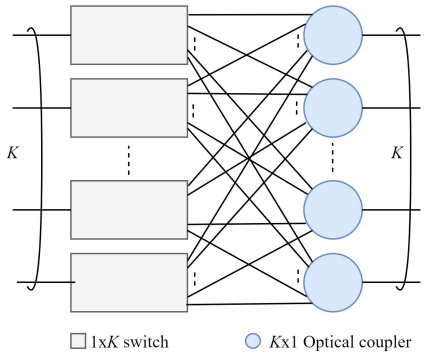

FIGURE 2.22: $K \times K$ DC-type Matrix Switch.

decreases because the switching occurs as an entire group, or band, and the number of bands switched simultaneously cannot be higher than W_B.

If we consider an 8-degree ROADM with 10 fiber links in each degree ($D = 8$, $f_D = 10$, $K = 80$), as in Sections 2.7.1 and 2.7.2, and 4 band groups ($W_B = 4$), the proposed node structure requires 160 1×4 WSSs and 4 80×80 matrices, while the conventional, using 1×20 WSSs, needs 320 or 640 WSSs, respectively, for a B&S and a R&S architecture. The total number of WSSs required by the FLEX structure is independent of the WSS size as in the conventional or interconnected architecture, and solely depends on the ROADM size (K).

2.7.4 Hardware cost comparison between interconnected, FLEX and conventional architectures

In this subsection, a comparison between the conventional and the two architectures types analyzed in Sections 2.7.2 and 2.7.3 is made, in terms of the number of WSSs required to achieve different ROADM sizes ($K \times K$), using different WSSs sizes. Today, WSS with sizes of 1×2, 1×4, 1×9, 1×20 or 1×35 are typically available [23]. For the FLEX architecture, we have considered the typical value $W_B = 4$ [13]. In Table 2.1, the expressions used for assessing this hardware cost comparison are shown.

	B&S	R&S
Conventional Node	$K \times \left\lceil \frac{K}{D_L} \right\rceil$	$2K \times \left\lceil \frac{K}{D_L} \right\rceil$
Inter-Connected A	$K + 2f_{intra} \left\lceil \frac{K}{D_S - 2f_{intra}} \right\rceil$	$2(K + 2f_{intra} \left\lceil \frac{K}{D_S - 2f_{intra}} \right\rceil)$
Inter-Connected B	$2K + 2f_{intra} \left\lceil \frac{2K}{D_S - 2f_{intra}} \right\rceil$	$2(2K + 2f_{intra} \left\lceil \frac{2K}{D_S - 2f_{intra}} \right\rceil)$
FLEX - Waveband	-	$2K$

TABLE 2.1: Comparison of the number of WSS required for each considered architecture.

In Figs. 2.23 a), b) and c), the number of WSSs required as a function of the WSS size is displayed for various ROADM sizes (K = 8, 40, 80) and for the 3 types of architectures considered in this work. Each architecture is considered for both B&S and R&S, except for the FLEX architecture which has only the R&S architecture option. Also, for the interconnected architecture, both A and B implementations are considered. For all the ROADM sizes, the number of WSSs is displayed in logarithmic scale.

For a small size 8×8 ROADM, the two new interconnected and FLEX architectures do not provide any advantages, regardless the number of WSSs, in comparison with the conventional architectures, as shown in Fig. 2.23 a). For either B&S or R&S, the interconnected architecture even requires more WSSs than the other two architectures. When the WSS size becomes larger than the ROADM size (K), the conventional R&S node requires a similar number of WSSs as the FLEX node, where the number of WSSs is independent of the WSS size.

For larger ROADM sizes, the two new architectures look more promising in reducing the number of WSS required, as shown in Figs. 2.23 b) and c). Notice that, in both figures, the interconnected A_{RS} line is superimposed with interconnected B_{BS}. For WSS sizes below 1×20, the interconnected architectures A, B and also the FLEX architecture, require quite less WSSs, 5 times less for K = 40 and 10 times less for K = 80, than the equivalent conventional nodes. For WSS sizes of 1×20 and 1×35, the WSSs number is not so drastically reduced (only 2 times less) but all the new architectures, except for the interconnected

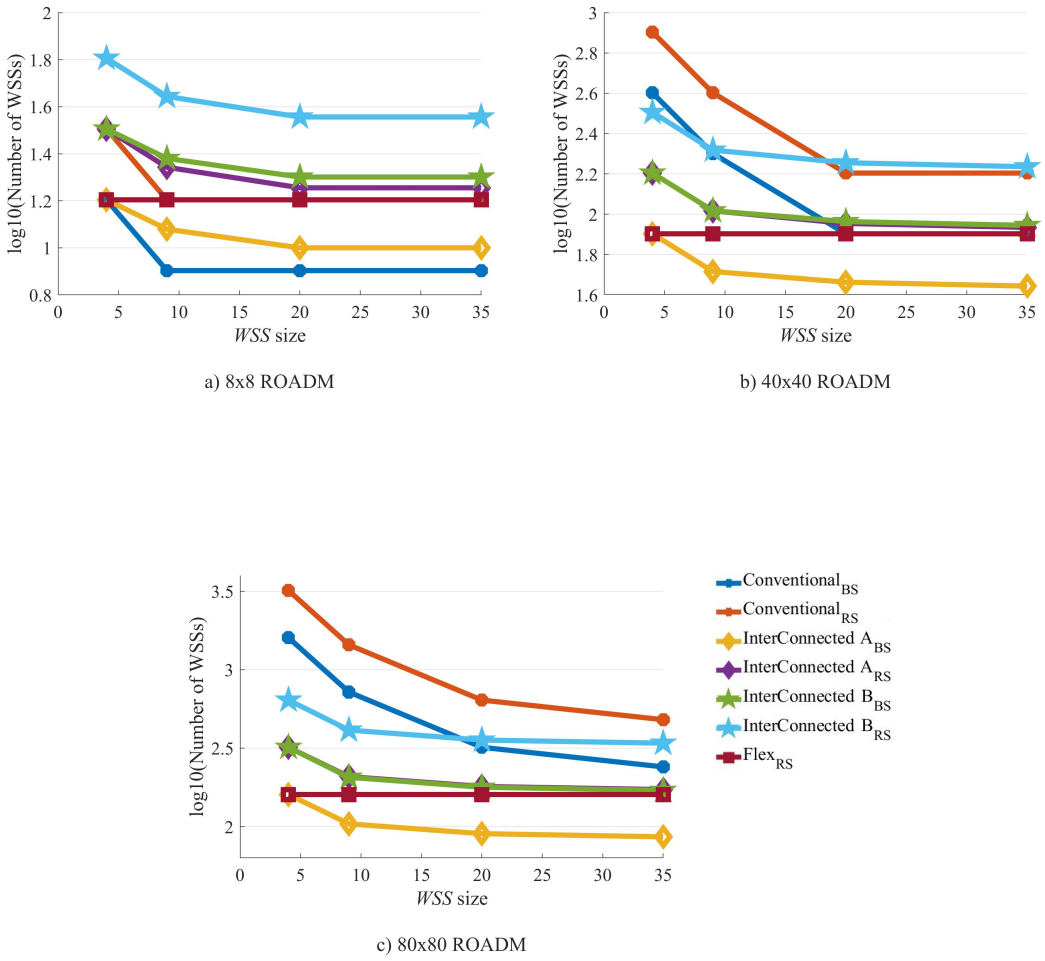

FIGURE 2.23: Number of required WSSs, as a function of the WSS size, for 8×8 a), 40×40 b) and 80×80 c) ROADMs, considering the 3 types of express architectures.

B R&S for $K = 40$, show less requirements in terms of the number of WSS needed in comparison with the conventional ones.

The FLEX node shows better results in terms of reducing the number of WSS needed than the interconnected R&S one, but as mentioned in Section 2.7.3, has the disadvantage that $K \times K$ matrix switches are needed, as many as the WSSs size. For the FLEX architecture, the decision on the WSS size relies on the number of bands that the node needs to group [13]. For the interconnected architecture, the ROADM becomes less expensive if smaller and more accessible WSSs like 1×9 are used instead of larger and more expensive 1×20 or 1×35 WSSs [12].

So, we can conclude that the two proposed architectures are a viable solution to the demands of the future optical networks based on large-scale ROADMs in terms of reducing the number of WSSs and therefore making larger ROADMs less expensive.

2.7.5 Bank-based A/D structure architecture

The previous new architectures were concerned with the design of the express structure of the ROADM, where the cost of the ROADM increases substantially as the ROADM degree is larger in order to accommodate higher traffic volumes. The A/D structure experiences also an increase in hardware count as these large-scale ROADMs are required in the network.

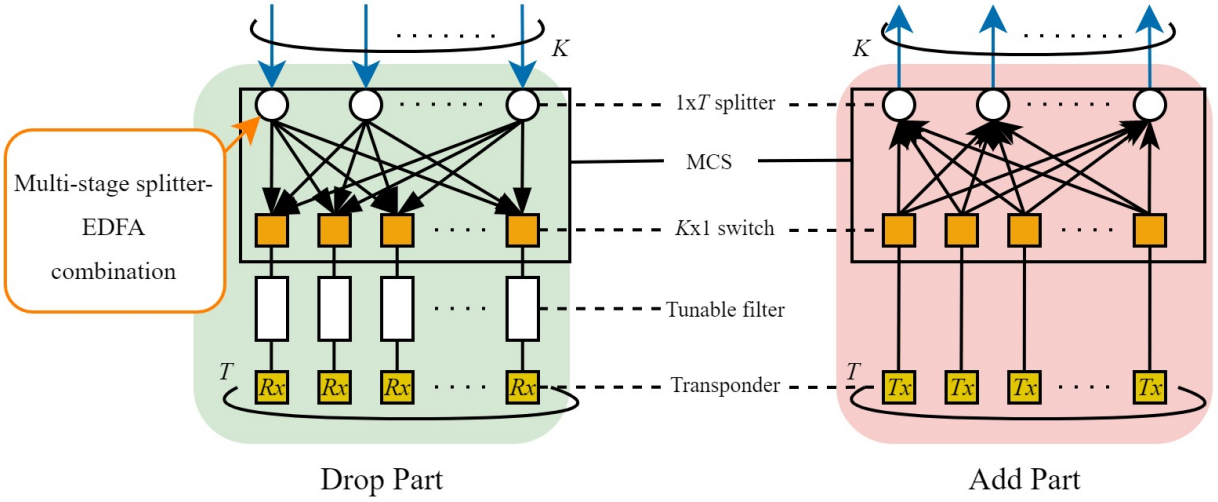

FIGURE 2.24: Conventional CDC A/D architecture using MCS.

In Fig. 2.24, an example of a conventional CDC A/D structure, using MCS, is depicted. In the drop part, the "drop fiber", represented by a blue arrow, is connected to a $1 \times T$ splitter that distributes the signal to T $K \times 1$ optical switches. Each optical switch is connected to a tunable filter that selects the desired channel to be dropped. In the add part, each transponder is connected to a $1 \times K$ optical switch that sends the added signal to a $T \times 1$ optical coupler that sends the signal through the "add fiber", represented by a blue arrow. When the number of transponders is large, a multi-stage splitter-erbium-doped fiber amplifier (EDFA) combination, such as the one depicted in Fig. 2.25 a), is required to compensate for the optical losses [14]. The switch dimension must also be increased, in comparison with today small scale ROADMs, so that each transponder can access any of the A/D fibers. Hence, this CDC A/D configuration is not particularly suitable for future, cost effectively, large-scale ROADMs [14].

Considering a ROADM scale of 8×8 and 96 channels per fiber, 154 transponders are required to accommodate a 20% A/D ratio. Since the required switch size is large, a multi-stage splitter-EDFA combination is required to compensate for the optical loss, as the one depicted in Fig. 2.25 b) using five 1×32 splitters. Each 1×8 and 1×32 splitter has approximately 11 dB and 19 dB insertion loss,

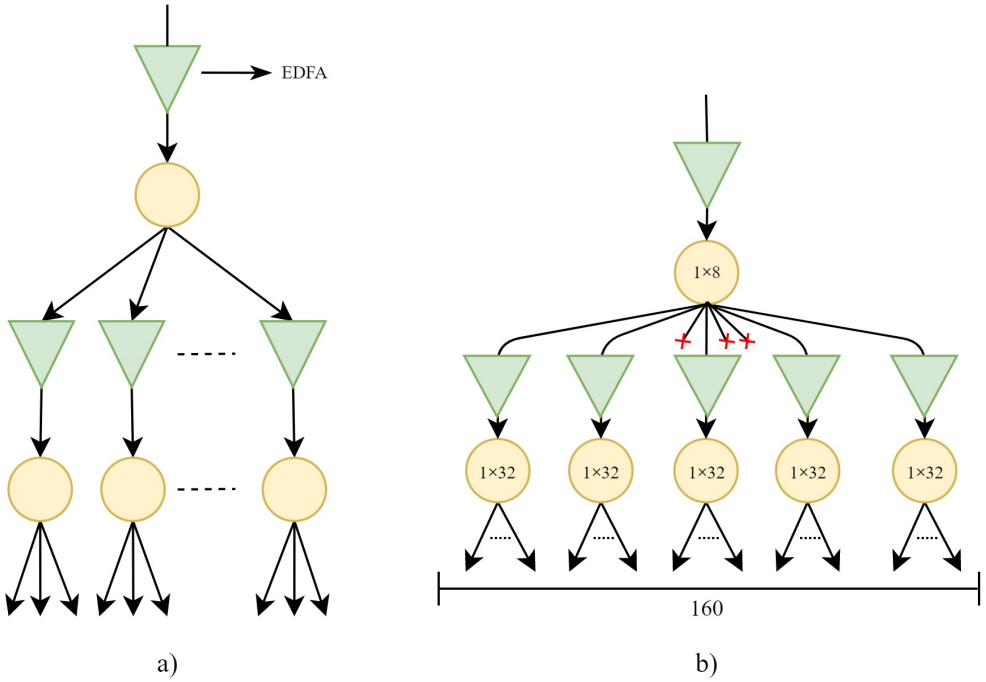

FIGURE 2.25: Multi-stage splitter-EDFA combination a) and a 1x160 splitter-EDFA example, using one 1×8 and five 1×32 splitters b).

respectively, that must be compensated by two EDFAs [37], thus, in the example, each ROADM A/D structure will require 6 EDFAs. The total number of EDFAs needed for a 8×8 ROADM with a 20% A/D ratio is therefore 48.

In order to reduce and ease the hardware cost of the A/D structure, a new solution has been proposed in [14], a solution named bank-based A/D architecture, whose schematic is shown in Fig. 2.26.

In Fig. 2.26, the proposed bank-based A/D architecture where the transponders are divided into groups named banks, is depicted. When dropping a signal, a "feeder" splitter distributes the dropped signals to bT/KT_{bank} banks out of the T/T_{bank} total banks, where K is the ROADM size, T is the total number of transponders, T_{bank} corresponds to the number of transponders in one bank and b is the number of input/output fibers of each bank [14].

Although there are no restrictions within each bank, only a limited number of A/D fibers can be accessed by each bank. Due to this restriction, the switch dimension of $b\times1$ and the total splitter degree of bT/KT_{bank} can be lowered, and the number of EDFAs needed to compensate for the splitter loss is also reduced [14].

In the bank-based A/D structure, routing flexibility and hardware requirements can be controlled by the parameter b. Smaller b enables fewer EDFAs due to reduced splitter losses, while larger b offers reduced A/D signal blocking, as the number of banks that can connect to each fiber A/D increases [14].

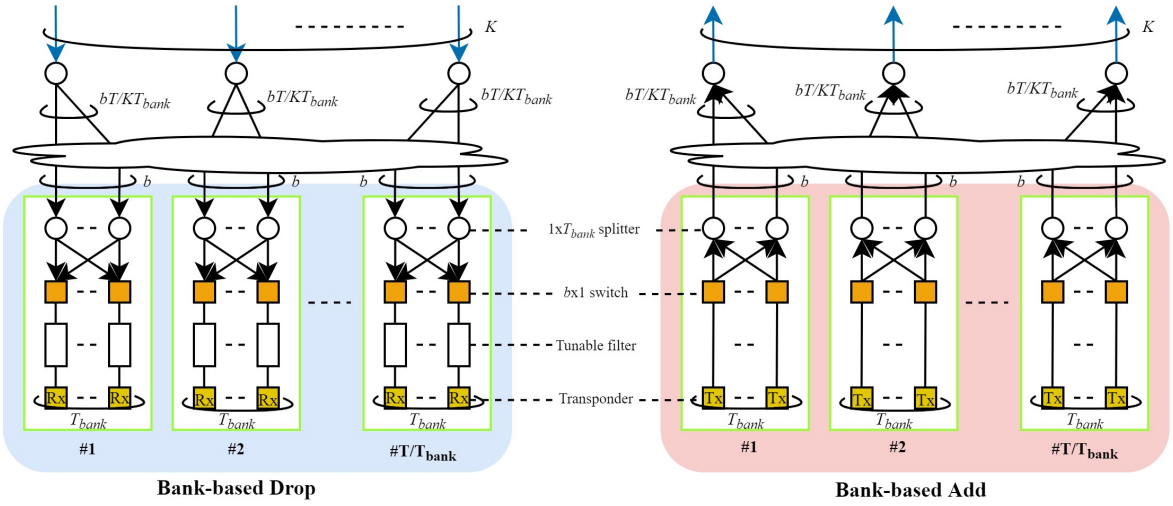

FIGURE 2.26: Bank-based A/D architecture

In order to compare the bank-based structure to the conventional A/D structure, we have performed an analysis considering different values of T_{Bank} and b. For the bank-based structure, for each drop fiber, the signal will go through the feeder splitter first, which splits the signal to *bT/KT* banks and, then, goes through the bank splitter that delivers the signal to every transponder in the bank (T_{Bank}), as depicted in Fig. 2.26.

In Tables 2.2 and 2.3, the splitter losses for various values of T_{Bank} and b for a K=8 and K=80 ROADM are displayed, respectively, considering 96 channels per fiber. Since the EDFA typical gain can range from 5 dB to 25 dB [38], we assume that when the total splitter loss is higher than 25 dB, we need two cascaded EDFAs in order to compensate the total loss. The splitters optical loss, $IL_{splitter}$, has been calculated using the following expression [37]:

$$IL_{splitter} = 10 \cdot \log(N) + IL_{excess} \tag{2.11}$$

where N is the splitter size and IL_{excess} is the excess loss in dB.

Excess losses of 1 dB were considered for 1×2 and 1×4 splitters and 2, 3 and 4 dB for 1×8, 1×16 and both 1×32 and 1×64 splitters, respectively [37].

Considering the splitter losses presented in Tables 2.2 and 2.3, the number of EDFAs required in the A/D structure has been calculated. In Fig. 2.27, the required number of EDFAs, for $K = 8$ and 80 bank-based and conventional A/D structure ROADMs, as a function of b, for T_{bank} values of (a) 8, (b) 16 and (c) 32 are shown. The number of EDFAs are displayed in a logarithmic scale.

Tbank	*b*	Number of banks	Feeder Splitter $1 \times \frac{bT}{KT_{bank}}$	Feeder Splitter Loss (dB)	Bank Splitter $1 \times T_{bank}$	Bank Splitter Loss (dB)	Total Splitter Loss (dB)
8	2	20	1×8	11	1×8	11	22
	4		1×16	15			26
	8		1×32*	19			30
	16		1×64*	23			34
16	2	10	1×4	7	1×16	15	22
	4		1×8	11			26
	8		1×16*	15			30
	16		1×32*	19			34
32	2	5	1×2	4	1×32	19	23
	4		1×4	7			26
	8		1×8*	11			30
	16		1×16*	15			34

*These feeder splitters size will not be considered in the following analysis, since they are greater than the available number of banks.

TABLE 2.2: Splitter losses for different values of T_{bank} and b parameters, for a $K = 8$ ROADM, considering 20% of A/D ratio (T=154).

Tbank	*b*	Number of banks	Feeder Splitter $1 \times \frac{bT}{KT_{bank}}$	Feeder Splitter Loss (dB)	Bank Splitter $1 \times T_{bank}$	Bank Splitter Loss (dB)	Total Splitter Loss (dB)
8	2	192	1×8	11	1×8	11	22
	4		1×16	15			26
	8		1×32	19			30
	16		1×64	23			34
16	2	96	1×4	7	1×16	15	22
	4		1×8	11			26
	8		1×16	15			30
	16		1×32	19			34
32	2	48	1×2	4	1×32	19	23
	4		1×4	7			26
	8		1×8	11			30
	16		1×16	15			34

TABLE 2.3: Splitter losses for different values of T_{bank} and b parameters, for a $K = 80$ ROADM, considering 20% of A/D ratio (T=1536).

As depicted in Fig. 2.27 a), for both $K = 8$ and $K = 80$, for a T_{Bank} of 8, the bank-based structure requires a reduced number of EDFAs for a lower b. When b=4 , for a larger ROADM scale size of 80, the bank-based A/D shows its advantages by reducing the number of required EDFAs significantly when compared to the conventional A/D structure from 3920 to 848 or 1616 for $b = 4$ and 8, respectively. If $b = 16$, the number of EDFAs is also reduced, but not so significantly, to 3152.

When increasing the number of transponders per bank, T_{Bank}, to 16 and 32, as depicted in Figs. 2.27 b)

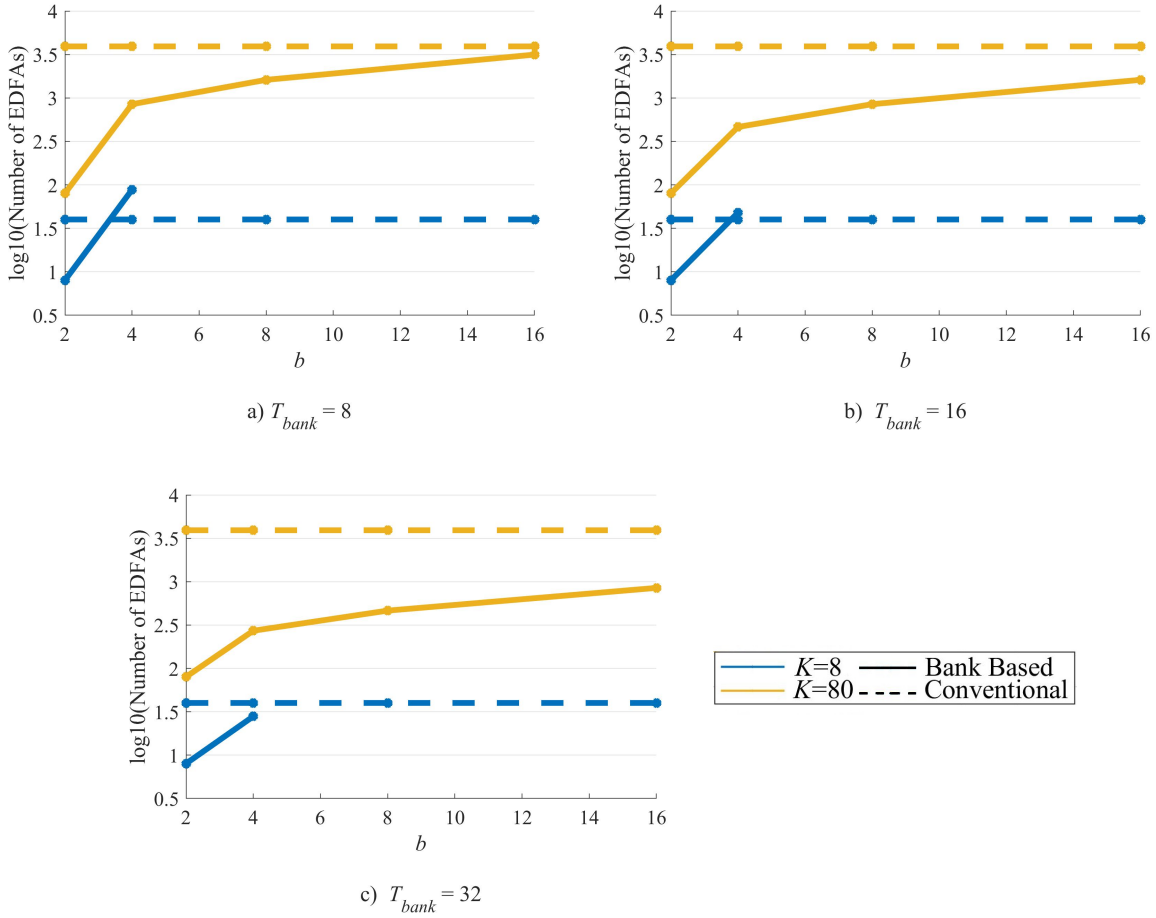

FIGURE 2.27: Number of required EDFAs in a conventional and bank-based A/D structures as a function of parameter b, for $K = 8$ and 80 and for T_{Bank}=8 (a), 16 (b) and 32 (c).

and c), the differences in the number of required EDFAs between the bank-based and the conventional A/D are marginal, for a ROADM scale of $K = 8$. However, for a $K = 80$ ROADM scale and T_{Bank}=16, the bank-based A/D requires much less EDFAs in comparison with $T_{bank} = 8$ due to the lower number of total banks, hence, reducing the number of EDFAs. For b=4, 8 and 16, the number of EDFAs is reduced to, respectively, 464, 848 and 1616, while in the conventional A/D structure, 3920 EDFAs are required. When T_{Bank}=32, the bank-based A/D structure requires 88% less EDFAs for $b = 8$ in comparison to the conventional A/D.

As a final example, to show the advantages of the bank-based structure for large-scale ROADMs, if we consider a 80×80 ROADM, with 20% A/D ratio, a total of 1536 transponders are required, for each add and drop structures, and 1536 tunable filters for the drop structure. For a conventional CDC drop structure, 4000 1×32 splitters and 3920 EDFAs are required, as well as 1536 80×1 switches. With the

bank-based A/D structure, considering T_{bank}=32, T=1536 and b=8, only 80 1×8 "feeder" splitters and 384 1×32 "bank" splitters are required. The switch size and EDFAs needed are significantly smaller, 1×8 and 464, respectively. This represents a reduction of 88% in the number of EDFAs and 88% in optical splitters.

2.8 Conclusions

In this chapter, the ROADMs state-of-the-art was presented, as well as their evolution and the possible approaches to future large-scale ROADMs. As the network requires more capacity and flexibility from the ROADM nodes, the scalability is an important characteristic.

To implement future large-scale ROADMs, the available components (e.g. WSS, MCS, splitters) size nowadays is not large enough, and thus implementing these ROADMs with conventional B&S and R&S architectures will become very much expensive, translating to less cascadeability and scalability. The conventional A/D architecture also becomes larger and more expensive. Hence, new architectures for the express and A/D structure have been proposed in the literature and analyzed and discussed in Section 2.7, in terms of hardware number and total cost. For example, for express structures of $K = 80$ ROADMs, the interconnected A, B and FLEX architectures require ten times less WSSs than conventional ones. Also, regarding the A/D structure and also for $K = 80$, the bank based A/D architecture requires 88% less EDFAs and optical splitters comparing with the conventional CDC A/D. All the architectures have shown that for the targeted large-scale ROADMs, the overall cost of the node can be significantly reduced.

Chapter 3

Generation of in-band crosstalk inside large-scale ROADMs

3.1 Introduction

This chapter is mainly focused in analyzing the in-band crosstalk generated inside the ROADM architectures studied in Chapter 2. The analysis is based on the worst case scenario for each architecture, i.e., the one that generates the highest number of interferers on the primary signal. In Section 3.2, the different crosstalk types are described and how their generation occurs in an optical network is explained. In Section 3.3, the generation of in-band crosstalk inside the two types of interconnected architectures, is investigated, for both B&S and R&S based subsystems. In Section 3.4, the generated in-band crosstalk inside the FLEX architecture is analyzed. Section 3.5 compares all the express structure architectures in terms of in-band crosstalk generation. Afterwards, in Section 3.6, the crosstalk generated inside the bank-based A/D is analyzed and compared to the one generated in a conventional A/D. Lastly, Section 3.7 presents the main conclusions of this chapter.

3.2 In-band versus out-of-band crosstalk

Optical crosstalk is a physical layer impairment that degrades the signal performance of optical networks [39]. The main cause of the existence of crosstalk signals in these networks is mainly due to the finite isolation of the components within the ROADMs [25], [39]. This imperfect isolation of the components (splitters, WSS, etc.) causes signal power leakage that accumulates along the node chain causing optical signal degradation at the optical receiver.

The crosstalk can be classified in two main types, in-band and out-of-band crosstalk [39]. Out-of-band crosstalk, also known as heterodyne crosstalk, occurs when the interference signals have a different wavelength than the selected signal. This crosstalk is not too much problematic as it can be removed with proper filtering at the receiver.

In-band, or homodyne, crosstalk occurs when the interference signals from different optical sources have the same nominal wavelength than the desired signal. Unlike out-of-band crosstalk, in-band interference cannot be removed at the receiver simply by filtering and accumulates along the path of the optical signal along several ROADMs [39].

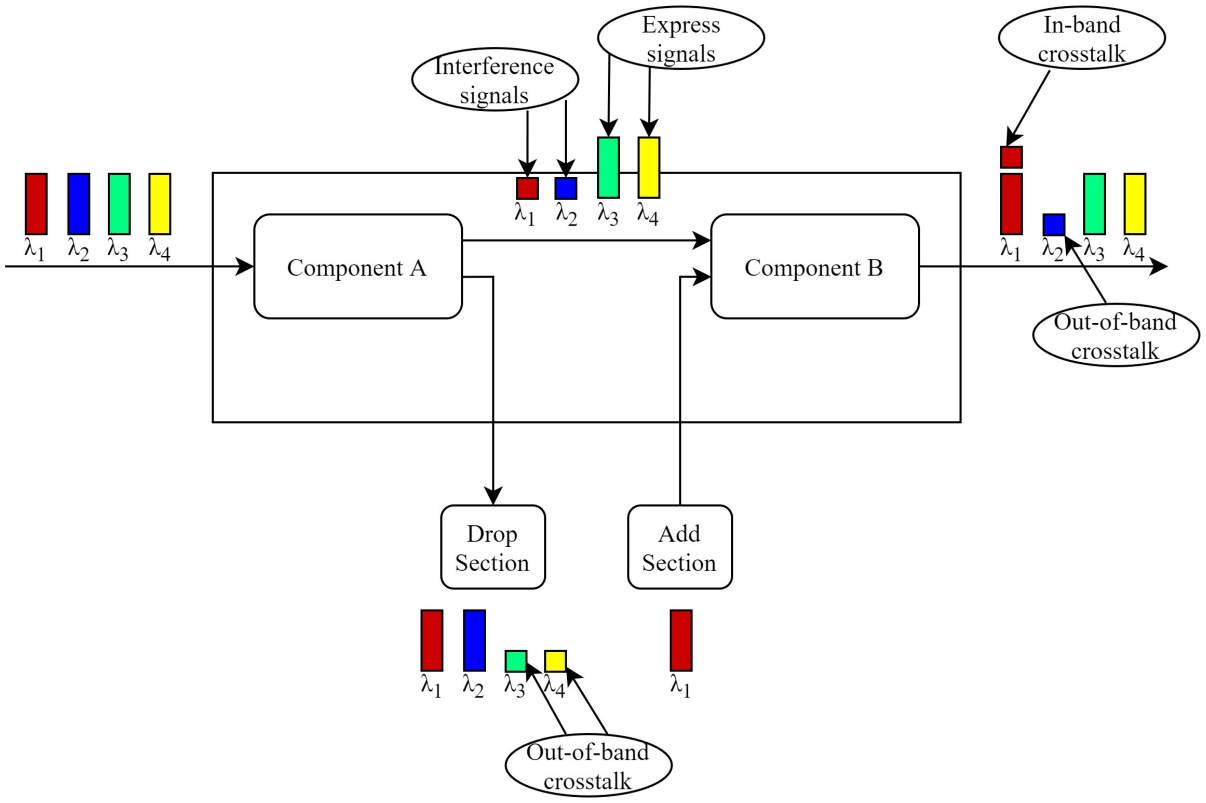

FIGURE 3.1: Generation of in-band and out-of-band crosstalk inside ROADMs nodes.

In Fig. 3.1, the process of generating crosstalk signals within a ROADM is outlined. At the ROADM input there are four optical signals with wavelengths λ_1, λ_2, λ_3 and λ_4. The first signal processing is performed in component A, which may be a WSS or an optical splitter, depending on the architecture of the ROADM [16], [28]. Signals λ_1 and λ_2 are extracted in the drop section and a new signal with wavelength λ_1 is added in the add section. The use of the same wavelength λ_1 for add and drop is known as wavelength reuse [16]. Signals λ_3 and λ_4 are express signals and therefore pass directly to component B.

At the ROADM output, the optical signals pass through component B, typically a WSS [28]. Thus, in Fig. 3.1, in terms of crosstalk signals, the output optical signal at λ_1 is impaired by an in-band crosstalk signal and an out-of-band crosstalk signal at wavelength λ_2. In the drop section, two out-of-band crosstalk

signals with wavelengths λ_3 and λ_4 appear. All these crosstalks appear due to imperfect isolation of the different optical components of the ROADM: components A, B and add/drop section components.

The components used in ROADMs are determined by the desired characteristics of the add/drop ports and express architectures used [28], as explained in Section 2.6. In this chapter, the impact of in-band crosstalk on interconnected ROADM-subsystems and FLEX architectures with different degrees, as well, as in ROADMs based on conventional B&S and R&S are investigated. For this study, it is important to understand the concept of 1st and 2nd order interfering terms [40]. Therefore, when an optical signal overcomes the isolation of only one optical component (e.g. a WSS), the crosstalk is considered 1st order. When it overcomes the isolation of two optical components, it is known as a 2nd order crosstalk [40]. Crosstalk signals with order above 2 are not considered in this work, because their impact on the network performance is negligible considering a typical isolation level between -20 dB and -40 dB [40].

3.3 In-band crosstalk generation in interconnected ROADM subsystems

In this section, the number of in-band crosstalk signals that will arise inside the express structure of a B&S or R&S interconnected ROADM-subsystems node is investigated. A similar study was done in [41] for the conventional B&S architecture.

3.3.1 Interconnected subsystems with A/D placed outside the express structure

First, the impact of the in-band crosstalk generated in an interconnected A subsystems architecture is analyzed. In this architecture, the maximum number of subsystems traversed, n_{hops}, known as hop-slug, is typically 2 [12]. After several analysis, we concluded that the worst case scenario for this node architecture is when all the traffic of a specific wavelength, is express and the considered signal traverses the maximum number of subsystems. In case of a full A/D traffic, all the ROADM output ports have zero in-band crosstalk signals, due to the small 1×2 WSSs connecting each input/output to the A/D structure represented in Fig. 3.2.

In Fig. 3.2, a diagram of the worst case scenario of generation of in-band crosstalk signals in the interconnected A sub-systems architecture is represented for 5×5 sub-ROADMs. The in-band crosstalk signals generated in each subsystem are represented by a dashed red line and the in-band crosstalk signals generated in adjacent subsystems are represented by a dashed black line. The input fiber Ⓐ is the primary signal input direction of the ROADM and Ⓑ is the signal output direction. The signal enters the node at the subsystem Sub0, and traverses Sub1 and Sub2, exiting the ROADM at Sub2 (2 hops). The crosstalk terms originated in adjacent subsystems will also impair the primary signal, when there are other signals

traversing different subsystems, such as the one entering at Ⓒ and exiting at Ⓓ with also 2 hops. Fig. 3.2 shows that, as expected, the in-band crosstalk impairment is worse when the primary signal transverses more subsystems.

When traveling to Sub1, at ①, the primary signal will be impaired by 2 in-band crosstalk terms generated inside Sub0, represented by the red dashed lines. In Sub1, the primary signal continues its path to Sub2 and is impaired by 3 more in-band crosstalk signals at ②. Once again, these terms join the optical path of the considered signal, being a total of 5 now. In the final subsystem, Sub2, the signal will exit the node at Ⓑ, but before exiting, at ③, it will be impaired by 3 more crosstalk signals generated inside Sub2. In total, the primary signal is going to be impaired by 8 in-band crosstalk signals generated inside the sub-ROADMs it transverses. These terms are 1st order in case of a B&S architecture and 2nd order in case of R&S architecture.

To study the interfering terms arising from the subsystems adjacent to the sub-ROADMs that the primary signal transverses (Sub 0, Sub 1 and Sub 2), we consider another express signal at the same wavelength as the primary signal that goes from Ⓒ to Ⓓ. When sent to Sub-1 at ④, this express signal is going to be impaired by 2 in-band crosstalk terms generated in Sub-2, that are added to the optical path of the primary signal. At Sub-1, the signal already with 2 in-band crosstalk terms, is sent to Sub0. At ⑤, 3 more in-band crosstalk terms will be added to the optical path, resulting in 5 in-band 1st or 2nd order interferers, respectively, for B&S and R&S architectures. Then, at Sub0, these terms will also impair the primary signal but as 2nd or 4th (negligible) order interferers, respectively, for B&S and R&S architectures. This situation is mirrored for a express signal going from Sub4 (not shown in Fig. 3.2 for simplicity) to Sub2, at ③, which results in more 5 in-band crosstalk terms, meaning that, in total, there are 10 interfering terms from adjacent subsystems.

Other adjacent subsystems that are more distant from Sub0 or Sub2, will not give rise to meaningful in-band crosstalk terms. For example, if there is a signal coming from Sub-3 to exit Sub-2, at ⑥, they will be 2nd order terms, in case of a B&S, but when arriving at ①, they are blocked, becoming 3rd order negligible terms.

Hence, the primary signal that goes from Ⓐ to Ⓑ is impaired by 8 1st order and 10 2nd order terms for a B&S or 8 2nd order terms for a R&S.

By generalizing this analysis, the total number of in-band crosstalk terms generated inside the interconnected A architecture that will impair the express signal, NX_{inter_A}, is therefore given by

$$NX_{inter_A} = NX_{prim} + NX_{adj} \tag{3.1}$$

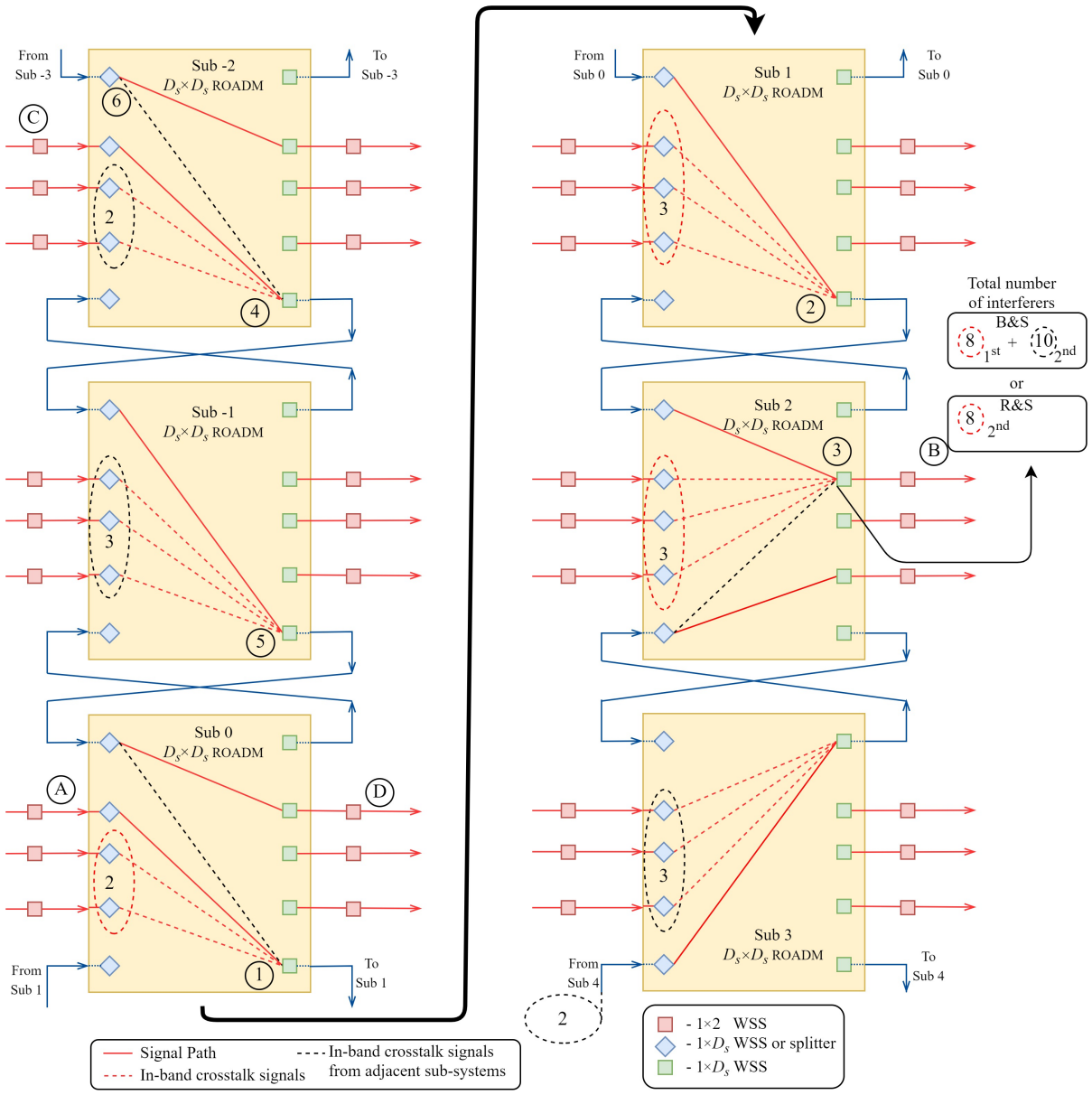

FIGURE 3.2: Generation of in-band crosstalk signals in the interconnected A subsystems architecture with $D_s = 5$ sub-ROADMs.

where NX_{prim} and NX_{adj} are the primary signal interferers and the adjacent subsystems interferers, respectively, calculated by:

$$NX_{prim} = D_s - 2f_{intra} - 1 + n_{hops} \times (D_s - 2f_{intra}) \tag{3.2}$$

$$NX_{adj} = 2 \times (D_s - 2f_{intra} - 1 + (n_{hops} - 1) \times (D_s - 2f_{intra})) \tag{3.3}$$

The NX_{prim} are 1st or 2nd order terms, for a B&S or R&S architecture, respectively, and NX_{adj} are 2nd order terms for a B&S and negligible for a R&S. This worst case shows that the number of crosstalk terms is independent of the ROADM scale (K), unlike in conventional architectures [24], and depends only on sub-ROADM parameters. Eqs. (3.2) and (3.3) can be only applied when the number of sub-ROADMs is equal or higher than 7. If lower, the number of interferers is also smaller.

3.3.2 Interconnected subsystems with A/D sharing the express structure

In interconnected nodes subsystems with A/D sharing the express routing capability, or interconnected B subsystems architecture, the in-band crosstalk must also be analyzed. In this architecture, the maximum number of subsystems traversed, n_{hops}, is also typically 2 [12]. After several analysis, we concluded that the worst case scenario for this node architecture is when all the traffic, of a specific wavelength is add/dropped and the considered primary signal traverses the maximum number of subsystems. In case of a full express traffic, since half the subsystem is dedicated to A/D traffic, the ROADM output ports would have half the number of in-band crosstalk signals.

In Fig. 3.3, a diagram of the worst case scenario of generation of in-band crosstalk signals in the interconnected B sub-systems architecture is represented. The in-band crosstalk signals generated in each subsystem are represented by a dashed red line and the in-band crosstalk signals generated in adjacent subsystems are represented by a dashed black line. The input fiber Ⓐ is the primary signal input direction and Ⓑ is the signal output direction. The signal enters the node at the subsystem Sub0, and traverses Sub1, exiting at the ROADM Sub2 (2 hops). The terms originated in adjacent subsystems will also impair when there are other signals at the same wavelength traversing different subsystems, such as the one entering at Ⓒ and exiting at Ⓓ with also 2 hops.

When traveling to Sub1, at ①, the primary signal will be impaired by 3 in-band crosstalk terms generated inside Sub0, represented by the red dashed lines. In Sub1, the signal continues its path to Sub2 and is impaired by 4 more in-band crosstalk signals at ②. In Sub2, the primary signal will exit the node at Ⓑ, but at ③, it will be impaired by 4 more crosstalk signals generated inside Sub2. In total, the primary signal is going to be interfered by 11 in-band crosstalk signals. These terms are 1st order in case of a B&S architecture and 2nd order in case of R&S architecture.

To study the adjacent subsystems interfering terms, we consider another express signal that goes from Ⓒ to Ⓓ. When sent to Sub-1 at ④, this express signal is going to be impaired by 3 in-band crosstalk

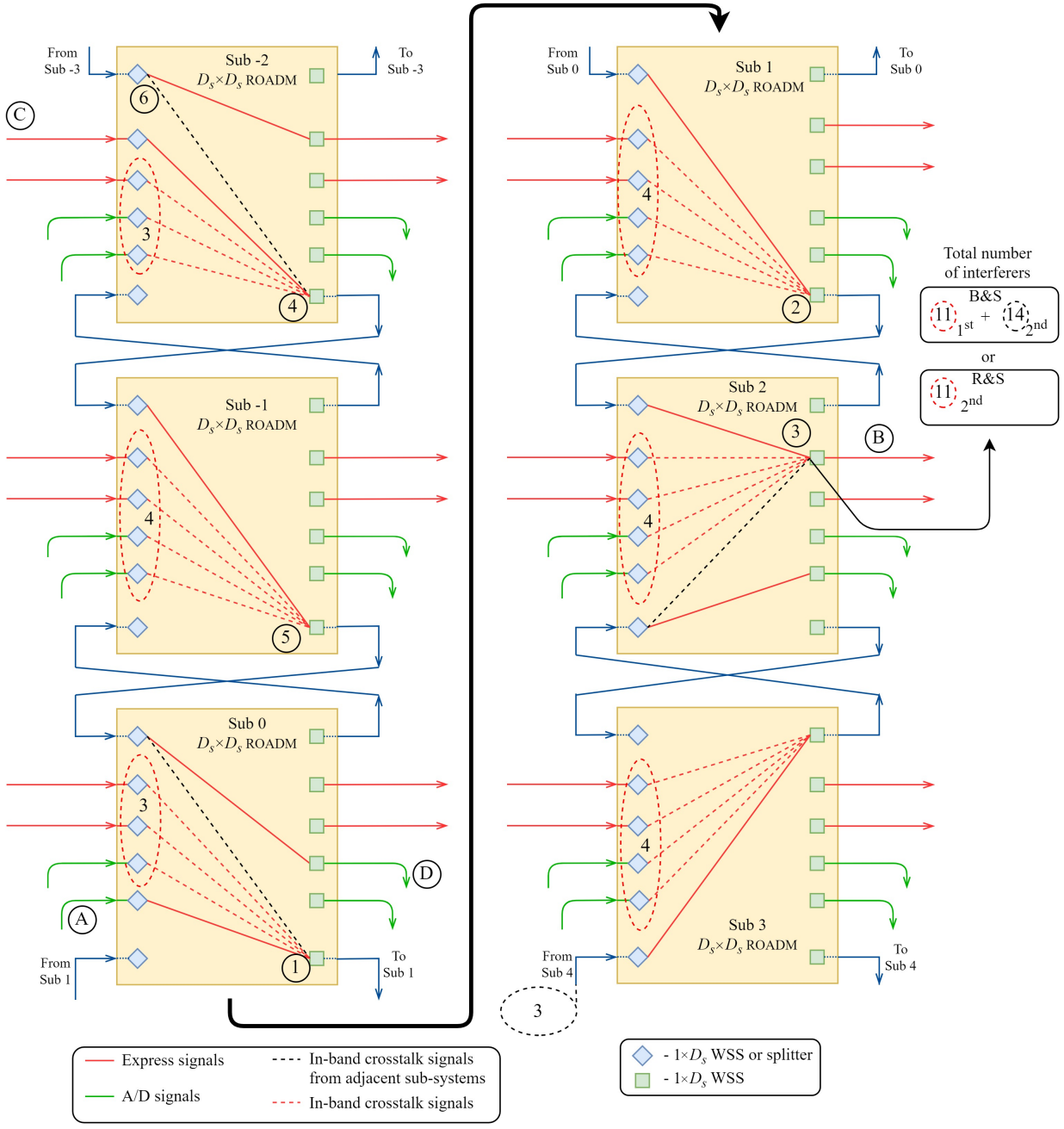

FIGURE 3.3: Generation of in-band crosstalk signals in the interconnected B subsystems architecture for $D_s = 6$, with half of each sub-ROADM input dedicated to A/D traffic.

terms generated in Sub-2. Afterwards, at Sub-1, the signal is sent, along with the 3 crosstalk terms, to Sub0 where it is going to exit the ROADM at Ⓓ. At ⑤, 4 more in-band crosstalk terms will be added to the optical path. Then, at Sub0, these terms will also impair the primary signal but as 2nd order for a B&S architecture and 4th order for a R&S (negligible). This situation is mirrored for a signal going from

Sub4 (not shown in Fig. 3.3 for simplicity) to Sub2, at ③, meaning that in total, there are 14 interfering terms originating in adjacent subsystems. The other possible adjacent subsystems that are more distant from Sub0 or Sub2, are negligible.

To conclude the reasoning, the signal that goes from Ⓐ to Ⓑ is impaired by 11 1st order and 14 2nd order terms for a B&S or 11 2nd order terms for a R&S.

By generalizing this analysis, the total number of in-band crosstalk terms generated inside the interconnected B architecture that will impair the express signal, NX_{inter_B}, is also given by Eq. (3.1), where NX_{prim} and NX_{adj} are given by Eqs. (3.2) and (3.3) presented in the previous section.

The NX_{prim} are 1st or 2nd order terms, for a B&S or R&S architecture, respectively, and NX_{adj} are 2nd order terms for a B&S and negligible for a R&S. This worst case shows that the number of crosstalk terms is also independent of the ROADM scale (K) as in the interconnected A, unlike the conventional architectures [24], and only applies when the number of sub-ROADMs is equal or higher than 7.

3.4 In-Band crosstalk generation in FLEX ROADM

In this section, the number of in-band crosstalk signals that will arise inside a FLEX ROADM architecture node express structure is investigated. After several analysis, we concluded that the worst case scenario for this node architecture is when all the traffic of a specific wavelength is express. In case of a full A/D traffic, all the ROADM output ports will experience negligible in-band crosstalk.

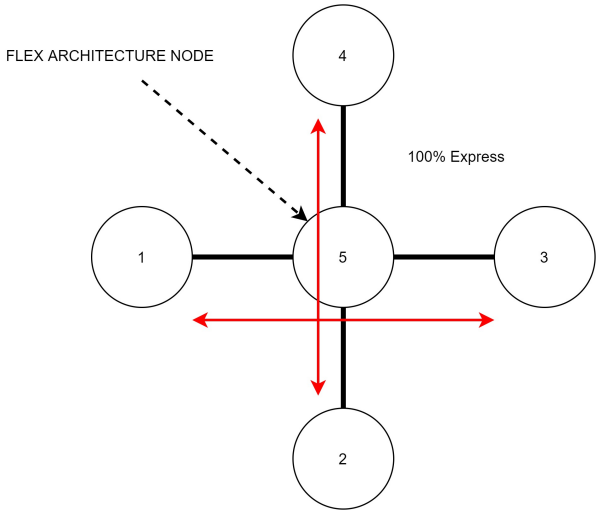

FIGURE 3.4: Five-node star network with a FLEX ROADM architecture.

Fig. 3.4 depicts an example of a 5 node star network, where the center node is a 4×4 FLEX ROADM and node 1 communicates with node 3 with the same wavelength as node 2 communicates with node 4, thus, the red wavelength is 100% express in the FLEX node. There are two possibilities for connecting these nodes depending on the network planning: using the same switching matrix for all the ROADM inputs or using different matrices, as depicted in Figs. 3.5 and 3.6, respectively, considering $W_B = 4$.

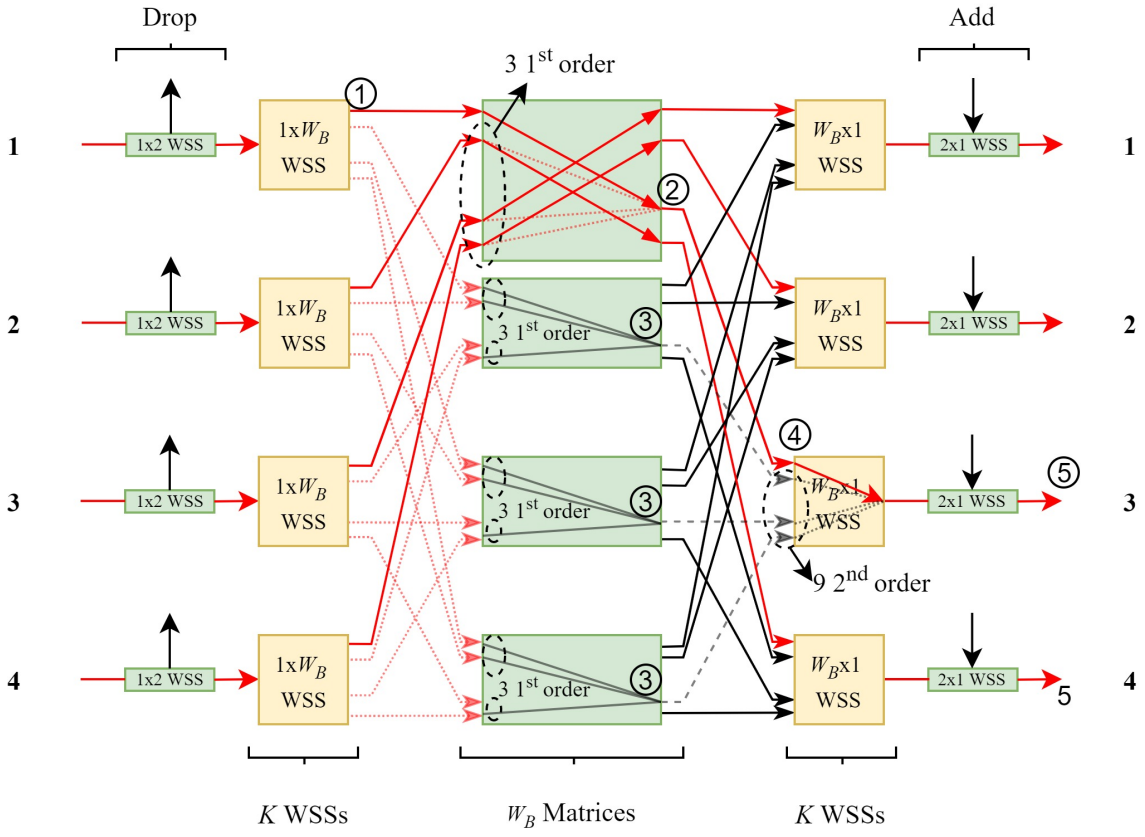

FIGURE 3.5: Example of the generation of in-band crosstalk signals in the FLEX architecture when the traffic is 100% express and only one matrix is used to switch the wavelength of the primary signal.

When the same matrix is used and considering fiber 1 and 3 as the primary signal input and output, as depicted in Fig. 3.5, at ①, each WSS output will have a 1st in-band crosstalk signal that is sent to the other matrices. At the selected matrix input, each optical switch will generate an in-band crosstalk signal, hence, at ②, each matrix output will be impaired by 3 1st order in-band interferers. The crosstalk signals generated at ① and sent to the other matrices, depending on the network planning, may impair the primary signal. These signals will continue travelling as 1st order crosstalk if other input signals of different wavelengths are switched to the same ROADM output as the primary signal. The worst case occurs when all inputs switch to the same output. At ③, considering the worst case, 3 1st order crosstalk

signals are sent, by each one of the other matrices, to the input of the $W_B \times 1$ WSS at ④, where they are blocked, becoming 2nd order interferers. Hence, at ⑤, the output express signal will be impaired by 3 1st order in-band crosstalk signals, and 9 2nd order crosstalk signals.

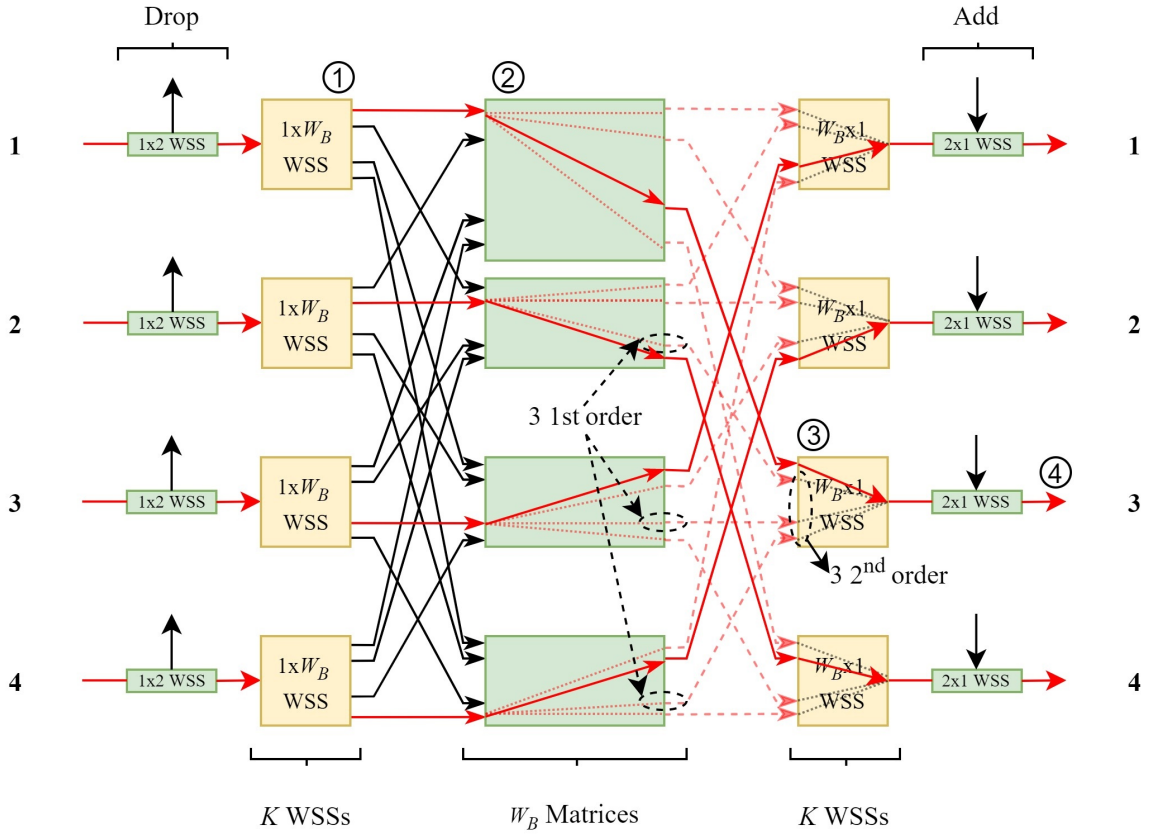

FIGURE 3.6: Example of the generation of in-band crosstalk signals in the FLEX architecture when the traffic is 100% express and different matrices are used.

The input signals can also be sent to different matrices, as depicted in Fig. 3.6, reducing the in-band crosstalk impairment. Considering the fiber 1 and 3 as, respectively, the signal input and output, at ①, the $1 \times W_B$ WSS sends the primary signal to the first matrix, while the other WSSs send the same wavelength to different matrices. At the input of each matrix ②, each optical switch will generate one 1st order in-band crosstalk signal in each matrix output (except for the output of the switched signal). At ③, the WSS block the crosstalk signals from the other matrices, becoming 2nd order interferers. At ④, the signal will be impaired by 3 2nd order in-band crosstalk signals.

If there is a mix of express and A/D signals, the overall in-band crosstalk impairment is also reduced because the A/D signals produce zero in-band crosstalk terms. Thus, considering the worst case scenario in terms of in-band crosstalk generation, as shown in Fig. 3.5, the output signal will be impaired by

3 1st order and 9 2nd order in-band crosstalk signals.By generalizing, the following expression can be considered to calculate the total number of interferers at the output signal in a FLEX node, NX_{FLEX}:

$$NX_{FLEX} = (K-1)_{1st} + ((K-1) \times (W_B - 1))_{2nd} \tag{3.4}$$

As a final example, for a K=80 ROADM with W_B=4, the output signal will be impaired by 79 1st order and 237 2nd order crosstalk signals. Even though this architecture has the advantage of reducing the overall cost of a large-scale ROADM [36], the in-band crosstalk impairment is worse than the interconnected architectures studied in Sections 3.3.1 and 3.3.2 .

3.5 In-band crosstalk comparison

In this section, a summary of the studied number of in-band crosstalk signals is presented and the comparison between all architectures is performed, considering the worst case scenario for each architecture. For the interconnected architectures, we have considered n_{hops} and f_{intra} to be 2 and 1, respectively.

	Broadcast&Select		Route&Select	
Term Order	1^{st}	2^{nd}	1^{st}	2^{nd}
Conventional Node	$K-1$	-	-	$K-1$
Inter-Connected A*	$3D_S-7$	$4D_S-10$	-	$3D_S-7$
Inter-Connected B*	$3D_S-7$	$4D_S-10$	-	$3D_S-7$
FLEX - Waveband	N/A	N/A	$K-1$	$(K-1)\times(W_B-1)$

* As mentioned in subsection 3.3, this only applies to $N_{SUB} \geq 7$.

TABLE 3.1: Number of in-band crosstalk signals generated inside each studied architecture.

In Figs. 3.7 a) and b), the number of 1st and 2nd order in-band crosstalk terms for different ROADM sizes, K, is depicted based on Table 3.1. Since the interconnected architectures are independent of the ROADM size, D_S sizes of 6 and 9 are considered [12], [42]. Also, since the number of interferers is equal in both interconnected A and B architectures, we only plotted one line for simplicity. We can see that the FLEX node, represented in green, has the worst performance in terms of the number of crosstalk terms, having the same or more 1st order crosstalk interferers than the conventional B&S architecture. For the considered K, the interconnected A B&S and R&S node shows a better performance against the corresponding conventional architecture. When a lower D_S is used, since the subsystems are smaller, the in-band crosstalk impairment is also lower.

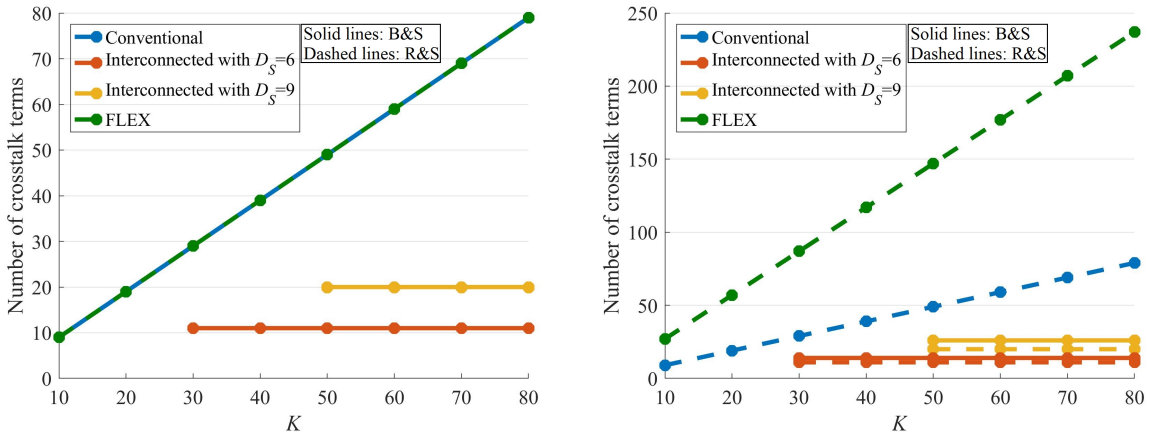

FIGURE 3.7: Number of 1st a) and 2nd b) order in-band crosstalk terms as a function of K.

We conclude that for large-scale ROADMs, the interconnected A or B R&S is the best choice in terms of in-band crosstalk generation, because all interfering terms are 2nd order interferers.Furthermore, the number of generated crosstalk terms in the interconnected architectures depends on D_s, the subsystem size, and is independent of the ROADM scale, K.

3.6 In-Band crosstalk generation in the conventional and bank-based A/D structures

In this section, the number of in-band crosstalk signals that will arise at the drop ports and at the ROADM outputs from the add ports in a conventional and bank-based A/D structure are analyzed and compared. A similar study was performed in [41], where the number of in-band crosstalk signals in A/D structures with MCSs or WSSs has been compared.

In a conventional CDC A/D structure, the A/D can be implemented using MCS or $N \times M$ WSSs. As concluded in [24], the number of interfering in-band crosstalk signals originated in the A/D structure depends on the ROADM scale (in [24], it was considered that $f_D = 1$). Considering that each ROADM degree can have several fibers ($f_D > 1$), the number of in-band crosstalk terms that arise at the drop ports and at the ROADM outputs from the add ports are presented in Table 3.2 for conventional B&S and R&S architectures.

Considering the bank-based A/D structure architecture presented in subsection 2.7.5, the structure of each bank is depicted in Figs. 3.8 and 3.9, for a drop and add bank, respectively.

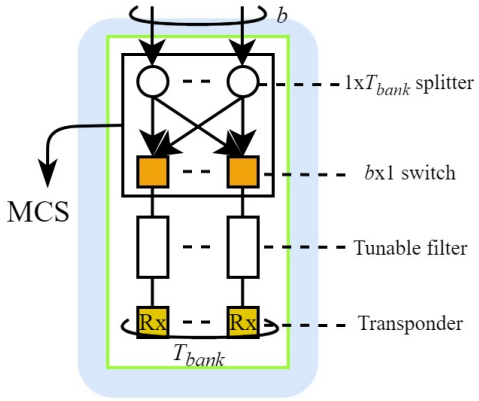

FIGURE 3.8: Bank-based A/D architecture: drop bank diagram.

In a drop bank, depicted in Fig. 3.8, b input fibers are connected to $1 \times T_{bank}$ splitters. The splitters split the signal to T_{bank} $b \times 1$ optical switches. Together, these components form a $b \times T_{bank}$ MCS. Each optical switch is then connected to a tunable filter that selects which wavelength to drop in the receiver transponder. Since each bank can be analyzed as a MCS, each drop bank output port is impaired by $b-1$ 1^{st} order in-band crosstalk terms.

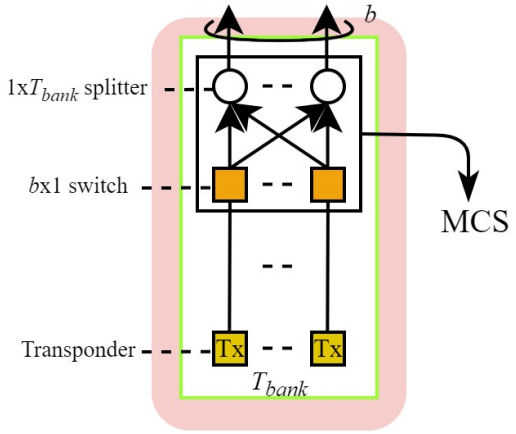

FIGURE 3.9: Bank-based A/D architecture: add bank diagram.

In a add bank, depicted in Fig. 3.9, each transponder is connected to a $1 \times b$ optical switch. Each optical switch is then connected to b $T_{bank} \times 1$ optical couplers. Again, these last two components form a $T_{bank} \times b$ MCS, where each MCS output is impaired by $b-1$ 1^{st} order in-band crosstalk terms. Each ROADM output fiber is connected to bT/KT_{bank} banks, hence, each ROADM output port is impaired by a total of $\frac{bT}{KT_{bank}} \times (b-1)$ 1^{st} order in-band crosstalk terms.

	Drop ports		Outputs (originated in Add ports)	
	1st order	2nd order	1st order	2nd order
Conventional MCS	K-1	-	K-1	-
Conventional WSS	-	K-1	-	K-1
Bank Based	$b-1$	-	$\frac{bT}{KT_{bank}} \times (b-1)$	-

TABLE 3.2: Number of in-band crosstalk terms generated in a conventional CDC A/D, conventional architectures with MCSs or WSSs, and in a bank-based A/D architecture.

Table 3.2 summarizes the expressions used to calculate the number of in-band crosstalk terms in both conventional CDC A/D and bank-based A/D structures. If we consider that there is no blocking in accessing each bank ($b = K$) and that there is only one bank ($T_{bank} = T$), the bank-based expressions become the same as the CDC A/D using MCS, which confirms the bank-based expressions that we found.

As a numerical example, considering a 20% A/D ratio 80×80 scale ROADM with a conventional A/D using MCS, we would have 79 1st order in-band crosstalk terms in both drop ports and add output ports, while in bank-based A/D architecture considering $b = 8$ and $T_{bank} = 32$, the number of in-band crosstalk terms drops to 7, in the drop ports, and 35, in the add ports. This is a significant performance improvement for large-scale ROADMs in terms of the in-band crosstalk impairment, representing a 90% and a 55% decrease, for the drop and add ports respectively, in a bank-based architecture in relation to the conventional MCS architecture. In comparison with a conventional WSS A/D architecture, the number of in-band crosstalk terms in the bank-based has also a 90% and a 55% decrease, for the drop and add ports, respectively, however, the in-band crosstalk terms are 2^{nd} order terms in the conventional WSS architecture.

3.7 Conclusions

In this chapter, the worst case scenario for each of the large-scale ROADM architectures, interconnected A, interconnected B, FLEX and bank-based A/D, was studied and analyzed. Regarding the A/D structure architectures, the proposed bank-based A/D shows a better performance in terms of in-band crosstalk impairment comparing to the conventional A/D. For the express structure, we concluded that the FLEX architecture is not a good option in terms of crosstalk impairment, since it performs the same as a conventional B&S, with the same number of 1^{st} order crosstalk terms. This proposed node can be outperformed by the conventional R&S, since the latter does not have 1^{st} order interferers impairing the

primary signal. However, as the ROADM scale increases, the interconnected A or B B&S and R&S shows better results than the equivalent conventional node, since the number of in-band crosstalk terms depends only on the D_S size. The number of crosstalk terms reduces for lower D_S.

On one hand, when considering a $K = 80$ B&S ROADM and $D_S = 9$, for example, the interconnected A or B has 20 and 26 1st and 2nd order interferers, respectively, while the conventional has 79 1st order interferers. On the other hand, considering a R&S ROADM with also $K = 80$ and $D_S = 9$, the interconnected A or B has 20 2nd order interferers while the conventional architecture has 79 2nd order interferers. The FLEX architecture, when considering $W_B = 4$, has 79 and 237 1st and 2nd order interferers, respectively, being the one with the worst performance in terms of in-band crosstalk generation.

Since the main goal of this work is to analyze both the conventional and the proposed architectures for future large-scale ROADMs, we conclude that the most promising one is the interconnected A or B architecture.

Chapter 4

Simulation Model

4.1 Introduction

In this chapter, the optical network simulation model is presented, as well as some key points needed for its implementation using MATLAB simulation. The model of the optical components of an optical network, such as the optical transmitter, the optical fiber, the WSS, the optical receiver and the optical amplifier, and their characteristics, are described in Section 4.2. The Monte Carlo (MC) simulator developed and implemented in MATLAB is described by a flow-chart in Section 4.3. This simulator is used to assess the performance of the optical network composed by the large-scale ROADMs described in the previous Chapter. In Section 4.4, we present the metrics used to evaluate the performance of the optical network using MC simulation, such as the bit error rate (BER) obtained by direct error counting (DEC) and optical-signal-to-noise ratio (OSNR). Lastly, the chapter conclusions are given in Section 4.5.

4.2 Model of a generic optical network

The simulation model used to study the optical network in this work is depicted in Fig. 4.1 with its main components. This network model represents a possible lightpath established in an optical network, from a source optical node to a destination node, which crosses several ROADM nodes along its path. Note that , in this work, only a single optical wavelength is considered, since one of the main aims of this work is to study in-band crosstalk. The consideration of WDM signal transmission could mask the in-band crosstalk crosstalk study due to the extra intercarrier crosstalk that can be added. The optical transmitter, that will be described in Section 4.2.1, is responsible for generating the optical signals with different characteristics, such as different modulation formats and symbol rates. Then, the generated signal enters the optical network and goes through a cascade of optical links, until it reaches the optical receiver. Each link is composed by an optical fiber, an optical pre-amplifier and a post-amplifier. The optical fiber characteristics and the filter model used to model the WSSs in the optical large-scale ROADM node are described in Sections 4.2.2 and 4.2.3, respectively. Throughout the optical path, the primary signal is impaired by ASE noise generated in each amplifier and interfering signals arising from imperfect (finite) isolation of the various optical components inside the nodes. The model of the optical amplifiers

is described in Section 4.2.4. The primary signal, impaired by the accumulation of ASE noise and interfering signals, reaches the optical receiver at the optical destination node. A coherent detection optical receiver is considered, which is described in Section 4.2.5. After detection at the optical receiver, the performance of the optical network is evaluated through the estimation of the BER, OSNR and OSNR penalty.

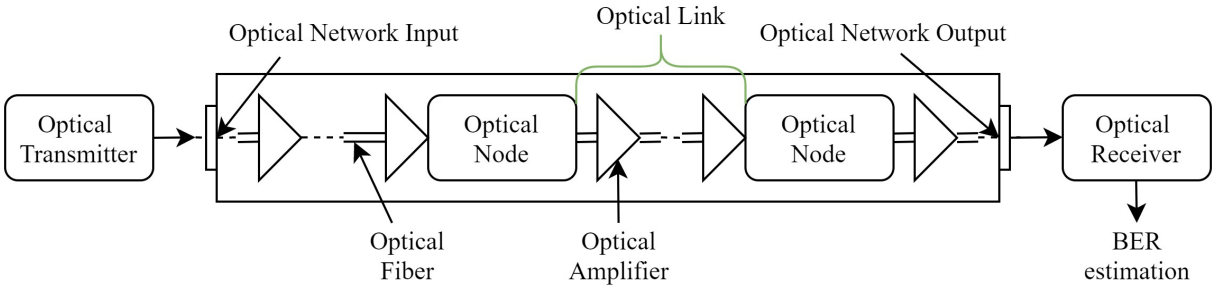

FIGURE 4.1: Optical communication network simulation model.

4.2.1 Optical transmitter

The optical transmitter is composed by four electrical blocks, as depicted in Fig. 4.2, whose functions are the generation of bits sequence, the mapping to QAM modulation, the sampling and the root raised cosine (RRC) shaping filter.

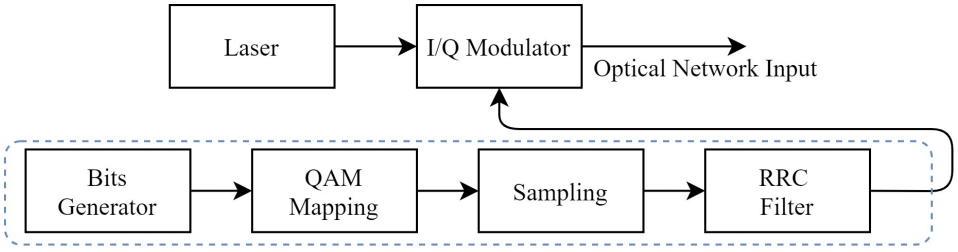

FIGURE 4.2: Optical transmitter simulation model.

An ideal optical transmitter is assumed in this work. This means that the electrical QAM signal is converted linearly to the optical domain without any impact from the optical transmitter limitations [43].

The most common modulation format in links with data rates of 200 and 400 Gb/s and coherent detection is the 16QAM modulation with 32 GBaud and 64 GBaud, respectively, hence being the main chosen modulation format to study in this work [27], [44]. The 32QAM has also been proposed for data rates of 250 and 500 Gb/s, but with a lower reach, and is also studied in this work [27], [44].

In order to obtain reliable results, it is important, in computer simulations, to choose an adequate symbol sequence for the data sequence. We simulate 16QAM and 32QAM signals in this work by generating a pseudo-random binary Bruijn sequence with 2^{12} bits and mapping it to 16QAM and 32QAM symbols using Gray coding. In our simulator, a sequence of 1024 and 819 symbols is generated, respectively, for the 16QAM and 32QAM. Tables 4.1 and 4.2 shows the mappings used for the 16QAM and 32QAM signals, respectively. The corresponding constellations and eye diagrams at the optical receiver output in a back-to-back scenario, are shown in Figs. 4.3 and 4.4, respectively.

Symbol	Bits	Mapped symbol	Symbol	Bits	Mapped symbol
1	0000	-3-3j	9	1000	3-3j
2	0001	-3-j	10	1001	3-j
3	0010	-3+3j	11	1010	3+3j
4	0011	-3+j	12	1011	3+j
5	0100	-1-3j	13	1100	1-3j
6	0101	-1-j	14	1101	1-j
7	0110	-1+3j	15	1110	1+3j
8	0111	-1+j	16	1111	1+j

TABLE 4.1: 16QAM bits to symbol mapping.

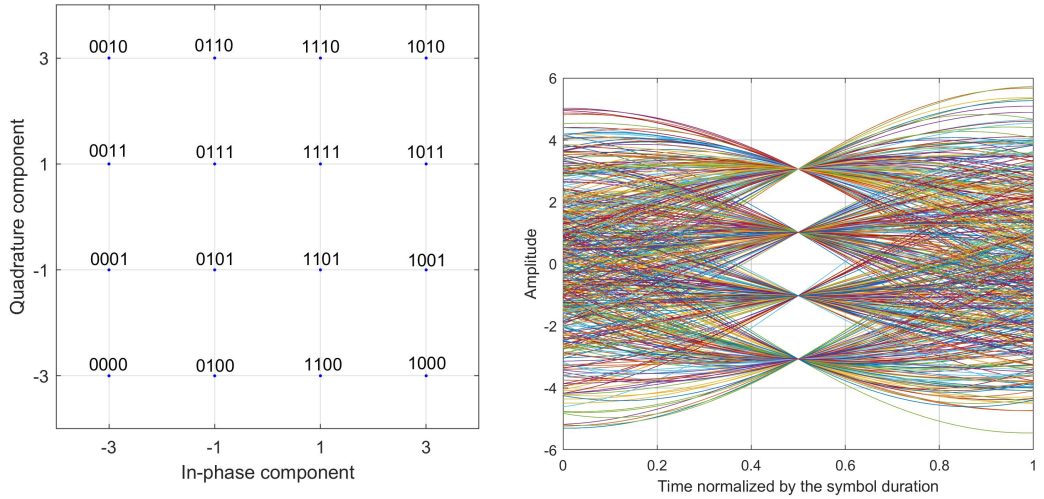

a) b)

FIGURE 4.3: Ideal 16QAM constellation (a) and eye diagram at the receiver output (b).

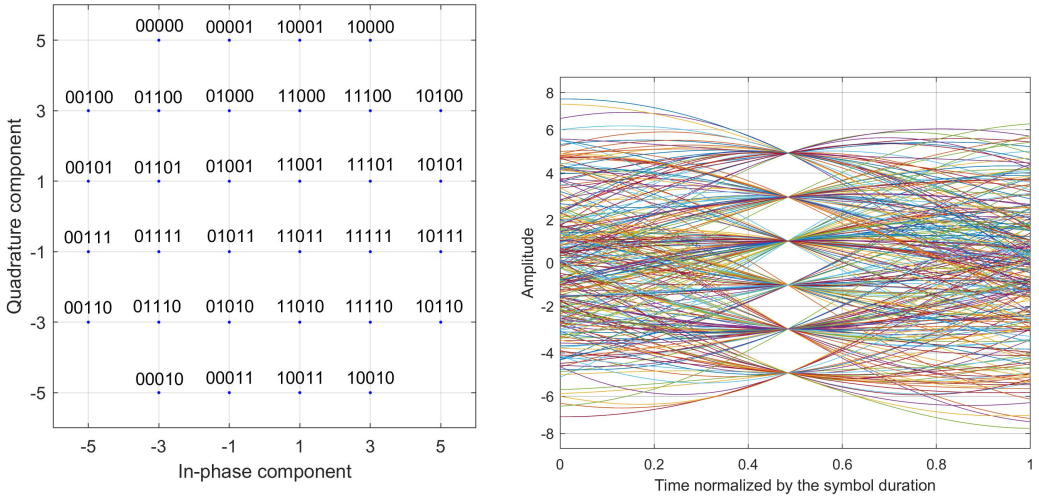

a) b)

FIGURE 4.4: 32QAM Constellation (a) and eye diagram (b) at the receiver output.

Symbol	Bits	Mapped symbol	Symbol	Bits	Mapped symbol
1	00000	-3+5*j*	17	10000	3+5*j*
2	00001	-1+5*j*	18	10001	1+5*j*
3	00010	-3-5*j*	19	10010	3-5*j*
4	00011	-1-5*j*	20	10011	1-5*j*
5	00100	-5+3*j*	21	10100	5+3*j*
6	00101	-5+*j*	22	10101	5+*j*
7	00110	-5-3*j*	23	10110	5-3*j*
8	00111	-5-*j*	24	10111	5-*j*
9	01000	-1+3*j*	25	11000	1+3*j*
10	01001	-1+*j*	26	11001	1+*j*
11	01010	-1-3*j*	27	11010	1-3*j*
12	01011	-1-*j*	28	11011	1-*j*
13	01100	-3+3*j*	29	11100	3+3*j*
14	01101	-3+*j*	30	11101	3+*j*
15	01110	-3-3*j*	31	11110	3-3*j*
16	01111	-3-*j*	32	11111	3-*j*

TABLE 4.2: 32QAM bits to symbol mapping.

In MATLAB the symbols sequences are represented by discrete vectors in the time or in the frequency domain. The time vector has $N_s N_a$ positions, where N_s is the number of simulated symbols and N_a is the number of samples per symbol. After mapping, the sequence is discretized with $N_a = 64$ samples per symbol using Nyquist pulse shaping. The frequency vector, which has the same number of positions as the time vector, is obtained by computing the Fast Fourier Transform of the time vector.

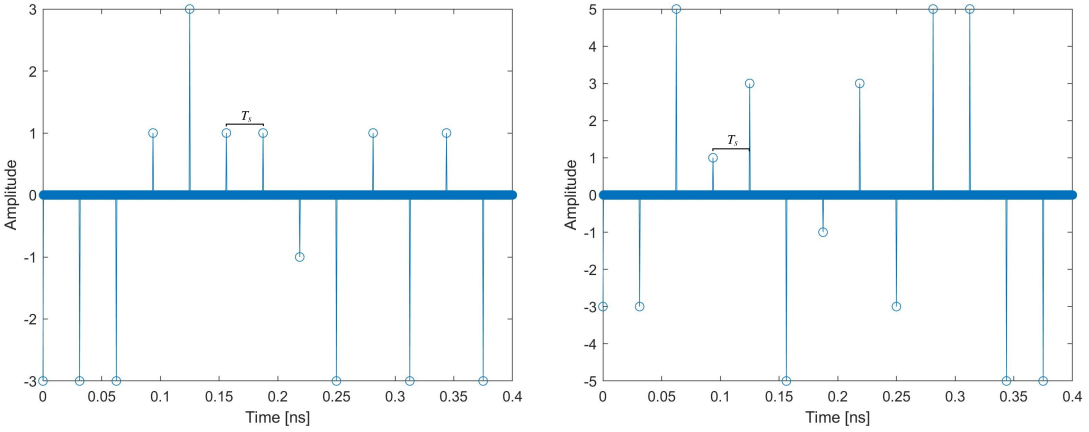

FIGURE 4.5: 16QAM (a) and 32QAM(b) Dirac impulses after sampling with 32 GBaud symbol rate.

The Nyquist pulse shaping is implemented by emulating a Dirac pulse at the beginning of each symbol, as shown in Fig. 4.5 for 13 generated 16QAM (a) and 32QAM (b) symbols in the in-phase component. Then, the signal composed by all the Diracs is applied to a RRC Nyquist pulse filter with a roll-off ρ of 0.1. This filter transfer function is obtained by applying a square root to the raised cossine (RC) filter transfer function, i.e. $H_{RRC}(f) = \sqrt{H_{RC}(f)}$. The RC filter transfer function assumes a rectangular shape in the frequency domain and a perfect *sinc* shape in the time domain for $\rho = 0$ and its transfer function is modeled by [45]:

$$H_{RC}(f) = \begin{cases} 1\,, & 0 \leq |f| < \frac{1-\rho}{2T_s} \\ \cos[\,\frac{\pi T_s}{2\rho}(|f| - \frac{1-\rho}{2T_s})]^2\,, & \frac{1-\rho}{2T_s} \leq |f| \leq \frac{1+\rho}{2T_s} \\ 0\,, & |f| > \frac{1+\rho}{2T_s} \end{cases} \tag{4.1}$$

where f is the low-pass equivalent frequency and T_s is the symbol duration.

The RRC filter bandwidth B_{RRC} is related to the symbol rate R_s and roll-off factor ρ by [45]

$$B_{RRC} = R_s \cdot (1 + \rho) \tag{4.2}$$

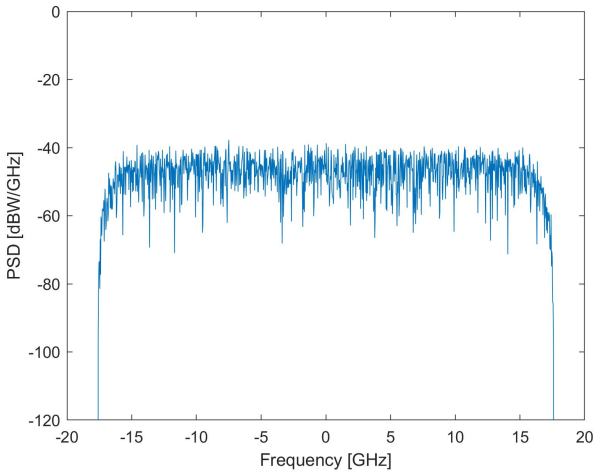

FIGURE 4.6: PSD of the 16QAM signal, with 32 GBaud and 0 dBm launch power, at the optical transmitter output (after RRC filtering).

After passing through the RRC filter, the signal power spectral density (PSD) assumes the shape of the filter, as shown in Fig. 4.6 for a 16QAM signal, and has a bandwidth of 32 GHz for the 32 GBaud symbol rate. The PSD for the 32QAM signal is similar to the one presented in Fig. 4.6.

4.2.2 Optical fiber

In order for the signal to travel through the network, it must be transmitted in a guided medium, such as an optical fiber. Besides other advantages, the optical fiber has an extremely large bandwidth and low attenuation, about 0.25 dB/km [16], that allows for a very high capacity transmission and long reach. Hence, nowadays, the optical fiber is the most important transmission medium that supports the overall telecommunications infrastructure and its increasing demand for data traffic.

However, the optical fiber can introduce different impairments such as signal attenuation, dispersion and non-linear effects, that degrade the transmission performance [46]. The optical signal attenuation can be compensated by optical amplification in the network. The optical dispersion, either chromatic or polarization mode dispersion, can be mitigated by the DSPs present in the coherent detectors [47]. Furthermore, the DSPs of the coherent receiver can also compensate some of the nonlinearities impact [48].

Our main focus is to study the impact of ASE noise, optical filtering and in-band crosstalk in the performance of the optical network, considering the node architectures studied in Chapter 2. We assume an ideal fiber transmission in the optical network simulation model, and neglect the optical fiber

impairments that can mask the impact of the physical layer impairments we intend to study on the network performance.

4.2.3 Optical filters, splitters and switches

In the simulation, we use two types of optical filters to model the WSS component: one to model the passband filter transfer function $H_p(f)$ and other to model the stopband filter transfer function $H_b(f)$. The signals that go through the WSS are filtered by the passband filter, while the signals that are blocked by the WSS are filtered by the stopband filter.

The optical passband filter is modeled by a super-Gaussian transfer function given by [49]

$$H_p(f) = \exp\left[-(f^2/2\sigma_{sg}^2)^n\right], \tag{4.3}$$

where n is the super-Gaussian order and σ_{sg} is related to the m-dB bandwidth of the super-Gaussian filter, BW_{mdB}, given by [49]

$$\sigma_{sg} = \frac{BW_{mdB}}{2\left[2\left(ln\sqrt{10^{\frac{m}{10}}}\right)^{\frac{1}{n}}\right]^{\frac{1}{2}}}. \tag{4.4}$$

The optical stopband filter is modeled by the inversion of the passband filter transfer function and by setting a blocking amplitude A, in dB. The transfer function of the stopband is given by [49]

$$H_b(f) = 1 - (1 - a) \times \exp\left[-(f^2/2\sigma_{sg}^2)^n\right], \tag{4.5}$$

where a is the blocking amplitude of the stopband filter $H_b(f)$ in linear units, $a = 10^{\frac{A[dB]}{20}}$. The transfer functions of a super-Gaussian filter with $BW_{-3dB} = 46.4$ GHz and $n = 5.5$ for the 50 GHz channel spacing [50] are represented in Fig. 4.7, a) represents the passband filter transfer function and b) represents the stopband filter transfer function for the WSS blocking amplitude of −40 dB and −60 dB.

The optical switches are modeled by considering a small insertion loss on the switched signal and the optical stopband filter, $H_b(f)$, is also used to model the signal leakage on optical switches present in the A/D structure. This signal leakage originates the in-band crosstalk that impairs the signal.

An important feature of the optical passband filtering occurs when the signal goes through a cascade of several nodes until its final destination. When the primary signal is filtered by several passband filters, the passband width will narrow and the signal can experience a severe distortion. This effect is known as passband narrowing effect [16], [46], [51]. This effect has a great impact on the network performance and it is more noticeable on networks based on R&S ROADM nodes, since they have, at least, one more filtering stage per node than B&S nodes [16]. On interconnected A architecture based ROADMs,

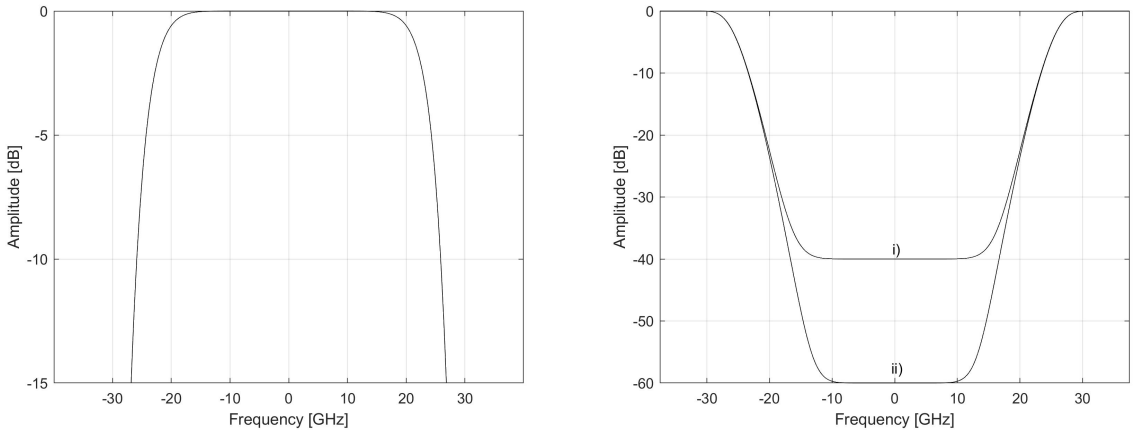

FIGURE 4.7: Transfer functions of the (a) super-Gaussian passband filter $H_p(f)$ and (b) the super-Gaussian stopband filter $H_b(f)$ with different blocking amplitudes i) -40 dB and ii) -60 dB.

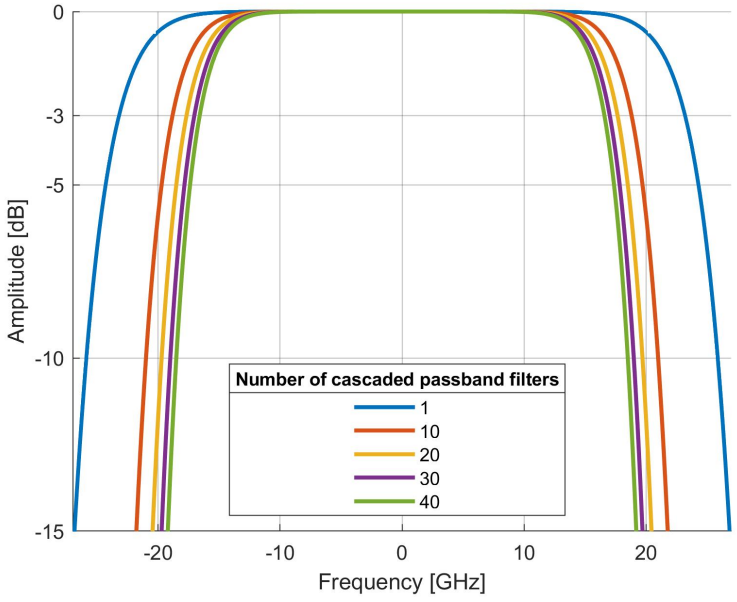

FIGURE 4.8: Passband narrowing of the optical filter $H_p(f)$ for a super-Gaussian filter with $B_o = 46.4$ GHz and $n = 5.5$ after passing through several passband filters.

the signal passes through more WSSs than in conventional B&S or R&S nodes. On a conventional architecture, for example, if the signal passes through 10 nodes until its destination, it crosses 10 or 20 WSSs filtering stages, in case of, respectively, B&S or R&S architectures. On the studied interconnected A sub-ROADMs architecture with zero hops, the signal undergoes at least two more WSSs (the small 1×2 WSSs that connect the A/D structure) per node, passing through 30 or 40 WSS filtering stages , in

case of, respectively, B&S or R&S architectures.

The passband narrowing effect is depicted in Fig. 4.8, for 1 to 40 filters ($\simeq$ 10 interconnected A nodes), where the −3 dB bandwidth narrows from 46.4 GHz to 33.2 GHz ($\simeq$13 GHz). This effect distorts the signal waveform and decreases its power, hence contributing to a lower OSNR at the optical receiver.

The optical splitters split the signal power equally by all the outputs and can be modeled by simulating a signal power reduction equal to the splitter optical loss calculated as a function of its splitting ratio, using Eq. (2.11).

4.2.4 Optical amplifier

As mentioned before, the optical fiber and also the different components in the optical nodes, introduce attenuation on the optical signal. In order to compensate the attenuation due to path losses, optical amplification is required [46]. At all optical nodes, optical amplifiers (OA) are used in order to compensate the path losses, at the ROADM input, and power losses inside the node, at the ROADM output [52].

There are three main types of OA: EDFAs, semiconductor optical amplifiers and Raman Amplifiers [46]. The one that is most commonly used in optical communications in the C-Band and considered in this work, is the EDFA. This type of OA is capable of achieving high gain, about 30 dB, and operates in the C band (1530 – 1565 nm) [53].

The downside is that optical amplification also adds ASE noise to the signal, that degrades the system performance [46]. The OAs used in this simulator are assumed to fully compensate the network losses, adding only ASE noise to the signal. The ASE noise power is defined by setting the OSNR at the OA output in the optical spectrum analyzer (OSA) bandwidth, defined by

$$OSNR = \frac{P_{out}}{P_{ASE}} , \tag{4.6}$$

where P_{out} is the average power of the signal at the OA output, and the P_{ASE} is the average power of the ASE noise added to the signal by the OA, which is defined by

$$P_{ASE} = N_{ASE} B_{OSA} , \tag{4.7}$$

where B_{OSA} is the OSA bandwidth with the typical value of 12.5 GHz and is related to the simulation bandwidth B_{sim} by [54]

$$B_{OSA} = \frac{B_{sim} N_{ASE}}{P_{ASE}} \quad . \tag{4.8}$$

In Eq. (4.7) and (4.8), the PSD of the generated ASE noise per signal polarization is represented by N_{ASE} and defined by

$$N_{ASE} = \frac{f_n}{2} (g - 1)\, h\, \upsilon_o \quad , \tag{4.9}$$

where f_n is the EDFA noise figure, g is the EDFA gain, h is the Planck constant and υ_o is the carrier frequency of the optical signal. The ASE noise is considered to be an Additive White Gaussian Noise (AWGN) [46], [55].

4.2.5 Optical coherent receiver

The model used for the optical coherent receiver is described in this subsection. Fig. 4.9 displays the optical coherent receiver block diagram with one single polarization, as considered in this study. Since, in this work, we assume an ideal receiver, the performance of the receiver can be evaluated for a single signal polarization using only the structure of Fig. 4.9 [56]. The optical coherent receiver structure for a single signal polarization consists of a 2x4 90º hybrid and two balanced photodetectors after the hybrid. The hybrid, as seen in Fig. 4.9, is composed by four 3 dB couplers and a 90º phase shifter in the lower branch. This allows the receiver to detect both the in-phase and quadrature signal components of the photodetected current, $I_i(t)$ and $I_q(t)$, respectively.

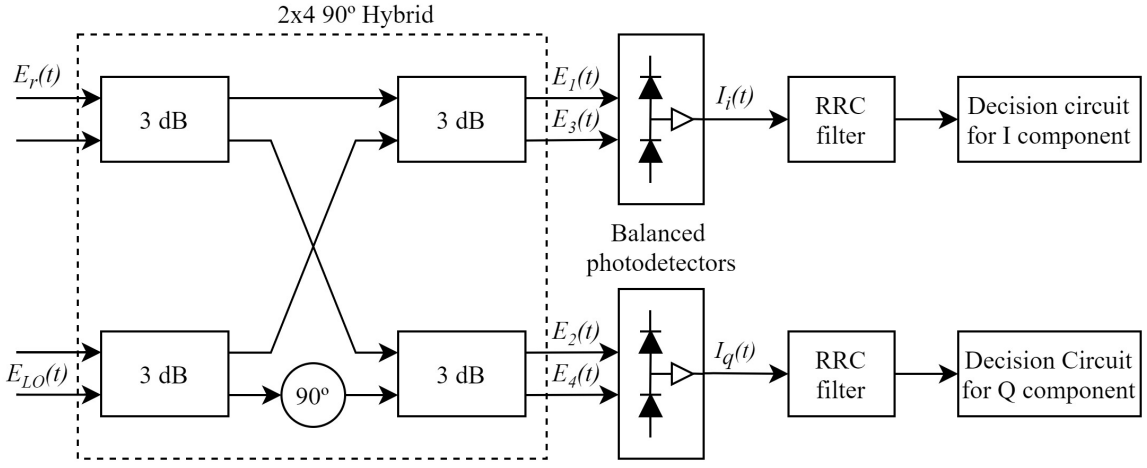

FIGURE 4.9: Optical coherent receiver block diagram, for a single polarization of the incoming optical signal.

In Fig. 4.9, $E_r(t)$ and $E_{LO}(t)$ represent the complex envelope of received signal (at the optical network output) and local oscillator (LO) field, respectively. The 2×4 90º hybrid is described by the following input/output relationship [57]:

$$E_1(t) = \sqrt{1-\varepsilon}E_r(t) + \sqrt{\varepsilon}E_{LO}(t) \tag{4.10}$$

$$E_2(t) = -\sqrt{\varepsilon}E_r(t) + \sqrt{1-\varepsilon}E_{LO}(t) \tag{4.11}$$

$$E_3(t) = \sqrt{1-\varepsilon}E_r(t) + j\sqrt{\varepsilon}E_{LO}(t) \tag{4.12}$$

$$E_4(t) = -\sqrt{\varepsilon}E_r(t) + j\sqrt{1-\varepsilon}E_{LO}(t) \tag{4.13}$$

where the sign of the signal term originates from energy conservation within the lossless beam splitters with power transmission ε (ideally, $\varepsilon = 0.5$), and the multiplication by j is due to the phase shift of the LO within the 90-degree optical hybrid.

The LO is an essential component of the coherent receiver as it allows it to detect both in-phase and quadrature components of the incoming QAM signal. To optimize the coherent performance of the receiver, the LO frequency must be as close as possible to the optical carrier frequency [58]. In this work, we considered that the LO is completely synchronized with the frequency of the optical carrier.

Each balanced photodetector shown in Fig. 4.9, often used in conjunction with the hybrid [59], transforms the optical signal into an electrical signal. The photodetection process can be represented by [46]

$$I_i(t) = 2R_\lambda\{E_s(t)E_{LO}^* + N(t)E_{LO}^*\} \tag{4.14}$$

$$I_q(t) = 2R_\lambda\{E_s(t)jE_{LO}^* + N(t)E_{LO}^*\} \tag{4.15}$$

where R_λ is each photodetector responsivity in [A/W]. In this study, for simplification, we will consider that the responsivity of each photodetector is $R_\lambda = 1$[A/W].

After photodetection, as shown in Fig. 4.9, each detected current passes through a matched filter [60] to reduce the ISI and noise and increase the OSNR [61]. Ideally, this filter shape has to be the same as the incoming signal. Hence, we consider an RRC filter as the one used at the optical transmitter. Finally, the decision circuit decides which symbol has been received.

4.3 MC simulation flowchart

The MC simulation method is a widely known technique used in statistical simulation in several scientific areas, where the influence of a stochastic process in a specific system must be characterized and described. The MC simulation flow-chart depicted in Fig. 4.10 [62], represents the simulator implemented in MATLAB to evaluate the performance of the optical communication network analyzed in this dissertation.

The first iteration of the MC simulation is used to save the reference signal (the transmitted signal), without adding any statistical sample function. With this reference signal, the receiver can obtain the propagation delay of the optical network and the optimum sampling instant from the received signal eye diagram. From the obtained delay, the synchronism between the received (impaired by statistical effects) and transmitted signal can be achieved.

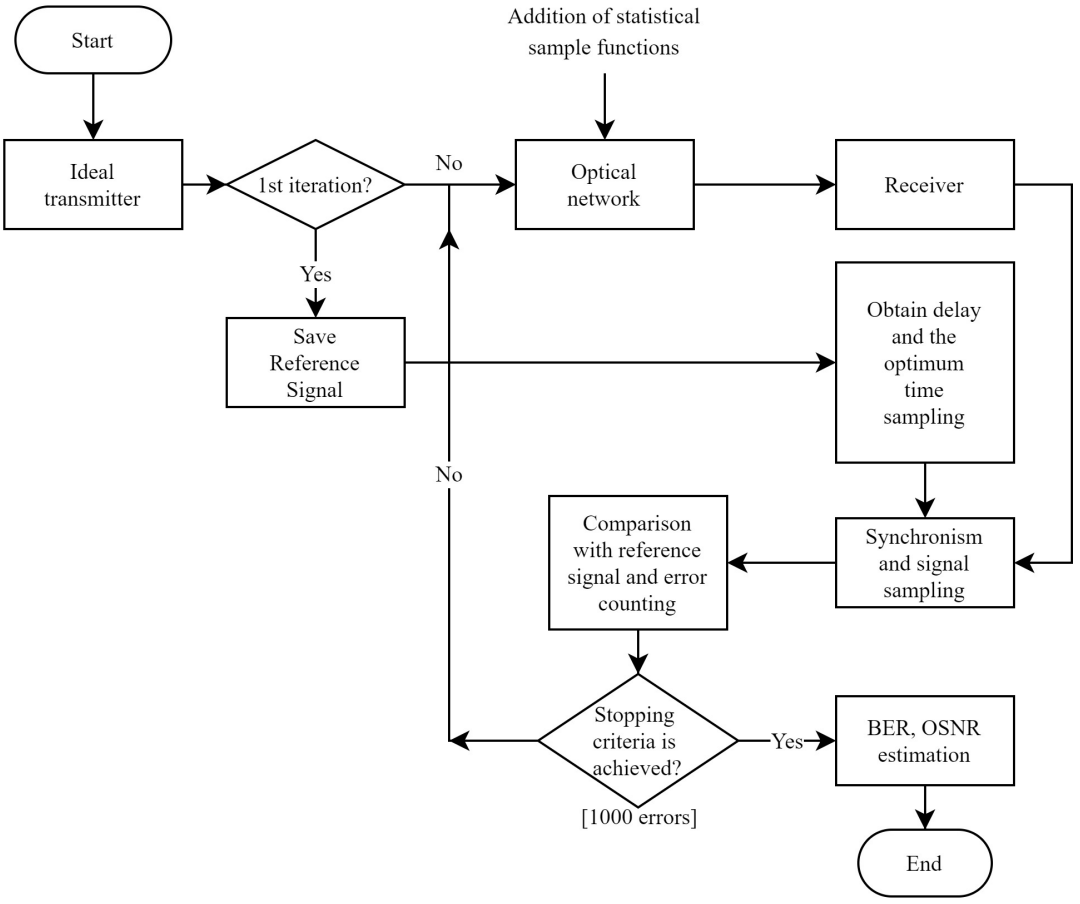

FIGURE 4.10: MC simulation flow-chart used to estimate the impact of the network impairments (ASE noise and in-band crosstalk) and obtain the BER and corresponding OSNR of the optical communication network.

Next, on the subsequent MC iterations, the statistical sample functions are applied to the signal along the simulated optical network. At the end of each iteration of the MC simulation, the received signal is compared to the reference signal to check if there are errors in the received signal. This process is called DEC. The MC simulator stops when a specific number of errors is reached, and the BER is calculated.

The ASE noise, filtering effect and interfering in-band signals will be the main cause of errors in our network simulation model. In each iteration of the MC simulator, statistical sample functions representing the ASE noise and in-band crosstalk are generated. The stopping criteria, in all MC simulation, is a total of 1000 symbol errors in order to obtain a BER estimation and corresponding OSNR as most accurate as possible, without demanding a significant simulation time [62].

In the simulation, the crosstalk signals are generated with the same characteristics of the primary signal (modulation format, number of symbols and transmitted signal power). In each iteration of the MC simulator, the bits of the interfering signals are generated randomly, and the interfering signal electrical field is generated with a random time delay that follows a uniform distribution between $]0, T_s]$ and a random phase difference uniformly distributed between $]0, 2\pi]$, in relation to the primary signal. The ASE noise is generated in two possible ways: using a noise loading circuit at the output of the optical network or generated discretely at each optical amplification stage. When noise loading is used, the noise power required to set a desired value of OSNR is calculated and then generated and added to the signal at the optical receiver input. When generated inside the OAs, the noise PSD is calculated using Eq. (4.9) as a function of the amplifier noise figure and gain, and then multiplied by the simulation bandwidth.

4.4 Performance evaluation methods

The BER performance metric used in this work is the most used metric in optical communication systems and is estimated by the DEC method. The BER is obtained by the ratio between the number of bits errors and the total number of transmitted bits in the simulation. By assuming Gray mapping, the BER is defined by [62], [63]

$$BER = \frac{N_e}{N_{MC} N_b (\log_2 M)} \tag{4.16}$$

where N_e is the number of counted bit errors, N_{MC} is the number of MC iterations, N_b is the number of transmitted bits in one MC iteration and M is the modulation order format. The system performance will be evaluated for a pre-FEC BER (or line BER) equal to 10^{-2}, since after the use of the forward error correction (FEC), the optical communication systems are able to achieve a much lower post-FEC BER,

around 10^{-15} or lower [64]. The FEC techniques are usually implemented at coherent detection optical receiver DSP circuits.

Another metric that is used in order to evaluate the performance of the optical communication network is the OSNR penalty. This metric consists of assessing the required OSNR at a specified BER without a particular impairment and, then, considering the desired impairment, the OSNR is obtained for the same BER. The OSNR penalty due to that physical impairment can be estimated from the difference between the required OSNRs with and without that specific impairment. The OSNR penalty due to in-band crosstalk and optical filtering is evaluated for a pre-FEC BER of 10^{-2}.

4.5 Conclusions

We have presented and described a generic model of the optical communication network, along with the MATLAB model used in the simulator. We also described in more detail the optical components and models used in this work, such as the RRC filter and WSSs, as well as the other network components, such as the optical fiber and optical amplifier. The generation of 16QAM and 32QAM signals was also described.

Lastly, the MC simulation was described with the help of a flow-chart and the performance evaluation methods used in this work, BER, estimated by DEC, and OSNR estimation and corresponding penalty were presented.

Chapter 5

Network performance assessment in the presence of physical impairments

5.1 Introduction

In this chapter, the performance of a 32 GBaud 16QAM and 32QAM signal, with 200 Gb/s and 250 Gb/s, respectively, impaired by the optical filtering effect, ASE noise and in-band crosstalk along a cascade of ROADMs based on interconnected A architecture with a bank-based A/D architecture is evaluated using MC simulation. We chose this architecture over the other large-scale architectures studied in Chapters 2 and 3, because the interconnected A has a significant cost reduction in hardware, as can be seen in Fig. 2.23, while having a similar performance in terms of in-band crosstalk generation, in comparison to the interconnected B and much less in-band crosstalk than the FLEX architecture. At the receiver, the BER is assessed with the DEC method and also through the OSNR. The OSNR penalty due to these impairments is also studied, by comparing the studied scenario with a reference scenario composed by two nodes, the add node and the drop node.

First, the simulator validation is made on a back-to-back scenario in Section 5.2 and a reference OSNR for each modulation format and architecture configuration is obtained. In Section 5.3, the optical filtering penalty induced by several cascaded nodes is analyzed using noise loading at the optical receiver input. In Section 5.4, each ASE noise term is added to the network model using lumped amplification. The OSNR degradation due to ASE noise accumulation is studied for several cascaded nodes and the maximum network reach is assessed. In Section 5.5, the OSNR penalty due to the presence of in-band crosstalk is evaluated for a network based on interconnected A architecture for the B&S and R&S configurations. The maximum network reach in presence of in-band crosstalk is also assessed. Section 5.6 presents the chapter main conclusions.

5.2 Back-to-back scenario validation

In this section, the implementation of the simulator that will be used to study the performance of the optical communication network, is firstly validated in back-to-back configuration without in-band

crosstalk and optical filtering, and considering only the ASE noise. The parameters used to study this scenario are shown in Table 5.1. The output signal is impaired by the addition of ASE noise through noise loading at the optical receiver input in order to study the BER in the simpler scenario shown in Fig. 5.1. The ASE noise power is set by imposing the OSNR at the coherent receiver input so that a BER = 10^{-2} is achieved.

Modulation format		16QAM	32QAM
Signal power at the transmitter	P_{Tx}	0 dBm	
Baud rate	R_s	32 GBaud	
RRC filter roll-off factor	ρ	0.1	
Information bit rate (per polarization)	$R_{b,\,i}$	100 Gb/s	125 Gb/s
Number of symbols	N_s	1024	819
Number of samples	N_a	64	
Reference optical bandwidth	B_{ref}	12.5 GHz	
Target BER		10^{-2}	
MC stopping criteria		1000 counted errors	

TABLE 5.1: MC simulation parameters used for validation.

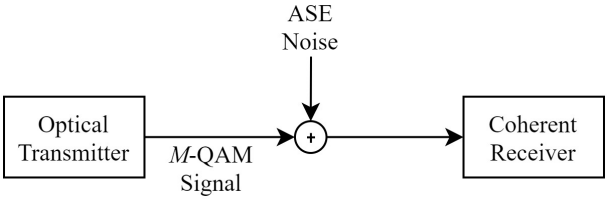

FIGURE 5.1: Simulation model in a back-to-back configuration for validation purposes.

The simulation model shown in Fig. 5.1 is used to find the reference OSNR, the OSNR required to reach the BER of 10^{-2}, in presence of ASE and absence of ISI, in a back-to-back configuration. In this case, the OSNR is imposed at the optical receiver input by changing the ASE noise power, while keeping the signal noise power constant. Fig. 5.2 shows the BER as a function of the required OSNR for two modulation formats: 16QAM and 32QAM at 32 Gbaud. The required OSNR, i.e., the reference OSNR, is 18 dB and 21 dB for the 16QAM and 32QAM modulations, respectively. The obtained results are in a

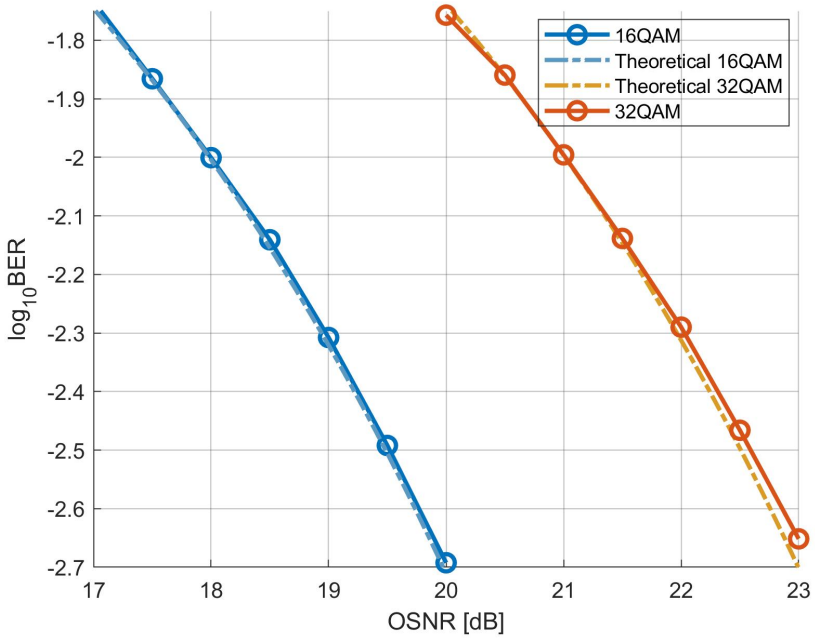

FIGURE 5.2: BER as a function of the required OSNR for a 32 GBaud Nyquist shaped 16QAM and 32QAM signal in a back-to-back configuration.

very good agreement with the theoretical values obtained using the following equations [6], [65]

$$P_{b,16\text{QAM}} \approx \frac{3}{8} \cdot \text{erfc}\left(\sqrt{\frac{4}{10} snr_b}\right), \tag{5.1}$$

$$P_{b,32\text{QAM}} \approx \frac{91}{240} \cdot \text{erfc}\left(\sqrt{\frac{snr_b}{4}}\right), \tag{5.2}$$

$$snr_b = \frac{2B_{ref} \cdot osnr_{req}}{R_{b,\,i}}, \tag{5.3}$$

where P_b is the BER for each modulation, snr_b is the electrical signal-to-noise ratio (SNR) per bit in linear units, $osnr_{req}$ is the required OSNR in linear units, p is 1 for single signal polarization and 2 for dual signal polarization. The results are also in agreement with other similar studies [57], [66]. This good agreement leads to the conclusion that the MC simulator and the BER assessment are well implemented for a back-to-back configuration with ASE noise loading.

5.3 Impact of optical filtering in a cascade of ROADM nodes with ASE noise loading

In order to study and analyze the impact of optical filtering in the network model using the interconnected A architecture and bank-based A/D structure, we considered the simulation model with an ASE noise loading approach at the end of the ROADM cascade, in order to set the OSNR level at the receiver input. Fig. 5.3 shows the simulation model used to study the optical filtering effect on the system performance. The additional simulation parameters considered, are presented in Table 5.2.

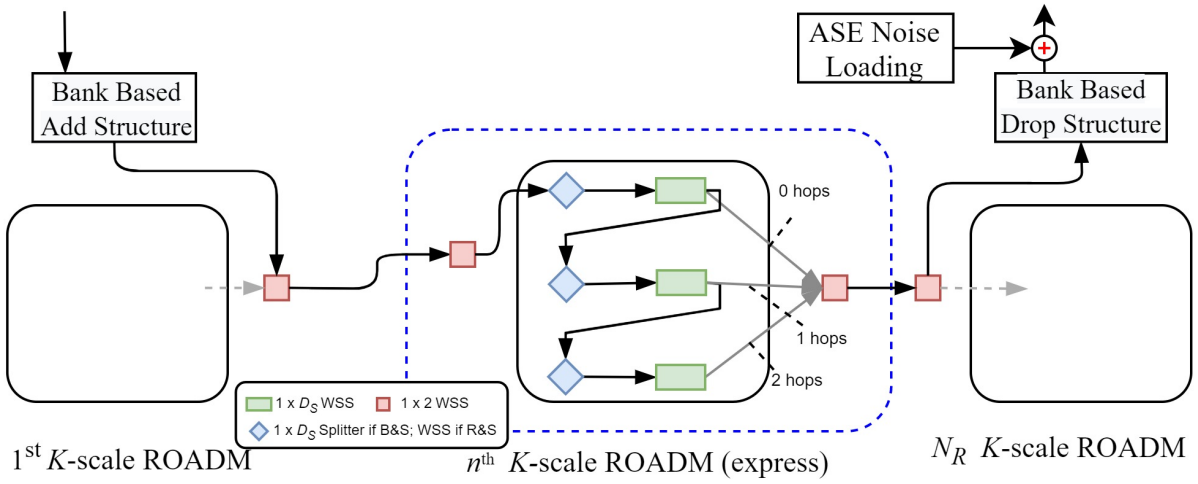

FIGURE 5.3: Simulation model of the optical network to study the optical filtering effect: reference situation with only 2 nodes, without the express ROADMs (inside the blue dashed line box), and with cascaded ROADM nodes between the add and drop nodes.

Number of hops between sub-ROADMs	n_{hops}	0, 1 and 2
WSS and splitter size in the sub-ROADMs	D_S	9
Maximum number of traversed ROADMs	N_R	10
ROADM scale	K	≥ 49

TABLE 5.2: Additional MC simulation parameters used for the optical filtering penalty study.

The primary signal coming from the optical transmitter output, passes through 2 to 10 nodes in the network, and for each case, the OSNR required to reach a target BER of 10^{-2} is estimated for the signal at the output of the optical network. The optical filtering penalty is extracted from the difference between the OSNR required to reach the target BER for a particular number of cascaded nodes and the OSNR required for the reference situation with only 2 nodes. The reference situation is the one where the

signal is added at the first ROADM node and dropped in the second node, without traversing the express ROADM nodes marked by a blue dashed line box in Fig. 5.3. When the number of ROADM nodes is larger than two, the express ROADM nodes are considered, where for each n^{th} node between the add and the drop one ($1 < n < N_R$), the signal is optically filtered by the small 1×2 and by the $1 \times D_s$ WSSs inside the express node, 3, 4 or 5 times, respectively, in case of 0, 1 or 2 hops configuration in the B&S interconnected A architecture. If a R&S architecture is considered, the signal is optically filtered 4, 6 or 8 times instead, respectively, in case of 0, 1 or 2 hops configuration. We considered a maximum number of 10 cascaded nodes, N_R, which gives us close to 500 km of reach, with 50 km fiber spans. Since the A/D structure considered is the bank-based, there is no incurred penalty due to WSS filtering inside these structures.

The WSS model used is a super-Gaussian filter [49] with a -3 dB bandwidth equal to 46.4 GHz for the 50 GHz channel spacing [50], which has been characterized in Section 4.2.3.

For a better comprehension of the effect of cascading optical filters, when using large-scale ROADM architectures, Fig. 5.4 quantifies the number of filtering stages as a function of number of hops and architecture configuration. As the number of hops increases, the total filtering stages increases linearly, as expected. The R&S also shows a higher number of filtering stages, due to the extra route WSS used in the configuration.

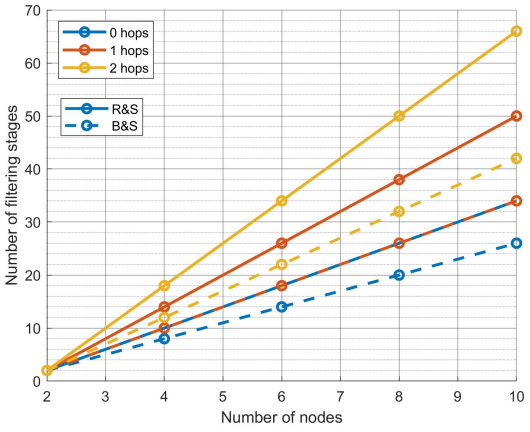

FIGURE 5.4: Number of filtering stages as a function of the number of cascaded interconnected A architecture nodes for 0, 1 and 2 hops and both B&S and R&S configurations.

Fig. 5.5 shows the BER as a function of the required OSNR for a signal that goes through 2, 4, 6, 8 and 10 R&S interconnected A architecture nodes with 2 hops, which is the most limiting case in terms of the number of filtering stages that the signal passes through. The OSNR penalty due to optical filtering can be extracted for a specific target BER from Fig. 5.5, by performing the difference between

the OSNR obtained for the reference situation with only 2 nodes and the OSNR estimated for a higher number of nodes. As the number of nodes increases, the required OSNR also increases, as expected, due to the enhanced signal distortion caused by the optical filtering. The 32QAM signal, which has a higher modulation format, is less robust to optical filtering.

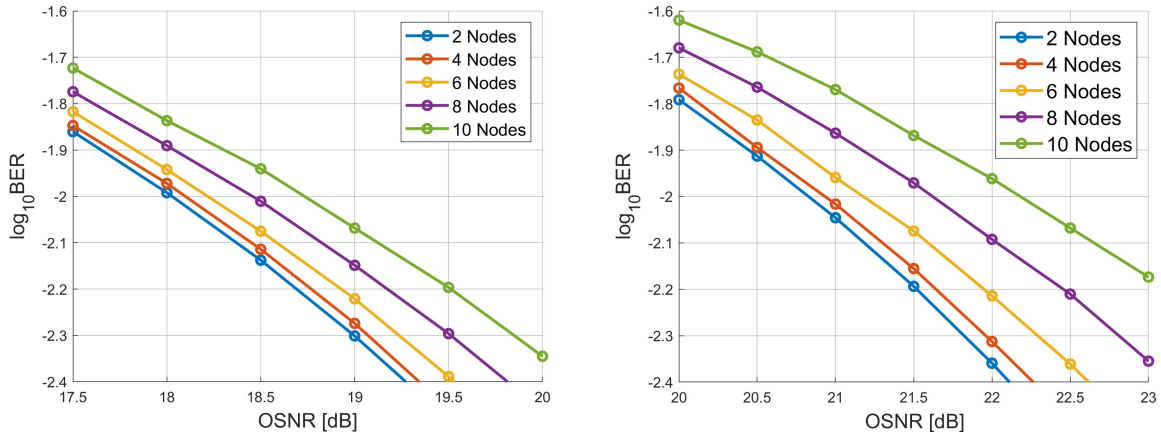

FIGURE 5.5: BER as a function of the required OSNR for a 32 GBaud Nyquist shaped 16QAM a) and 32QAM b) signals, with 2 hops for several cascaded interconnected R&S nodes.

The OSNR filtering penalty is depicted in Fig. 5.6, for a target BER of 10^{-2}, for different hop number configurations and both B&S and R&S architectures. Fig. 5.6 a) refers to a 32 Gbaud 16QAM signal and Fig. 5.6 b) to a 32QAM signal. The B&S architecture has a very low OSNR penalty for 0 and 1 hops, reaching less than 0.2 dB and 0.4 dB, respectively, for 16QAM and 32QAM modulation, after 10 cascaded nodes. On the other hand, the R&S architecture exhibits a higher OSNR penalty, that reaches 0.2 dB and 0.4 dB, for the 16QAM signal, and 0.4 dB and 0.8 dB, for the 32QAM signal, respectively, for 0 and 1 hops. The OSNR penalty, after 10 nodes with 2 hops, reaches about 0.3 dB and 0.7 dB for the 16QAM modulation, and 0.6 dB and 1.4 dB for the 32QAM modulation, respectively, for B&S and R&S architectures. The 32QAM exhibits practically twice the OSNR penalty of the 16QAM, regardless of the architecture configuration. As expected, as the number of hops increases, the optical filtering penalty also increases, due to the 1 or 2 additional filtering stages per hop, respectively, in case of B&S or R&S configurations. Regarding the comparison between the ROADM architectures, the B&S architecture shows a better performance, in comparison with the R&S architecture, as it has less filtering stages in the nodes. For 10 nodes with 2 hops, the B&S architecture has 24 less filtering stages in total than the R&S architecture, 3 in each express ROADM, translating into an improved performance of 0.4 dB and 0.8 dB for, respectively, 16QAM and 32QAM signals.

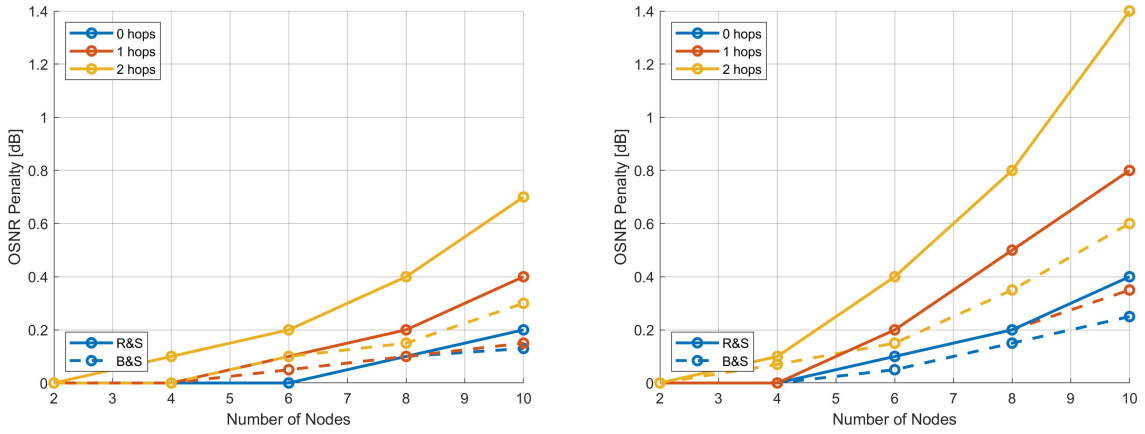

FIGURE 5.6: OSNR filtering penalty as a function of the number of cascaded nodes for a 32 GBaud Nyquist shaped 16QAM a) and 32QAM b) signals, for 0, 1 and 2 hop configurations.

Other optical filtering studies [10], [50], [66], typically study the optical filtering impact on the communication network performance only for a maximum of 20 cascaded WSS, which is equivalent to 10 R&S or 20 B&S conventional nodes. All these studies revealed a very marginal filtering penalty for a 16QAM signal with 50 GHz channel spacing, like in our study shown in Fig. 5.6 a). For 10 cascaded nodes, with the large-scale interconnected A ROADM node architecture and 2 hops, we have roughly two (B&S) or three (R&S) times the amount of cascaded WSSs (as shown in Fig. 5.4), in comparison with these other works that use conventional architectures. This much higher number of filtering stages lead to a non-negligible higher optical filtering penalty after 10 cascaded nodes.

Also in [24], albeit for a 25 GBaud non-return-to-zero (NRZ) QPSK signal, the OSNR filtering penalty for conventional R&S CDC ROADM nodes reaches 1.2 dB for 32 cascaded conventional nodes (64 filtering stages), with WSSs modelled as 4^{th} order Super-Gaussian filters with 41 GHz -3 dB bandwidth and a target BER of 10^{-3}. Note that in our study, the node architecture has two more filtering stages than in conventional ROADM nodes and also a higher modulation format. Although, not directly comparable, for a very high number of cascaded nodes, the optical filtering penalty shown in [24] becomes above 1 dB.

5.4 Impact of ASE noise and optical filtering in a cascade of ROADM nodes with lumped amplification

In this subsection, the impact of ASE noise arising from lumped amplification on a network composed by a cascade of interconnected A sub-ROADMs architecture nodes, using the bank-based A/D, is analyzed.

We considered, again, that the reference scenario corresponds to a signal that travels only through 2 nodes, the add node and the drop node. This scenario is depicted in Fig. 5.7, considering that the 1^{st} K-scale ROADM is connected directly to the last K-scale ROADM (i.e., by neglecting the express ROADMs). The corresponding amplification stages and amplifier characteristics are also depicted.

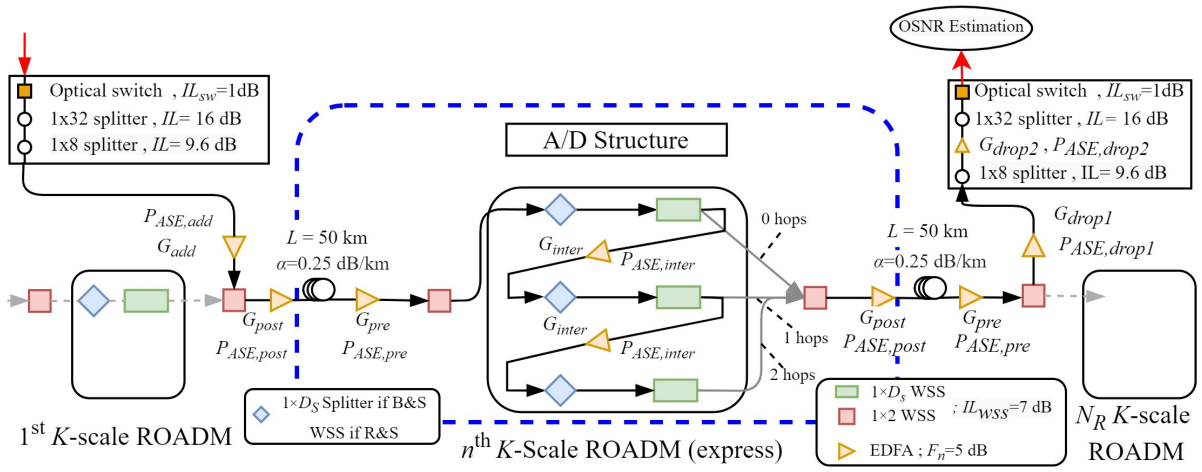

FIGURE 5.7: Simulation model of the optical network to study the accumulation of ASE noise and optical filtering impact.

The signal enters the network in the add structure followed by an EDFA with small gain G_{add} and generated noise power $P_{ASE,add}$ that partially compensates the add losses and a 2×1 WSS that makes the connection between the add structure and the express path. After this WSS, a post-amplifier with gain G_{post} and generated noise power $P_{ASE,post}$ compensates the express structure losses and uncompensated add structure losses. At the input of the last node, there is a pre-amplifier with gain G_{pre} and generated noise power $P_{ASE,pre}$ that fully compensates the fiber losses. Since the signal is to be dropped, it is sent to the drop structure by a 2×1 WSS. In our case, the drop losses are very high (33.7 dB) and an EDFA to compensate them would generate too much noise. In order to reduce the ASE noise generation, we use 2 EDFAs at the drop node, similarly to the multi-stage amplification solution shown in Fig. 2.25. In this way, the signal then passes by an amplifier named G_{drop1} with generated noise power $P_{ASE,drop1}$ and then goes to the bank-based drop structure, where before entering the bank, the losses are compensated by a second amplifier named G_{drop2} with generated noise power $P_{ASE,drop2}$.

When the number of ROADM nodes is larger than two, the model considered is the one depicted in Fig. 5.7 considering the nodes inside the dashed line box, where in each express node between the first and last nodes, regarding the optical amplification, the signal goes through a pre-amplifier and a post-amplifier, if the number of hops is 0. If the number of hops is 1 or 2, the signals passes through more, respectively, 1 or 2 amplifiers named G_{inter} with generated noise power $P_{ASE,inter}$, that compensate

the losses between the sub-ROADMs. In all subsequent studies, we always consider that $n_{hops} = 2$, which is the worst-case in terms of noise accumulation, in-band crosstalk and optical filter bandwidth narrowing. The optical losses of the optical splitters depicted in Fig. 5.7 are estimated using Eq. (2.11). The additional simulation parameters considered are presented in Table 5.3.

WDM channel spacing	Δf	50 GHz
Number of channels	N_{ch}	96
Number of transponders per bank	T_{bank}	32
Number of input fibers per bank	b	8
Number of hops between sub-ROADMs	n_{hops}	2

TABLE 5.3: Additional MC simulation parameters used for studying the optical filtering penalty and ASE noise accumulation.

The amplifier gains and corresponding generated ASE noise power at each amplifier depend on the architecture type used, where in case of a B&S configuration, the blue diamond component represents a $1 \times D_S$ splitter, and in case of a R&S configuration is a $1 \times D_S$ WSS. The gains considered in this work and corresponding ASE noise powers are shown in Table 5.4.

	Gain (dB)			$P_{ASE}(\mu W)$	
Architecture Type	B&S	R&S	Architecture Type	B&S	R&S
G_{add}	3.05	5.7	$P_{ASE_{add}}$	0.002	0.007
G_{post}	30.6	28	$P_{ASE_{post}}$	2.761	1.55
G_{pre}	12.5	12.5	$P_{ASE_{pre}}$	0.043	0.043
G_{inter}	16.6	14	$P_{ASE_{inter}}$	0.12	0.06
G_{drop_1}	16.6	16.6	$P_{ASE_{drop_1}}$	0.12	0.12
G_{drop_2}	17	17	$P_{ASE_{drop_2}}$	0.14	0.14

TABLE 5.4: EDFA gains and corresponding ASE noise powers used to study the optical filtering penalty and the ASE noise impact on the network performance.

First, we varied the transmitted signal power obtained for the reference scenario of Fig. 5.7, as depicted in Fig. 5.8, and obtained the transmitted signal power that leads to the target BER of 10^{-2}, and to the respective OSNRs of 18 dB and 21 dB, respectively, for the 16QAM and 32QAM formats. The transmitted signal powers extracted from Fig. 5.8 are displayed in Table 5.5. The B&S architecture requires about 1.5 dB higher signal power than the R&S architecture to reach the target BER, for both modulation formats. This happens due to the broadcast splitter in the B&S architecture having a higher loss in comparison with the WSS in the R&S architecture. Hence, the gain of the post-amplifier, G_{post}, is higher to compensate the additional losses and the corresponding degradation due to the increased ASE noise power, $P_{ASE_{post}}$, is higher for the B&S architecture. The total accumulated noise power measured at the optical receiver input in the reference scenario, before the OSNR estimation depicted in Fig. 5.7, is

-24.5 dBm and -26 dBm, respectively, for the B&S and R&S architectures, matching the 1.5 dB signal power difference found.

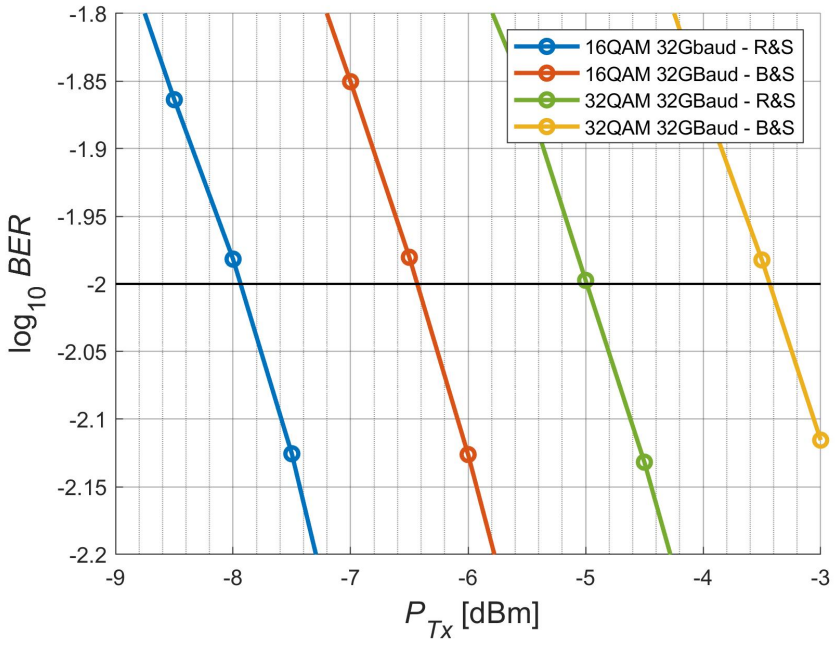

FIGURE 5.8: BER as a function of the transmitted signal power for 32 GBaud Nyquist shaped 16QAM and 32QAM signals, in both B&S and R&S configurations, in the reference situation.

	Architecture	
Modulation	BS	RS
16QAM	-6.4 dBm	-7.9 dBm
32QAM	-3.4 dBm	-5 dBm

TABLE 5.5: Transmitted signal powers for each modulation format for the target BER of 10^{-2} in the reference scenario, for B&S and R&S architectures.

Then, after obtaining the signal powers in the reference situation, we varied the number of nodes from 2 to 10, while maintaining the signal power at the transmitter output at the reference levels. Fig. 5.9 depicts the OSNR at the optical receiver input as a function of the number of cascaded nodes, considering the transmitted signal powers shown in Table 5.5. In this way, the ASE noise contribution to the OSNR degradation can be quantified by the difference between the reference scenario OSNR and the OSNR estimated for each number of cascaded nodes.

As depicted in Fig. 5.9 the degradation induced by the ASE noise on the OSNR is higher on the B&S architecture, for both modulations. This happens mainly because the post-amplifiers with gain G_{post} and the amplifiers between sub-ROADMs, with gain denoted as G_{inter}, have at least a 2 dB higher

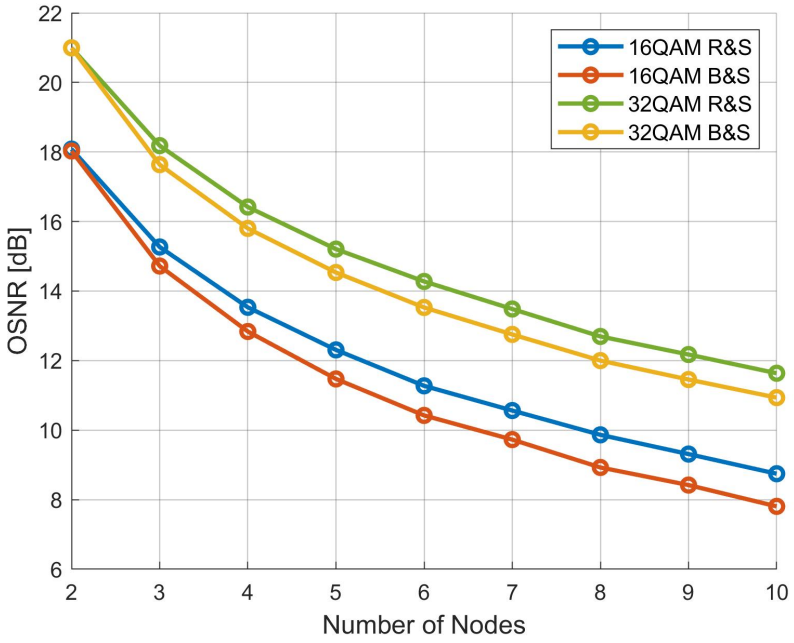

FIGURE 5.9: OSNR as a function of the number of cascaded interconnected A nodes with 2 hops for 32 GBaud Nyquist shaped 16QAM and 32QAM signals, in both B&S and R&S configurations, considering the ASE noise accumulation along the network.

gain in the B&S architecture due to the higher broadcast splitter losses in comparison to the route WSS used in the R&S architecture, hence, generating a higher ASE noise power. For 10 cascaded nodes, the 16QAM system has a OSNR reduction of 9.4 dB and 10.3 dB, in comparison with the OSNR for the reference scenario, for the R&S and B&S architectures, respectively, while the 32QAM system has a OSNR reduction of 9.1 dB and 9.8 dB, for the R&S and B&S, respectively.

Since the optical path losses are fully compensated, the decrease of OSNR with the number of cascaded nodes, due to the ASE noise power increase, and the optical filtering penalty can be compensated by raising the signal power output at the optical transmitter. To perform the next study, we establish two design considerations based on what is typically used in optical networks. First, we set the maximum signal power per WDM channel, $P_{max_{ch}}$, by considering a power level of 1 dBm at each ROADM input [10]. At the bank-based drop structure due to overcompensation of the optical losses, the amplifier with gain G_{drop_2} must have a maximum output power above 30 dBm [67]. Another possible implementation is to decrease the gain of this amplifier and compensate the remaining losses at the receiver DSP circuits. The second design consideration is setting a safety margin, SM, to the signal OSNR at the receiver input in order to account for additional system performance degradation caused by, for example, optical filtering, crosstalk between carriers and material aging [10]. The safety margin is defined in [10] as

$$SM\ [dB] = 0.05 \times N_R + P_{filt}\ + P_{interXT} \tag{5.4}$$

where $0.05 \times N_R$ is the considered penalty by material aging, P_{filt} is the optical filtering penalty in dB and $P_{interXT}$ is the intercarrier crosstalk penalty in dB, which, in this work, is considered as 0.5 dB [10]. Since the optical filtering penalty is already included in the MC simulator with lumped amplification, we set $P_{filt} = 0$. The safety margin is related to the required OSNR at the optical receiver input for the target BER, $OSNR_{req}$, by the relationship [10]

$$OSNR_{tot}\ [dB] = OSNR_{req}\ [dB] + SM\ [dB] + RM\ [dB] \tag{5.5}$$

where $OSNR_{tot}$ is the total required OSNR that must be met at the optical receiver input to account for the additional system performance degradation and RM is a residual margin. In our work, we have considered $RM = 0$ dB.

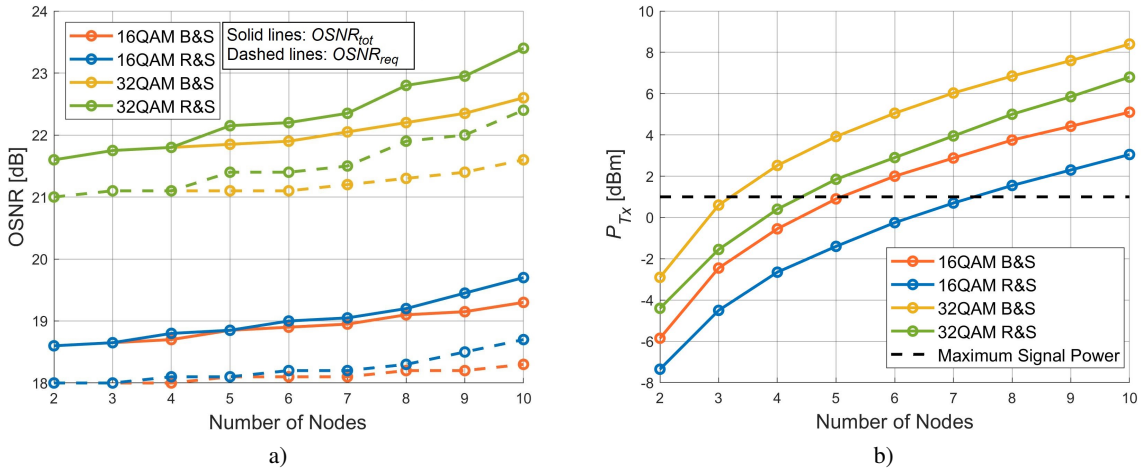

FIGURE 5.10: Required OSNR at the optical receiver input a) and transmitted signal power b) as a function of the number of cascaded interconnected A nodes with 2 hops, for 32 GBaud Nyquist shaped 16QAM and 32QAM signals and a target BER of 10^{-2}, in both B&S and R&S configurations.

In order to address the maximum reach in terms of cascaded ROADM nodes, the required OSNR at the optical receiver input and the required signal power at the transmitter for a BER of 10^{-2} as a function of the number of ROADM nodes transversed is shown in Figs. 5.10 a) and b), respectively. In Fig. 5.10 a), the dashed lines represent $OSNR_{req}$ and the solid lines show $OSNR_{tot}$ obtained by the simulator, including the optical filtering and ASE noise accumulation. In order to obtain the OSNRs at the optical receiver input accounting the additional margin, $OSNR_{tot}$, the transmitted signal powers must

be raised to the levels depicted in Fig. 5.10 b), for each number of nodes considered. The constraint regarding the maximum signal power of 1 dBm at the ROADM inputs is also plotted using a dashed black line. The optical filtering is already included in the simulator with lumped amplification and the optical filtering penalty can be extracted from Fig. 5.10 a), by subtracting the OSNR obtained for a specific number of cascaded nodes by the OSNR obtained for the reference situation of 2 nodes. From the results of Fig. 5.10, the optical filtering penalty with lumped amplification is very similar to the one estimated in Section 5.3, for ASE noise loading at the end of the filters cascade. For example, for 10 nodes, the optical filtering penalty is 0.7 dB and 1.4 dB, respectively, for a 16QAM and 32QAM signal in a R&S architecture, in agreement with the results of Fig. 5.6.

From Fig. 5.10 b), and considering 1 dBm signal power per channel as the limiting power, it can be concluded that the 16QAM signal allows a higher network reach of 5 and 7 nodes, while the 32QAM only allows 3 and 4 cascaded nodes, respectively, for B&S and R&S architectures. For a residual margin of 3 dB, the 16QAM signal would only allow 3 and 4 cascaded nodes, respectively, for B&S and R&S architectures, while the 32QAM signal only reaches 2 cascaded nodes for B&S and R&S architectures. The higher modulation format, 32QAM, is less resilient to node cascading, as expected [27], mainly due to the higher signal power required to achieve the target BER, in the reference scenario, which reduces the OSNR budget (or system margin). As predicted, the B&S architecture leads to a lower reach in comparison with the R&S architecture due to the ASE noise power accumulated along the optical path, whose effect in the performance degradation is stronger than the optical filtering penalty.

5.5 Impact of in-band crosstalk in a cascade of ROADM nodes with lumped amplification

In this subsection, the in-band crosstalk impairment is added to the simulation model and its impact on a network composed by a cascade of interconnected A sub-ROADMs architecture nodes, using the bank-based A/D structure is analyzed.

The interfering in-band signals follow the same path of the primary signal in the optical network, and also go through optical amplification stages at the ROADM inputs, outputs and also in the bank-based A/D structure, as depicted in Fig. 5.11. The number of in-band crosstalk signals originated in the A/D structure depends on the bank-based structure parameters, while the ones originated in express ROADMs differ in case of B&S or R&S configurations. As discussed in Section 3.3.1, we expect that the in-band crosstalk penalty is higher in the B&S interconnected A, which has 1^{st} order interferers than in a R&S interconnected A architecture, which has only 2^{nd} order interferers.

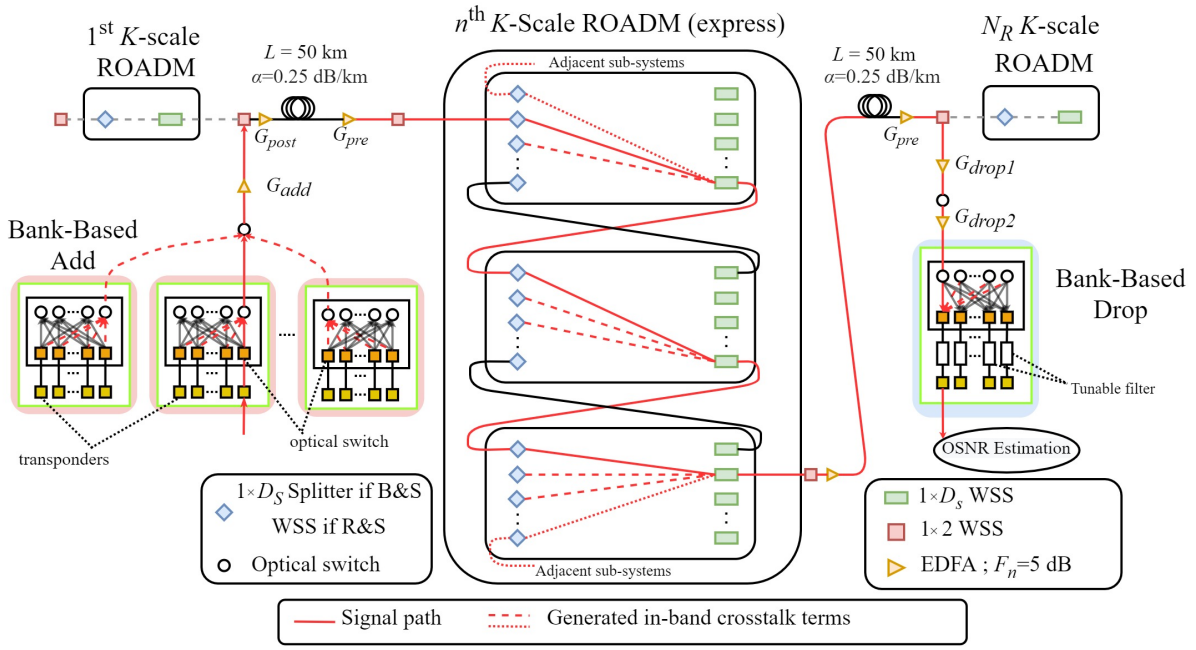

FIGURE 5.11: Simulation model of the optical network to study the in-band crosstalk impact.

The isolation level considered for the optical switches existing in the MCS and the blocking amplitude for the WSSs is -60 dB and -40 dB, respectively [50], [68].

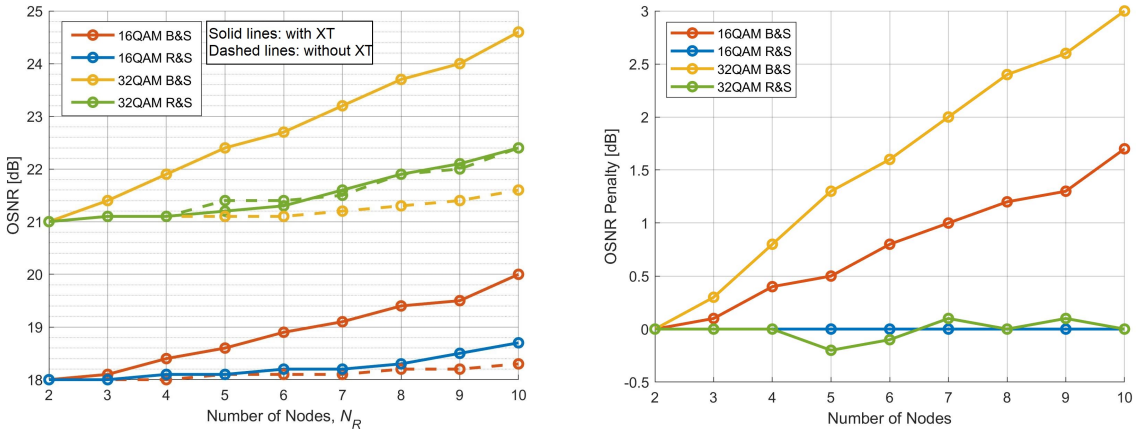

a) b)

FIGURE 5.12: Required OSNR a) and OSNR penalty due to in-band crosstalk b) at the optical receiver input as a function of the number of cascaded nodes, for 32 GBaud Nyquist shaped 16QAM and 32QAM signals and a target BER of 10^{-2}, in both B&S and R&S configurations.

Figs. 5.12 a) and b) depict the required OSNR and OSNR penalty due to in-band crosstalk at the optical receiver input, respectively, for the target BER of 10^{-2} as a function of the number of nodes, for 16QAM and 32QAM signals, in B&S and R&S configurations, considering the system with (solid

lines) and without (dashed lines) crosstalk. The OSNR penalty is extracted by the difference between the required OSNR with crosstalk and the required OSNR without crosstalk, for each number of cascaded nodes. It is very noticeable that the B&S architecture is less resilient to the presence of in-band crosstalk having a OSNR penalty of 1.7 dB and 3 dB after 10 cascaded nodes, for 16QAM and 32QAM signals, respectively. The R&S architecture is much more resilient to the in-band crosstalk , showing a negligible OSNR penalty for both modulations, as in Fig 5.12 a), the lines with and without in-band crosstalk are practically superimposed. This is mainly due to the additional blocking stage existing in the R&S architecture, meaning that all interferers are of 2nd order and have a negligible contribution to the OSNR degradation, as discussed in Section 3.5.

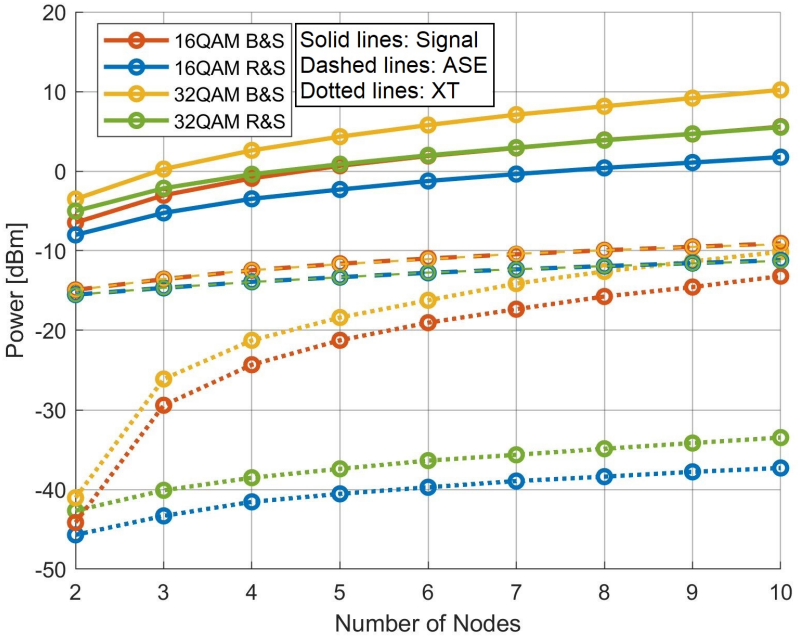

FIGURE 5.13: Signal, ASE noise and in-band crosstalk powers at the optical receiver input as a function of the number of cascaded interconnected A nodes with 2 hops for 32 GBaud Nyquist shaped 16QAM and 32QAM signals, in both B&S and R&S configurations.

In Fig. 5.13, the signal, ASE noise and in-band crosstalk powers at the optical receiver input are depicted as a function of the number of cascaded nodes. The accumulated ASE noise power only depends on the architecture configuration and reaches around -9.5 dBm and -11 dBm, for B&S and R&S architectures, respectively, after 10 nodes. As noted previously, the accumulated in-band crosstalk signal power is much higher in the B&S architecture, being around 24 dB higher than in a R&S configuration after 10 nodes. As discussed previously in Chapter 3, this higher in-band crosstalk power is due the higher number of 1st order interferers for this architecture, being around 41, 124, and 201, for, respectively, 2,

6 and 10 cascaded nodes. In the interconnected A R&S architecture nodes, the in-band crosstalk signals power is much lower than the ASE noise power, more than 20 dB, which confirms that the in-band crosstalk impairment is negligible in this case. For both architectures, for 32QAM, the total in-band crosstalk power is slightly higher (between 3 and 4 dB) than in the case of 16QAM, although only meaningful for the B&S, mostly due to the higher signal power at the generation of the in-band crosstalk terms.

Similarly as in previous section, the performance of the system is also evaluated by the maximum reach considering a maximum ROADM input power per channel of 1 dBm and by setting a safety margin on the required OSNR using Eqs. (5.4) and (5.5).

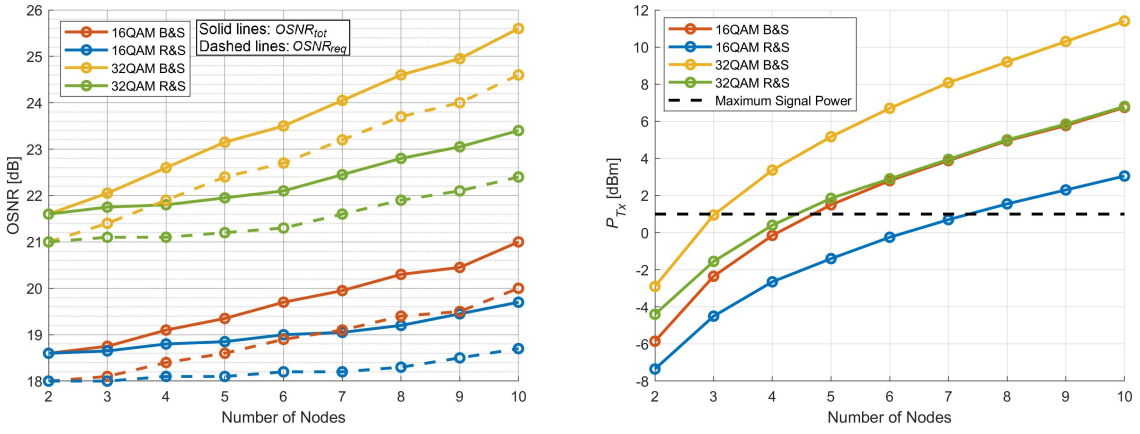

FIGURE 5.14: Required OSNR at the optical receiver input a) and transmitted signal power b) as a function of the number of cascaded interconnected A nodes with 2 hops, for 32 GBaud Nyquist shaped 16QAM and 32QAM signals and a target BER of 10^{-2}, in both B&S and R&S configurations with the presence of in-band crosstalk.

Fig. 5.14 shows that, regardless of the modulation format, the B&S architecture leads to a lower reach, in comparison with the R&S architecture and, that the 16QAM signal allows a higher network reach of 4 and 7 cascaded nodes, while the 32QAM allows only 3 and 4 cascaded nodes, respectively, for B&S and R&S architectures, as depicted in Fig. 5.14 b). The maximum reach of a network with in-band crosstalk in comparison with the reach of a network without in-band crosstalk is similar, being the only difference in the 16QAM system with the B&S interconnected A nodes that reduces from 5 to 4 cascaded nodes. This maximum reach after a few cascaded nodes results from a compromise between the maximum signal power per channel at the ROADM inputs and the stronger influence of the accumulated ASE noise along the network in comparison with the effect of the in-band crosstalk and optical filtering.

5.6 Conclusions

In this chapter, the impact of optical filtering, ASE noise from lumped amplification and in-band crosstalk on the performance of an optical network with cascaded interconnected A ROADM nodes with bank-based A/D structure has been studied and analyzed considering 32 GBaud 16 and 32QAM Nyquist shaped signals.

First, in Section 5.2, we performed the MC simulator validation in back-to-back scenario in presence of ASE noise from a loading circuit at the optical receiver input, and a very good agreement with theoretical values and similar studies has been found.

In Section 5.3, the effect of cascading optical filters was added to the simulator with ASE noise loading at the end of the filter cascade and its penalty was evaluated for different number of cascaded nodes and node configurations. For 10 cascaded interconnected A architecture nodes with $n_{hops} = 2$, an optical filtering penalty of 0.3 dB and 0.7 dB was obtained for a 16QAM signal in, respectively, B&S and R&S configurations, while the optical filtering penalty of 0.6 dB and 1.4 dB was obtained for a 32QAM signal in B&S and R&S configurations, respectively. The 32QAM signal shows practically twice the optical filtering penalty obtained for a 16QAM signal, for both node configurations.

In Section 5.4, we changed the ASE noise loading technique and considered the generation of the ASE noise contributions from lumped amplification along the optical path. The degradation induced by the ASE noise on the OSNR was higher on the B&S architecture, mainly due to the higher post-amplifier gain. The optical filtering penalty showed the same results as with the ASE noise loading at the optical receiver input. The optical network performance in terms of maximum cascaded nodes was evaluated and we have verified a maximum reach of 5 and 7 cascaded interconnected A architecture nodes, respectively, for B&S and R&S architectures, for the 16QAM modulation, while the 32QAM signal allowed a maximum network reach of 4 and 5 cascaded nodes, respectively, for B&S and R&S architectures.

Lastly, in Section 5.5, the in-band crosstalk impairment was studied and the in-band crosstalk penalty was evaluated for both 16QAM and 32QAM signals and both B&S and R&S architectures. The B&S architecture with 2 hops showed a in-band crosstalk OSNR penalty of 1.7 dB and 3 dB for a 16QAM and 32QAM signals, respectively, while the R&S architecture showed a negligible OSNR penalty for both modulations. The optical network reach was evaluated again, in the presence of optical filtering, ASE noise and in-band crosstalk. The 16QAM signal allows a maximum reach of 4 and 7 cascaded nodes, while the 32QAM only allows 3 and 4 cascaded nodes. The maximum reach is similar to a network without in-band crosstalk, the only difference being in the B&S interconnected A nodes that reduces from 5 to 4 cascaded nodes for a 16QAM signal. We have also concluded that the network reach is achieved

due to a compromise between the maximum signal power per channel at the ROADM inputs and the higher impact of the accumulated ASE noise. The penalties due to in-band crosstalk and optical filtering cascading have a smaller contribution to the performance degradation.

Chapter 6

Conclusions and future work

In this chapter, the main conclusions of this dissertation are presented, as well as some suggestions for possible future work.

6.1 Final conclusions

In this dissertation, several architectures for future large-scale ROADMs have been studied. The performance of the most promising of these architectures, named interconnected A ROADM sub-systems architecture with bank-based A/D has been investigated considering 16QAM and 32QAM Nyquist shaped signal transmission in optical networks impaired by optical filtering cascading, ASE noise from lumped amplification and in-band crosstalk.

In Chapter 2, the evolution of the ROADM nodes and its components has been presented and the architectures that allow building large-scale ROADMs and their advantages have been discussed. All the discussed architectures show a significant cost reduction in hardware in relation to large-scale ROADMs based on conventional architectures, with the interconnected A B&S architecture showing the lowest cost implementation, due to the reduced number of components.

In Chapter 3, an investigation on the generation of in-band crosstalk terms in the new proposed architectures has been performed and compared to the conventional ones. As in conventional nodes, the new large-scale architectures show a reduction on the in-band crosstalk on R&S architectures, since the majority of interferers are 2^{nd} order. The FLEX architecture shows the worst performance similar to the performance of a conventional B&S architecture, due to the high number of generated 1^{st} order interferers. In interconnected architectures, the number of generated in-band crosstalk interferers increases with the number of hops. We concluded also that the best architectures in terms of in-band crosstalk generation are the interconnected A and B. As the interconnected A shows a significant cost reduction in hardware in comparison to the interconnected B architecture, the subsequent analysis of the performance of an optical network is performed for ROADM nodes based on the interconnected A architecture.

In Chapter 4, the simulation model used in MATLAB to emulate the optical network based on interconnected A B&S and R&S architectures has been described. We provide details regarding the models of the optical components that compose the optical network such as the optical transmitter, fiber,

filters, amplifiers and coherent receiver. The MC simulation method used to assess the optical network performance and the performance metrics considered have also been presented.

In Chapter 5, the performance of 16QAM and 32QAM signals transmission with 32 GBaud on a interconnected A architecture based ROADM cascade, considering the impact of ASE noise, filtering and in-band crosstalk is assessed using MC simulation. Initially, the simulator is validated in a back-to-back scenario with ASE noise by comparison with theoretical values and other works, and a very good agreement is verified. Then, the optical filtering penalty is studied for an optical network with 2 to 10 cascaded interconnected A nodes with ASE noise loading at the optical receiver input. The optical filtering penalty reaches 0.3 dB and 0.7 dB for a 16QAM signal and 0.6 dB and 1.4 dB for a 32QAM signal, respectively, for B&S and R&S architectures when the number of hops is 2. Then, the impact of both optical filtering and ASE noise generation from lumped amplification on the optical network performance has been studied. The optical filtering penalty showed the same results as with ASE noise loading at the optical receiver input. The maximum number of cascaded nodes is 5 and 7 for a 16QAM signal, respectively, for B&S and R&S architectures, and for a 32QAM signal is 3 and 4 cascaded nodes, respectively, for B&S and R&S architectures. For the 32QAM modulation format, the B&S architecture shows a lower reach, mainly due to the higher ASE generation on the post-amplifier. With the addition of in-band crosstalk, the maximum reach achieved is 4 and 7 for a 16QAM signal, respectively, for B&S and R&S architectures, and, for a 32QAM signal, is 3 and 4 cascaded nodes, respectively, for B&S and R&S architectures. We concluded that the optical network reach, based on interconnected A architecture nodes, is mainly reached due to the high ASE noise generation along the network. The influence of in-band crosstalk and optical filtering penalty due to cascading has a smaller contribution to the network reach reduction.

6.2 Future work

For future investigation, we propose the following topics that were not addressed in this work:

- Study the network performance considering 64 GBaud 16QAM and 32QAM Nyquist shaped signals with 75 GHz channel spacing;
- Study the network performance considering different interconnected A and bank-based related parameters, such as D_s, b and T_{bank};
- Study the network performance considering an optical network based on interconnected B architecture ROADM nodes;

- Investigation of the influence of the fiber non-linear effects in each span with a simplified model such as the non-linear interference (NLI) [69];
- Comparison of the maximum reach achieved with the large-scale interconnected A and B architectures with the one attained by large-scale ROADMs based on conventional architectures.

References

[1] Cisco, "Cisco Global Cloud Index: Forecast and Methodology, 2016–2021," *White Paper*, pp. 1–46, February 1 2018.

[2] P. J. Winzer, D. T. Neilson, and A. Chraplyvy, "Fiber-Optic Transmission and Networking: The Previous 20 and the Next 20 Years," *Optics Express*, vol. 26, no. 18, pp. 24190–24239, September 2018.

[3] J. Kahn and K. Ho, "Spectral Efficiency Limits and Modulation/Detection Techniques for DWDM Systems," *IEEE J. Sel. Topics Quantum Electron.*, vol. 10, no. 2, pp. 259–272, April 2004.

[4] O. Gerstel, M. Jinno, A. Lord, and S. Yoo, "Elastic Optical Networking: a New Dawn for the Optical Layer?," *IEEE Commun. Mag.*, vol. 50, no. 2, pp. s12–s20, February 2012.

[5] P. J. Winzer, "High-Spectral-Efficiency Optical Modulation Formats," *J. Lightwave Technol.*, vol. 30, no. 24, pp. 3824–3835, December 15 2012.

[6] E. Ip, A. Lau, D. Barros, and J. Kahn, "Coherent Detection in Optical Fiber Systems," *Optics Express*, vol. 16, no. 2, pp. 753–791, January 2008.

[7] S. Gringeri, B. Basch, V. Shukla, R. Egorov, and T. Xia, "Flexible Architectures for Optical Transport Nodes and Networks," *IEEE Commun. Mag.*, vol. 48, no. 7, pp. 40–50, July 2010.

[8] "Spectral Grids for WDM Applications: DWDM Frequency Grid." ITU-T Recommendation G.694.1, 2012 [Online] Available: https://www.itu.int/rec/T-REC-G.694.1/.

[9] M. Jinno, "Elastic Optical Networking: Roles and Benefits in Beyond 100-Gb/s Era," *J. Lightwave Technol.*, vol. 35, no. 5, pp. 1116–1124, March 1 2017.

[10] J. Pedro, "Designing Transparent Flexible-Grid Optical Networks for Maximum Spectral Efficiency," *IEEE J. Opt. Commun. Netw.*, vol. 9, no. 4, pp. C35–C44, April 2017.

[11] D. Xie, D. Wang, M. Zhang, Z. Liu, Q. You, Q. Yang, and S. Yu, "LCoS-Based Wavelength-Selective Switch for Future Finer-Grid Elastic Optical Networks Capable of All-Optical Wavelength Conversion," *IEEE Photon. J.*, vol. 9, no. 2, pp. 1–12, April 2017.

[12] Y. Iwai, H. Hasegawa, and K.-I. Sato, "OXC Hardware Scale Reduction Attained by Using Interconnected Subsystem Architecture," *Optical Fiber Communication Conference and Exhibition (OFC)*, Anaheim, CA, USA, March 2013, paper NW1J.2.

[13] H. Hasegawa, S. Subramaniam, and K.-I. Sato, "Node Architecture and Design of Flexible Waveband Routing Optical Networks," *IEEE J. Opt. Commun. Netw*, vol. 8, no. 10, pp. 734–744, October 2016.

[14] M. Niwa, Y. Mori, H. Hasegawa, and K.-I. Sato, "Tipping Point for the Future Scalable OXC: What Size M×M WSS Is Needed?," *IEEE J. Opt. Commun. Netw*, vol. 9, no. 1, pp. A18–A25, January 2017.

[15] B. Ramamurthy, H. Feng, D. Datta, J. Heritage, and B. Mukherjee, "Transparent vs. Opaque vs. Translucent Wavelength-routed Optical Networks," *Optical Fiber Communication Conference and Exhibition (OFC)*, vol. 1, San Diego, CA, USA, February 1999, paper TuF2-1.

[16] J. M. Simmons, *Optical Network Design and Planning*. Springer, 2nd ed., 2014.

[17] S. Woodward, M. Feuer, and P. Palacharla, "ROADM-Node Architectures for Reconfigurable Photonic Networks," *Optical Fiber Telecommunications VIB*, pp. 683–707, I. Kaminov, T. Li, and A. Willner, eds., Academic Press, 2013.

[18] G. Papadimitriou, C. Papazoglou, and A. Pomportsis, "Optical Switching: Switch Fabrics, Techniques, and Architectures," *J. Lightwave Technol.*, vol. 21, no. 2, pp. 384–405, February 2003.

[19] G. Baxter, S. Frisken, D. Abakoumov, H. Zhou, I. Clarke, A. Bartos, and S. Poole, "Highly Programmable Wavelength Selective Switch Based on Liquid Crystal on Silicon Switching Elements," *Optical Fiber Communication Conference and Exhibition (OFC)*, Anaheim, CA, USA, March 2006, paper OTuF2.

[20] S. Han, T. J. Seok, N. Quack, B.-W. Yoo, and M. C. Wu, "Monolithic 50×50 MEMS Silicon Photonic Switches with Microsecond Response Time," *Optical Fiber Communication Conference and Exhibition (OFC)*, San Francisco, CA, USA, March 2014, paper M2K.2.

[21] N. Fontaine, R. Ryf, and D. Neilson, "$N \times M$ Wavelength Selective Crossconnect with Flexible Passbands," *Optical Fiber Communication Conference and Exhibition (OFC)*, Los Angeles, CA, USA, March 2012, paper PDP5B.2.

[22] H. Yang, B. Robertson, P. Wilkinson, and D. Chu, "Low-Cost CDC ROADM Architecture Based on Stacked Wavelength Selective Switches," *IEEE J. Opt. Commun. Netw*, vol. 9, no. 5, pp. 375–384, May 2017.

[23] Lumentum, "Optical Communications Products." Available: `https://www.lumentum.com/en/optical-communications/all-products`, 2019.

[24] D. Sequeira, L. Cancela, and J. Rebola, "Impact of In-Band Crosstalk in an Optical Network based on Multi-Degree CDC ROADM." Master's dissertation in Telecommunications and Computer Engineering, ISCTE-IUL, October 2017.

[25] S. Tibuleac and M. Filer, "Transmission Impairments in DWDM Networks With Reconfigurable Optical Add-Drop Multiplexers," *J. Lightwave Technol.*, vol. 28, no. 4, pp. 557–598, February 15 2010.

[26] T. Zami, "High Degree Optical Cross-Connect Based on Multicast Switch," *Optical Fiber Communication Conference and Exhibition (OFC)*, San Francisco, CA, USA, March 2014, paper W2A.36.

[27] T. Zami and B. Lavigne, "Advantages at Network Level of Contentionless $N \times M$ adWSS," *Optical Fiber Communication Conference and Exhibition (OFC)*, San Diego, CA, USA, March 2019, paper M1A.2.

[28] B. C. Collings, "Advanced ROADM Technologies and Architectures," *Optical Fiber Communication Conference and Exhibition (OFC)*, Los Angeles, CA, USA, March 2015, paper Tu3D.3.

[29] M. D. Feuer, S. L. Woodward, P. Palacharla, X. Wang, I. Kim, and D. Bihon, "Intra-Node Contention in Dynamic Photonic Networks," *J. Lightwave Technol.*, vol. 29, no. 4, pp. 529–535, February 15 2011.

[30] R. Shankar, M. Florjanczyk, T. J. Hall, A. Vukovic, and H. Hua, "Multi-Degree ROADM Based on Wavelength Selective Switches: Architectures and Scalability," *Optics Communications*, vol. 279, no. 1, pp. 94–100, 2007.

[31] L. Zong, H. Zhao, Z. Feng, and Y. Yan, "Low-cost, Degree-expandable and Contention-free ROADM Architecture Based on M × N WSS," *Optical Fiber Communication Conference and Exhibition (OFC)*, Anaheim, CA, USA, August 2016, paper M3E.3.

[32] M. D. Feuer and S. L. Woodward, "Advanced ROADM Networks," *Optical Fiber Communication Conference and Exhibition (OFC)*, Los Angeles, CA, USA, March 2012, paper NW3F.3.

[33] W. Wei, C. Wang, and J. Yu, "Cognitive Optical Networks: Key Drivers, Enabling Techniques, and Adaptive Bandwidth Services," *IEEE Commun. Mag.*, vol. 50, no. 1, pp. 106–113, 2012.

[34] A. Boskovic, M. Sharma, N. Antoniades, and M. Lee, "Broadcast and Select OADM Nodes Application and Performance Trade-offs," *Optical Fiber Communication Conference and Exhibition (OFC)*, Anaheim, CA, USA, March 2002, paper Tux2.

[35] M.-E. Ganbold, T. Yasuda, Y. Mori, H. Hasegawa, and K.-I. Sato, "Assessment of Optical Cross-Connect Architectures for the Creation of Next Generation Optical Networks," *2018 23rd Opto-Electronics and Communications Conference (OECC)*, Jeju, Korea, July 1 2018.

[36] J. Wu, M. Xu, S. Subramaniam, and H. Hasegawa, "Joint Banding-Node Placement and Resource Allocation for Multigranular Elastic Optical Networks," *IEEE J. Opt. Commun. Netw*, vol. 10, no. 8, pp. 27–38, August 2018.

[37] T. F. O. A. Inc., "Testing Fiber Optic Couplers, Splitters Or Other Passive Devices." Available: `https://www.thefoa.org/tech/ref/testing/test/couplers.html`, 2019.

[38] Lumentum, "Optical Amplifier Portfolio - High-Power EDFAs." Available: `https://www.lumentum.com/en/products/optical-amplifier-portfolio`, 2019.

[39] I. Monroy and E. Tangdiongga, *Crosstalk in WDM Communication Networks*. Norwell, MA: Springer, 2002.

[40] X. Wu, C. Lu, Z. Ghassemlooy, and Y. Wang, "Evaluation of Intraband Crosstalk in an FBG-OC-Based Optical Cross Connect," *IEEE Photon. Technol. Lett.*, vol. 14, pp. 212–214, February 2002.

[41] L. Cancela, D. Sequeira, B. Pinheiro, J. Rebola, and J. Pires, "Analytical Tools for Evaluating the Impact of In-band Crosstalk in DP-QPSK Signals," *21st European Conference on Networks and Optical Communications (NOC)*, pp. 6–11, Lisbon, June 2016.

[42] R. Hashimoto, S. Yamaoka, Y. Mori, H. Hasegawa, K.-I. Sato, K. Yamaguchi, K. Seno, and K. Suzuki, "First Demonstration of Subsystem-Modular Optical Cross-Connect Using Single-Module 6 × 6 Wavelength-Selective Switch," *J. Lightwave Technol.*, vol. 36, no. 7, pp. 1435–1442, April 1 2018.

[43] V. López and L. Velasco, *Elastic Optical Networks*. Springer, 2016.

[44] T. Zami, B. Lavigne, and M. Bertolini, "How 64 GBaud Optical Carriers Maximize the Capacity in Core Elastic WDM Networks With Fewer Transponders per Gb/s," *IEEE J. Opt. Commun. Netw.*, vol. 11, no. 1, 1 January 2018.

[45] Chia-Yu Yao and Chiang-Ju Chien, "Design of a Square-Root-Raised-Cosine FIR filter by a Recursive Method," *2005 IEEE International Symposium on Circuits and Systems*, vol. 1, pp. 512–515, Kobe, Japan, 23-26 May 2005.

[46] G. Agrawal, *Fiber-Optic Communication Systems*. New York: Wiley, 4th ed., 2010.

[47] E. Ip and J. Kahn, "Fiber Impairment Compensation Using Coherent Detection and Digital Signal Processing," *J. Lightwave Technol.*, vol. 28, no. 4, p. 502–519, February 15 2010.

[48] X. Zhou and C. Xie, *Enabling Technologies For High Spectral-efficiency Coherent Optical Communication Networks.* New Jersey: John Wiley & Sons, 2016.

[49] C. Pulikkaseril, L. A. Stewart, M. A. F. Roelens, G. W. Baxter, S. Poole, and S. Frisken, "Spectral Modeling of Channel Band Shapes in Wavelength Selective Switches," *Optics Express*, vol. 19, no. 9, pp. 4–11, April 2011.

[50] A. Morea, J. Renaudier, T. Zami, A. Ghazisaeidi, and O. Bertran-Pardo, "Throughput Comparison Between 50 GHz and 37.5 GHz Grid Transparent Networks," *J. Opt. Commun. Netw.*, vol. 7, no. 2, pp. A293–A300, February 2015.

[51] Y. Hsueh *et al.*, "Passband Narrowing and Crosstalk Impairments in ROADM-Enabled 100G DWDM Networks," *J. Lightwave Technol.*, vol. 30, no. 24, pp. 3980–3986, December 15 2012.

[52] T. Zami, "Current and Future Flexible Wavelength Routing Cross-Connects," *Bell Labs Technical Journal*, vol. 18, no. 3, pp. 23–38, December 2013.

[53] R. Ramaswami, K. Sivarajan, and G. Sasaki, *Optical Networks: A Practical Perspective*. 3rd ed. San Francisco, CA: Morgan Kaufmann, 2009.

[54] R. Hui and M. O'Sullivan, *Fiber Optic Measurement Techniques*. Burlington, MA: Academic, 2009.

[55] J. G. Proakis and M. Salehi, *Communication Systems Engineering*. Prentice-Hall, 2nd ed., 2001.

[56] M. Seimetz and C. Weinert, "Options, Feasibility, and Availability of 2×4 90º Hybrids for Coherent Optical Systems," *J. Lightwave Technol.*, vol. 24, no. 3, pp. 1317–1322, March 2006.

[57] R.-J. Essiambre, G. Kramer, P. J. Winzer, G. J. Foschini, and B. Goebel, "Capacity Limits of Optical Fiber Networks," *J. Lightwave Technol.*, vol. 28, no. 4, pp. 662–701, February 15 2010.

[58] L. Binh, *Digital Processing: Optical Transmission and Coherent Receiving Techniques*. Taylor and Francis, 2013.

[59] C. Doerr and P. Winzer *et al.*, "Monolithic Polarization and Phase Diversity Coherent Receiver in Silicon," *J. Lightwave Technol.*, vol. 28, no. 4, pp. 520–525, 15 February 2010.

[60] J. Proakis and M. Salehi, *Digital Communications*. McGraw-Hill, 5th ed., 2008.

[61] M. Seimetz, *High-Order Modulations for Optical Fiber Transmission*. Springer, 2009.

[62] B. Pinheiro, J. Rebola, and L. Cancela, "Impact of In-Band Crosstalk on the Performance of Optical Coherent Detection Communication Systems." Master's dissertation in Telecommunications and Computer Engineering, ISCTE-IUL, 2015.

[63] M. Jeruchim, P. Balaban, and K. Shanmugan, *Simulation of Communication Systems: Modeling, Methodology, and Techniques*. 2nd ed. New York: Kluwer, 2000.

[64] B. Li, K. J. Larsen, D. Zibar, and I. T. Monroy, "Reconfigurable Forward Error Correction Decoder for Beyond 100 Gbps High Speed Optical Links," *IEEE Commun. Lett.*, vol. 19, no. 2, pp. 119–122, February 2015.

[65] P. Vitthaladevuni, M.-S. Alouini, and J. Kieffer, "Exact BER Computation for Cross QAM Constellations," *IEEE Trans. on Wireless Comm.*, vol. 4, no. 6, pp. 3039–3050, November 2005.

[66] P. Pereira, J. Rebola, and L. Cancela, "Superchannel Transmission over Flexible-Grid Optical Networks." Master's dissertation in Telecommunications and Computer Engineering, ISCTE-IUL, October 2019.

[67] OEQuest, "+30 dBm C-Band In-Line EDFA." Available: `https://www.oequest.com/getproduct/18533/cat/1101/page/1`, 2020.

[68] T.-W. Yeow, K. Law, and A. Goldenberg, "MEMS Optical Switches," *IEEE Commun. Magazine*, vol. 39, pp. 158–163, November 2001.

[69] P. Poggiolini, G. Bosco, A. Carena, V. Curri, Y. Jiang, and F. Forghieri, "The GN-Model of Fiber Non-Linear Propagation and its Applications," *J. Lightwave Technol.*, vol. 32, no. 4, pp. 694–721, February 15 2014.